Hes·so VALAIS WALLIS
Haute Ecole Spécialisée de Suisse occidentale
Fachhochschule Westschweiz
University of Applied Sciences Western Switzerland

TOHOKU UNIVERSITY

Studiengang Systemtechnik

Vertiefungsrichtung Design and Materials

Diplom 2007

David Jossen

Flux growth of ZnO microcrystals and growth of doped homoepitaxial ZnO films by liquid phase epitaxy

Dozent	Efrain Carreño-Morelli
Experte	Dirk Ehrentraut

Sendai, 15. Februar 2008

Timetable

September 2007	October 2007	November 2007	December 2007	January 2008	February 2008
- Literature studies: papers, journal, and books. - Teaching by Prof. Ehrentraut (asking questions, theory about ZnO, examination methods, LPE, applications, flux growth, doping, etc.).	- Several pages about LPE and hydrothermal growth were written. - Abstract and poster for the "KACG fall meeting" in Korea. - First structure of the diploma thesis. - First instruction of the LPE machine. - Abstracts and poster for the "IMRAM workshop" (poster presentation) in December. - Abstract for the "flux growth conference" (oral presentation) in December. - Flux experiments were prepared.	- "KACG fall meeting". - Study of characterization methods. - I gave a presentation on PV cells. - The first pages of the report were discussed with Prof. Ehrentraut. - The abbreviations for the report were written, charts, pictures, etc. were drawn by Inventor, Visio, Paint, etc. About 20 pages were written so far. - 5 K_2CO_3 tablets were sintered and 2 flux experiments were done. - Preparation for the flux growth conference.	- Translation and summarize of a temperature sensor patent from German into English. - Study of XRD and XRC. - Further drawings for the report. - SEM-EDX, XRD, and PL of the crystals obtained in the two first flux experiments. - 2 Research meetings. - Poster presentation "IMRAM workshop" Sendai. - Oral presentation "flux growth conference" in Sendai. - Structure of the appendix for the report. - 5 flux experiments and XRD of the obtained microcrystals. - 7 K_2CO_3 tablets were sintered.	- Abstract for "CGCT conference" in Sendai. - 2 LPE experiments and examination of the films by PL, SEM-EDX, and DIC. - The abstract for the report was written. - SEM-EDX, PL of the crystals obtained in the last 5 flux experiments. - 1 Research meeting. - 1 page about ZnO for the "Annual Report Book". - SEM-EDX of 4 hydrothermal grown microcrystals for comparison.	- XRC of the two films grown by LPE - 1 Research meeting - 2 flux experiments Mo-doped ZnO (for India) - Presentation of the work at IMRAM. - Diploma thesis was finished and sent to Sion.

Abbreviations

General

α-Al_2O_3	*Alumina (Sapphire, written as Al_2O_3)*
AFM	*Atomic force microscopy*
Al	*Aluminum*
Ar	*Argon*
Au	*Gold*
Bi	*Bismuth*
BiO	*Bismuth(II) oxide, metastable phase, used for calculations*
Bi_2O_3	*Bismuth(III) oxide*
$Bi_{0.02}Zn_{0.98}O$	*Solid solution 2 mol% BiO and 98 mol% ZnO*
BSE	*Back scattered electron*
CdO	*Cadmium oxide*
Cl	*Chlorine*
CMP	*Chemical mechanical polishing*
CuO	*Copper(II) oxide*
CsCl	*Caesium chloride*
CT	*Computed tomography*
DAP	*Donor acceptor pair*
DIC	*Differential interference contrast microscopy*
D^0X	*Neutral donor bound exciton*
D^+X	*Ionized donor bound exciton*
e.g.	*lat.: Exempli gratia (for example)*
EDX	*Energy dispersive x-ray analysis*
etc.	*lat.: et cetera*
FDG	*Fluorodeoxyglucose*
FWHM	*Full width half maximum*
FX_A	*Free exciton A*
FX_B	*Free exciton B*
Ga	*Gallium*
GaN	*Gallium nitride*
Ga_2O_3	*Gallium(III) oxide*
Ge	*Germanium*
GeO_2	*Germanium(IV) oxide*
H_2O_2	*Hydrogen peroxide*
H_2O	*Water*
He-Cd	*Helium-Cadmium*
ICP-MS	*Inductively coupled plasma-mass spectroscopy*
i.e.	*lat.: id est (that means)*
i	*inert, undoped*
In	*Indium*
$InCl_3$	*Indium(III) chloride*
In_2O_3	*Indium(III) oxide*
$In_{0.02}Zn_{0.98}O$	*Solid solution 2 mol% InO and 98 mol% ZnO*
$In_{0.001}Zn_{0.999}O$	*Solid solution 0.1 mol% InO and 99.9 mol% ZnO*
IR	*Infrared*
K	*Potassium*
KCl	*Potassium chloride*
K_2CO_3	*Potassium carbonate*
KOH	*Potassium hydroxide*
LD	*Laser diode*
LED	*Light emitting diode*
Li	*Lithium*
LiCl	*Lithium chloride*
Li_2CO_3	*Lithium carbonate*
LiOH	*Lithium hydroxide anhydrous*
LOs	*Phonon replicas*
LPE	*Liquid phase epitaxy*
MBE	*Molecular beam epitaxy*
Mo	*Molybdenum*
MoO	*Molybdenum(II) oxide, metastable phase, used for calculations*
MoO_3	*Molybdenum(VI) oxide*
$Mo_{0.001}Zn_{0.999}O$	*Solid solution 0.1 mol% MoO and 99.9 mol% ZnO*
$Mo_{0.02}Zn_{0.98}O$	*Solid solution 2 mol% MoO and 98 mol% ZnO*
$Mo_{0.05}Zn_{0.95}O$	*Solid solution 5 mol% MoO and 95 mol% ZnO*
MgO	*Magnesium oxide*
N	*Nitrogen*
n	*N-type*
NaCl	*Sodium chloride*
NaOH	*Sodium hydroxide*
NBE	*Near band edge emission*
NDIM	*Nomarski differential interference microscopy*
Ni	*Nickel*
nLO	*Phonon replica number n*
no	*Number*
O	*Oxygen*
p	*P-type*
PET	*Positron emission tomography*
PL	*Photoluminescence*
Pt	*Platinum*
RL	*Radioluminescence*
RTM	*Repeated temperature modulation*
SAW	*Surface acoustic wave*
Sb	*Antimony*
SbO	*Antimony(II) oxide, metastable phase, used for calculations*
Sb_2O_5	*Antimony(V) oxide*
$Sb_{0.02}Zn_{0.98}O$	*Solid solution 2 mol% SbO and 98 mol% ZnO*
Sc	*Scandium*
SCAM	*$ScAlMgO_4$*
SC H_2O	*Supercritical water*
SE	*Secondary electron*
SEM	*Scanning electron microscopy*
SIMS	*Secondary ion mass spectroscopy*
SiO_2	*Silicon(IV) oxide*
TCO	*Transparent conductive oxide*
TEM	*Transmission electron microscopy*
TES	*Two-electron satellite*
UV	*Ultraviolet*
WDX	*Wavelength dispersive x-ray analysis*
XRC	*X-ray rocking curve*
XRD	*X-ray diffraction*
Y_2O_3	*Yttrium(III) oxide*
Zn	*Zinc*
$ZnCl_2$	*Zinc chloride*
ZnO	*Zinc oxide*
ZPL	*Zero phonon line*
ZrO_2	*Zirconium(IV) oxide*

Symbols and units

Å	*Angstrom*
A	*Surface area, Ampere*
A	*Plane of hexagonale structure*
Arcsec	*Arcsecond*
a_0	*Lattice parameter in a direction*
B	*Magnetic field*
c	*Speed of light, plane of hexagonale structure*
cm	*Centimeter, 10^{-2} meter*
c_0	*Lattice parameter in c direction*
°C	*Degree Celsius*
C	*Concentration*
d	*Distance, thickness*
E_{el}	*Electric power*
E_g	*Band gap energy*
E_{kin}	*Kinetic energy*
eV	*Electron volt*
f	*Frequency*
fm	*Femtometer, 10^{-15} meter*
F_{cent}	*Centrifugal force*
$F_{Lorentz}$	*Lorentz force*
g	*Gram*
h	*Hour*
I	*Current*
K	*Kelvin*
keV	*Kilo electron volt, 10^3 electron volt*
km	*Kilometer, 10^3 meter*
kV	*Kilovolt, 10^3 volt*
l	*Liter*
µm	*Micrometer, 10^{-6} meter*
m	*Meter, plane of hexagonal structure*
M	*Mass*
M^+	*Secondary ions*
mA	*Milliampere, 10^{-3} Ampere*
meV	*Milli electron volt, 10^{-3} eV*
MeV	*Mega electron volt, 10^6 eV*
mg	*Milligram, 10^{-3} g*
min	*Minute*
ml	*Milliliter, 10^{-3} Liter*
mm	*Millimeter, 10^{-3} meter*
Mm	*Megameter, 10^6 meter*
mmol	*Millimol, 10^{-3} mol*
mol%	*Mol·10^2*
MPa	*Megapascal, 10^6 pascal*
n	*Number*
nm	*Nanometer, 10^{-9} meter*
ns	*Nanosecond, 10^{-9} second*
p-T	*Pressure-temperature*
p	*Pressure*
p_c	*Critical pressure*
pm	*Picometer, 10^{-12} meter*
ps	*Picosecond, 10^{-12} second*
q	*Charge*
r	*Radius*
rpm	*Rotations per minute*
RT	*Room temperature*
s	*Second*
T	*Temperature*
T_c	*Critical temperature*
T_G	*Growth temperature*
T_H	*High temperature*
T_L	*Low temperature*
T_m	*Melting temperature*
t	*Time*
U	*Voltage*
V	*Volt, five, volume*
v	*Ionic speed*
$V_{(0001)}$	*Growth rate in (0001) direction*
W	*Watt*
Z	*Atomic number*
δ	*Distance delta*
θ	*Angle theta*
λ	*Wavelength lambda*
ρ	*Density roh*
ω	*Angle omega*
#	*Number*
°	*Degree*
Δ	*Difference*
%	*Per cent*

Abstract

Zinc oxide is known as an outstanding material with desirable properties and a wide application range in optoelectronics, transparent electronics, etc.
An increasingly important aspect is the fabrication of materials like ZnO by technologies which not only guarantee reproducibly high quality, but also facilitate one-step fabrication of the functional materials with a minimum effort in producing them by so-called green technologies. Moreover, mechanically untouched ZnO surfaces are desirable to exclude radiative losses due to a damaged surface layer.
As the doping of hydrothermal grown bulk ZnO appears rather difficult and time consuming, LPE was employed to obtain high-quality single crystal films of several micrometer thickness. With the LPE growth technique the damaged surface layer is neutralized, at the same time doping can be realized and the sample surface is mechanically untouched.
LPE is an advancement of the flux growth. Before growing films by LPE several flux experiments were done. Homoepitaxial ZnO films and microcrystals were grown from a LiCl solution at 640°C under ambient air conditions. ZnO is produced by a reaction of $ZnCl_2$ with K_2CO_3, such way providing the feeding for continous growth. Doping and formation of solid solutions with ions such like Bi, Sb, Mo, and In was enabled through employment of the relevant pure metal, metal halogenide or metal oxide. The crystal quality has been investigated by SEM, EDX, XRD, DIC and PL.

Table of contents

1. Introduction

Zinc oxide is a wide bandgap semiconductor (E_g = 3.3 eV at RT) with a large exciton binding energy of 60 meV. It therefore has a wide application field in modern technology such as transparent conductor in the full visible-IR wavelength range, as UV and blue light-emitting device, for ferromagnetic devices, as a piezoelectric transducer, for surface acoustic devices (SAW filter), as photocatalyst, as superfast scintillator, for spin functional devices, as gas sensor, as varistor, as sunblock, etc.

Desirable scintillation properties include high light output, high density, high speed of response, proprotional response, mechanical robustness, and chemical stability [1,2]. ZnO is an ideal material for this type of application. ZnO has a relatively high light output, is easily detectable (emission around 400 nm), has a relatively high density (increased radiation stopping power), an ultra-fast scintillation decay (high speed of response), proportional response, the transparency at RT is 80%, mechanical robustness, chemical stability and low cost [3]. A disadvantage of ZnO is the self-absorption. This problem may be overcome by doping.
To realize any type of device technology, it is important to have control over the concentration of intentionally introduced impurities, called dopants, which are responsible for the electrical properties of ZnO. For ZnO, n-type conductivity is relatively easy to realize via excess Zn or with Al, Ga, or In doping. However the important market of light emitting devices (LED, LD) is not yet accessible as long as the acceptor doping problem (p-type doping) is not solved. Although many groups have successfully achieved p-type ZnO [4], the reliability and reprocucibility are still the main issues that hinder the development of ZnO-based optoelectronic devices.
An increasingly important aspect is the fabrication of materials by technologies which not only guarantee reproducibly high quality, but also facilitate one-step fabrication of the functional materials with a minimum effort in producing them by so-called green technologies. Mechanically untouched ZnO surfaces are desirable to exclude radiative losses due to a damaged surface layer.
The hydrothermal method for the growth of ZnO single crystals has been known as a technology to grow highly crystalline and large-size crystals under a relatively low temperature [5]. Moreover, its growth rate of 0.3 mm/day is reasonably high compared with the value of 0.5 mm/day for the industrialized quartz crystal growth. The wafers sliced from the crystals are suitable for a wide band gap device.
In the ZnO thin film technologies, a sapphire has been conventionally used as substrate. However, dense dislocations exist in the devices, caused by the large lattice mismatch between the sapphire substrate and device materials. ZnO single crystal substrates are promising for homoepitaxy of ZnO active layers, and could be useful for heteroepitaxy of GaN-based active layers. It was shown that doping of ZnO during the hydrothermal growth process did not lead to high quality single crystals and the surface of the sliced wafers has to be polished what means radiative losses [6].
The mentioned problems can be solved by a recently developed technique for ZnO films called LPE. LPE serves as a fast screening tool, the damaged surface layer is neutralized, at the same time, doping can be realized and a mechanically untouched surface is obtained. LPE is an advancement of the flux growth.

Basic properties of ZnO

ZnO is a direct band gap conductor with E_g = 3.3 eV (at RT). It belongs to the hexagonal crystal system and normally forms in the wurtzite crystal structure with a_0 = 3.2495 Å and c_0 = 5.2069 Å (Figure 1). Table 1 shows a compilation of basic properties for ZnO. It should be noted that there still exist uncertainty in some of these values. For example, there are few reports on p-type ZnO and therefore the hole mobility and effective mass are still under debate.

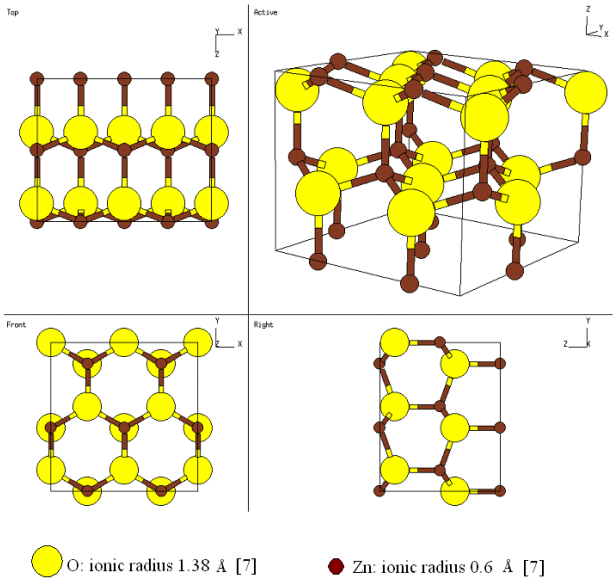

Figure 1. The wurtzite structure (after: [8]).

Table 1. Properties of ZnO

Property	Value	References
Lattice parameters at 300 K		
a_0	0.32495 nm	[9]
c_0	0.52069 nm	[9]
a_0/c_0	1.602 (ideal hexagonal structure shows 1.633)	[9]
Density	5.606 g/cm^3	[9]
Stable phase at 300 K	Wurtzite	[9]
Melting point	1975°C	[9]
Thermal conductivity at 298		
a_0	49.1 W/(mK)	[10]
c_0	57.2 W/(mK)	[10]
Linear expansion coefficient at 298 K		
$(11\bar{2}0)$ direction	6.06 x 10^{-6} K^{-1}	[10]
(0001) direction	4.16 x 10^{-6} K^{-1}	[10]
Static dielectric constant	8.656	[9]
Refractive index	1.93-2.23	[10]
Energy gap	3.3 eV	[3]
Intrinsic carrier concentration	<10^6 cm^{-3}	[9]
max n-type doping	>10^{20} cm^{-3} electrons	[9]
max p-type doping	<10^{17} cm^{-3} holes	[9]
Exciton binding energy	60 meV	[9]
Electron effective mass	0.24	[9]
Electron Hall mobility at 300 K for low n-type conductivity	200 cm^2/Vs	[9]
Hole effective mass	0.59	[9]
Hole Hall mobility at 300 K for low p-type conductivity	5-50 cm^2/Vs	[9]

2. Doping and main applications of ZnO

2.1 Doping issues

Intentionally introduced impurities are called dopants. The dopants determine whether the current, and ultimately the information processed by the device, is carried out by electrons or holes. There may also be unintentional impurities introducing during the growth of ZnO that have a deleterious effect on the properties of the material.
For ZnO n-type conductivity is relatively easy to realize via excess Zn or with Al, Ga, or In doping. With respect to p-type doping, ZnO displays significant resistance to the formation of shallow acceptor levels. There have been several approaches put forward in explaining doping difficulties in wide bandgap semiconductors [11]. First, there can be compensation by native point defects or dopant atoms that locate on interstitial sites. The defect compensates for the substitutional impurity level through the formation of a deep level trap. In some cases, strong lattice relaxations can drive the dopant energy level deeper within the gap. In other systems, one may simply have a low solubility for the chosen dopant limiting the accessible extrinsic carrier density. In ZnO, most candidate p-type dopants introduce deep acceptor levels. It appears that the most promising dopants for p-type material are the group V elements. Table 2 gives an overview of the undoped and differently doped ZnO films grown by LPE.

Table 2. Doped and undoped ZnO films by LPE.

Dopant	Results and comments	References
Undoped	The concentration of ZnO determines the growth mechanism, which evolves from island growth at C_{ZnO} < 2 mmol ZnO (per mol LiCl) to columnar growth at C_{ZnO} = 2.5 ± 0.5 mmol ZnO, to porous columnar film at 3.5 ± 0.5 mmol ZnO, to closed columnar film at C_{ZnO} = 5 mmol ZnO, to step-flow growth at C_{ZnO} = 12 ± 0.5 mmol ZnO. High structural quality, single-crystalline films, were fabricated in the concentration range 12 ≤ C_{ZnO} ≤ 13 mmol ZnO.	[10]
MgO	Magnesium is widely used for band gap engineering of ZnO to achieve a UV shift.	[10]
CdO	CdO can be employed to achieve a red shift.	[10]
Ga_2O_3	Ga in ZnO is very effective in enhancing the electrical conductivity.	[10]
In_2O_3	Indium in ZnO acts similarly to Ga (increase in the n-type conductivity of the ZnO films). TCO application.	[10]
GeO_2	Only a few reports attempted to change the electronic structure of ZnO by doping with Ge. The doping with Ge led to a lattice distortion and the solubility of Ge in ZnO is rather limited to about 0.7 mol%.	[10]
Sb_2O_5	Antimony might be a candidate as p-type dopant in ZnO if oxygen substitutes for Sb on the oxygen site.	[10]
CuO	SIMS revealed that Cu had been easily incorporated into the ZnO film. The XRC measurement using the (0002) reflection gives a FWHM of 17.3 arcsec. This was the lowest FWHM value ever measured with ZnO.	[10]

Doping can influence the decay time, the light intensity and the emission wavelength of ZnO. Acceptor, donor co-doping is interesting for superfast scintillators with an emission in the blue spectrum (high DAP recombination) [10]. Li could be used as acceptor (already in the system by reason of LiCl as solvent). However, Li behaves as a deep acceptor that means for p-type doping Li cannot be used.
An advantage of ZnO is that the exciton is stable enough under RT (relatively high emission intensity of the blue curve, Figure 2). With rising temperature the emission curve is shifted to higher wavelength but the emission peak is still beyond the absorption edge what leads to self-absorption. This problem has to be solved by doping.

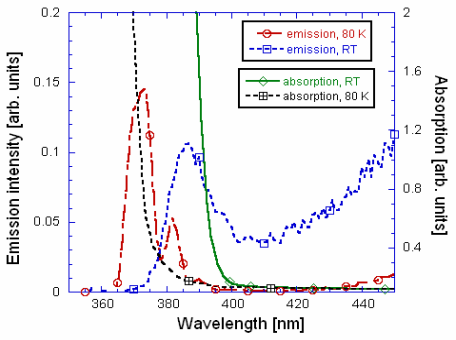

Figure 2. Radioluminescence (RL) of an undoped hydrothermal grown ZnO crystal. Temperature-dependent absorption edge vs. excitonic emission. Self-absorption becomes increasingly troublesome with rising temperature (taken from: [12]).

The absorption edge is given by the material whereas the emission can be influenced by doping. That could be a solution to the self-absorption problem: shift of the emission wavelength by doping, Figure 3. The shift is also desired to facilitate the detection in the visible light. The green curve shows In-doped ZnO. The triangles show the time-resolved emission spectra. Doping ZnO with Ge shows almost no influence (red curve).

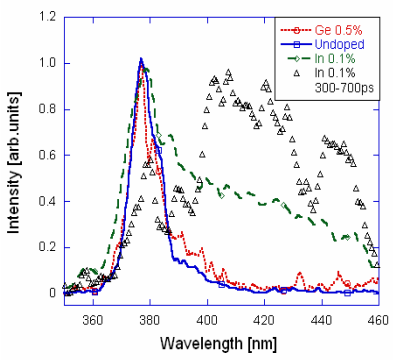

Figure 3. Time-resolved photoluminescence (PL) emission spectra of LPE grown films doped with In and Ge in comparison to the undoped film (taken from: [12]).

In this work ZnO was doped with Sb, Bi_2O_3, $InCl_3$, and MoO_3.

- P-type doping of ZnO was shown by other groups using N [13]. Sb and Bi are group V elements like N. For this reason these elements could be candidates for doping ZnO p-type. Arsenic was excluded because of its toxicity.
- Indium with Li together could build a DAP which is interesting for superfast scintillators [10].

- Mo doping leads to a strong enhancement of the photocatalytic effect of ZnO [14]. Photodegradation of model pollutants was already shown [15] (photoexcitation of Mo-doped ZnO leads to a change on its surface, e.g. increasing of electron density. If toxic color slowly flows over the excited material, the toxic part can be degraded).

2.2 Scintillator-basics and applications

Scintillator basics

Scintillation detectors consist of a scintillator material followed by an optional relay element and a photodetector. A scintillator converts high energy photons in low energy photons, which than can be detected by a photodetector diode (Figure 4).

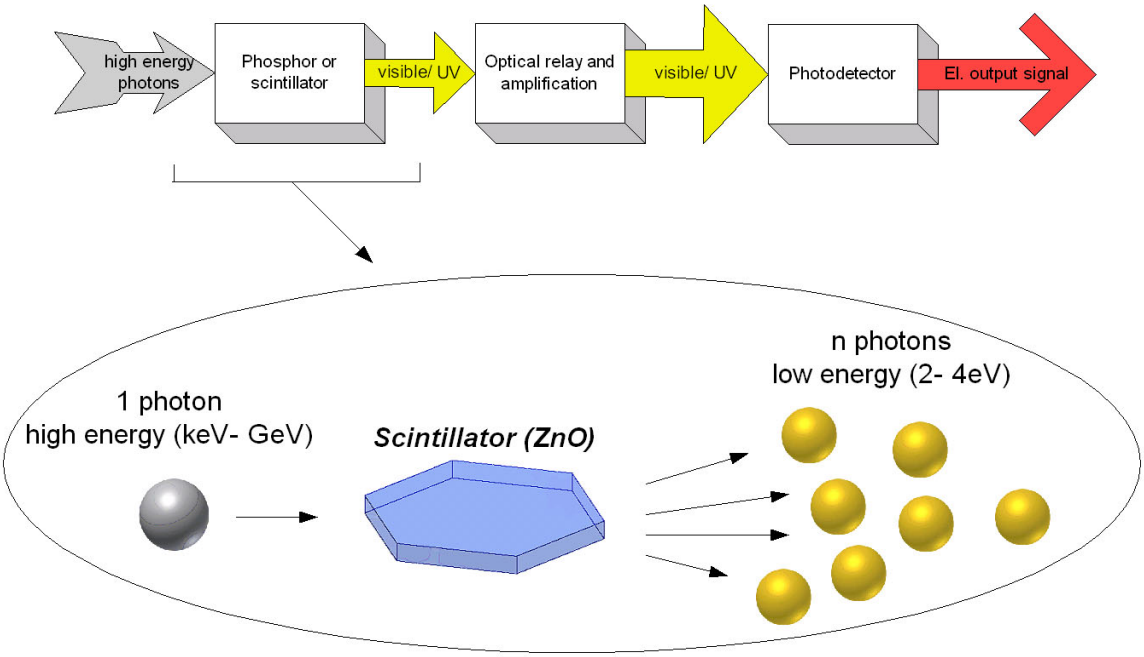

Figure 4. Principle of a scintillator (after: [16,17]).

Wide band-gap materials like ZnO (Table 3) are employed for transformation of high energy photons to UV/ visible light. Current standard material is $PbWO_4$ although its slow decay hampers for use in ultrafast decay devices. Figure 5 shows the electromagnetic spectrum with the visible light. Scintillation conversion is a relatively complicated issue, which can be divided into three consecutive sub-processes; conversion, transport and luminescence (Figure 6).

Table 3. Scintillator materials.

Chemical composition	ρ [g cm^{-3}]	$\lambda_{emission}$ [nm]	Decay time [ns] Fast / slow	Light yield [Photons/MeV]	References
CsI:Tl	4.51	400-565	- / 1000	4-5x10^4	[16]
$PbWO_4$	8.23	410-500	2-10 / 100-10^4	1-3x10^2	[16]
$Bi_4Ge_3O_{12}$	7.13	490	- / 300	4-5x10^3	[16]
Ce-doped Lu_2SiO_5	7.41	420	40 / -	2.7-3x10^4	[16]
ZnO	5.61	390	0.250–0.850 / -	9x10^2-9x10^3	[3]

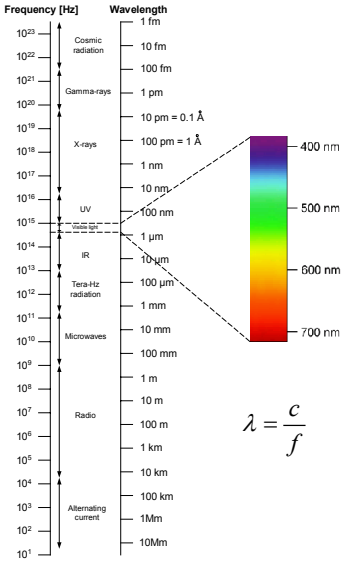

Figure 5. Electromagnetic spectrum (after: [18]).

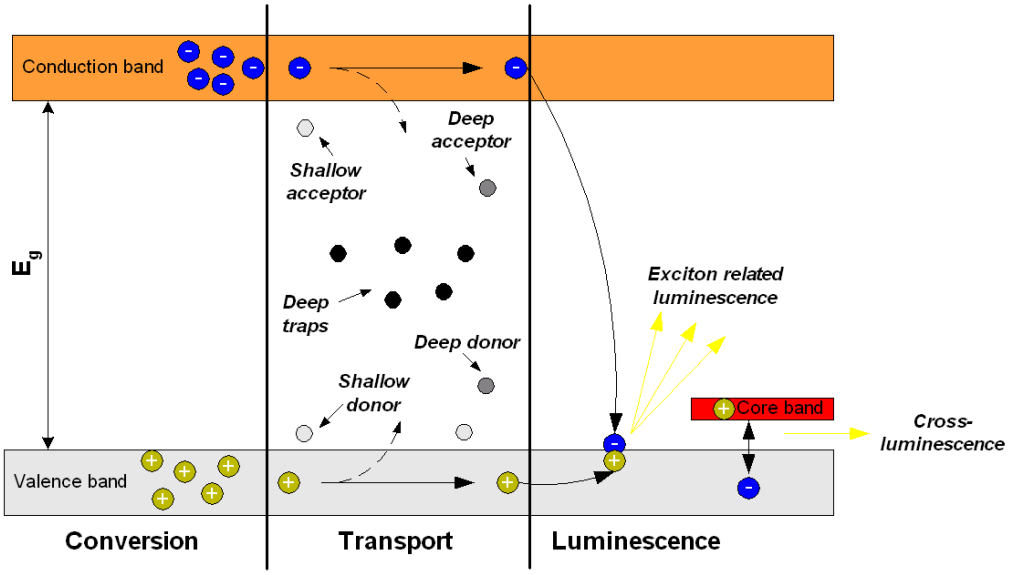

Figure 6. A sketch of the scintillator conversion mechanism in a wide band-gap single crystal solid state (after: [17]).

During the initial conversion a multi-step interaction of a high-energy photon with the lattice of the scintillator material occurs through the photoelectric effect and Compton scattering effect. Many electron-hole pairs are created and thermalized in the conduction and valence bands, respectively. This first stage is concluded within less than 1 ps. In the transport process, electrons and holes migrate through the material, repeated trapping at defects may occur, energy losses are probable due to nonradiative recombination, etc. There are two kinds of traps, shallow and deep traps. Shallow traps have a short lifetime whereas deep traps have a lifetime up to weeks or months. The final stage, luminescence, consists in consecutive trapping of the electron and hole at the luminescence centre and their radiative recombination. In particular groups of materials (like ZnO) the light generation occurs in radiative transitions between the valence and first core bands as sketched in Figure 6. These are so-called cross-luminescence scintillators. The latter mechanism enables very fast, even subnanosecond, scintillation response, which is, however, usually accompanied by much slower exciton-related luminescence.

Optimum scintillator requirements are [1]:

- superfast response time (below 1 ns) and fast signal rise time for good time resolution and handling of high counting rates,
- high light yield (>50000 photons per MeV of absorbed gamma ray energy) for good energy, time and position resolution,
- proportional response for good energy resolution,
- high ρ, and high Z for high gamma ray detection efficiency.

Applications

A major field of application of scintillators is medicine. PET is a nuclear medicine imaging technique which produces a three-dimensional image or map of functional processes in the body. A short-lived radioactive tracer isotope, which decays by emitting a positron, which also has been chemically incorporated into a metabolically active molecule (most commonly used is FDG), is injected into the living subject (usually into blood circulation). There is a waiting period while the metabolically active molecule becomes concentrated in tissues of interest. The research subject or patient is placed in the imaging scanner.
As the radioisotope undergoes positron emission decay, it emits a positron. After travelling up to a few millimeters the positron encounters and annihilates with an electron, producing a pair of photons moving in opposite direction. These pairs are detected when they reach a scintillator material in the scanning device. With the collected information an image can be reconstructed (Figure 7).

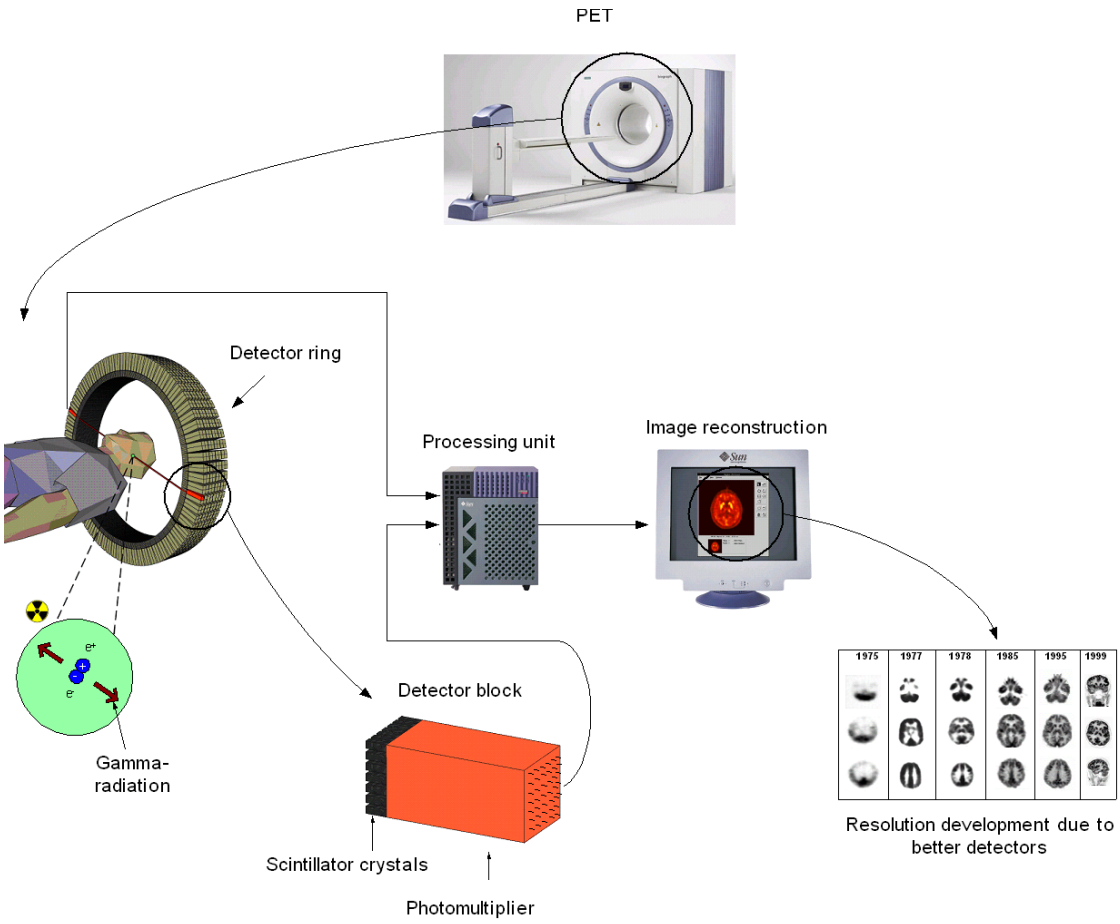

Figure 7. PET an important application for scintillators (after: [19,20,21]).

Other scintillator applications are:

- high energy physics (particle physics,…)
- security check (x-ray scanning)
- nondestructive analysis (CT)
- neutron-based check (remote detection)
- etc.

So far, ZnO is not used as scintillator material. LPE is promising for reproducible and cheap production of high quality crystals which can be used as scintillators in future, for two dimensional thin film detectors.

2.3 ZnO based light emitting diode

ZnO has the following advantages for LED's and lasers:

- a high exciton binding energy.
- it is possible to tune the bandgap from 2 eV to 4.5 eV upon alloying with CdO and MgO, respectively.
- large and high-quality single-crystal wafers are commercially available.

Figure 8 shows a homostructural p-i-n junction. A SCAM substrate is covered by a 100 nm thick buffer layer followed by a 400 nm thick n-type ZnO layer. An inert ZnO layer of 50 nm connects the p-type ZnO layer (300 nm) with n-type ZnO. Ni and Au were used to obtain ohmic contacts.

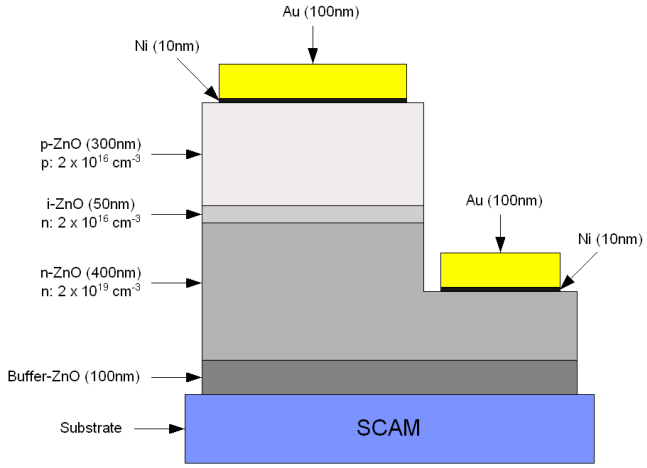

Figure 8. Structure of a p-i-n junction LED based on ZnO (after: [4]).

A light emitting diode based on ZnO was recently demonstrated by a technology called RTM. Thin films of ZnO and junction devices were grown by laser MBE using N as p-type dopant (T_g = 950°C). This layer-by-layer growth mode is possible with an atomically smooth ZnO buffer layer on SCAM substrate produced by high temperature annealing. However, N as one of the most promising p-type dopant, cannot be incorporated into ZnO at such high T_g. C_N decreases with increasing temperatures. RTM was developed to satisfy high cristallinity and high C_N. It was repeated a growth sequence in which a N-doped ZnO layer 10-15 nm thick is deposited at T_L = 400°C, followed by rapid ramp to T_H = 950°C, and growth of a 1-nm-thick layer at T_H.

3. Flux growth, film growth and characterization methods

3.1 Flux growth

The term “flux” is deceptive but widely used for the growth of crystals from a liquid solution. Before ZnO films were grown by LPE, several flux experiments were done. The conditions were similar to LPE, same solvent and solutes, same temperatures, air atmosphere and atmospheric pressure. Compared to LPE, there was no substrate used. Only natural convection in the crucible serves to transport the ZnO. Although the furnace is a closed system, the temperature of the solution is not homogeneous. On the surface of the solution there is contact to air and around the solution is the ZrO_2 crucible. The obtained microcrystals from the flux experiments were used for investigation on dopant concentration and crystallinity. The production of these crystals is quite easy and their properties are mostly similar to films grown by LPE. These microcrystals could find applications in sunblock or as micro-lasers. For laser application the crystals have to be aligned e.g. by a magnetic field, electric field, chemical influence of the growth process, etc., to bundle the emitted light beam.
A film could also be grown by flux growth. All materials are put in a crucible and a substrate is added, but the film would be of low quality (island growth, many inclusions, etc. due to the lack of forced convection, see section 3.2.2). There is the risk that the crystals would be ordered randomly on the substrate, that means many interfaces what leads to radiation losses.

3.2 Film growth

Often due to the lack of high-quality ZnO substrates, most of the device structures are based on heteroepitaxial ZnO films, i.e. ZnO deposited on foreign substrates with different crystallographic and thermal properties. The resulting disadvantages in ZnO films on Al_2O_3 or GaN involve, i.e. a temperature-dependent lattice misfit that often makes buffer layers indispensable, and the out-diffusion of ions like Al and Ga from the substrate into the ZnO film [10]. This has accelerated the quest for large-size ZnO substrates of excellent crystallinity and low defect concentration. The largest high-quality crystals are currently produced by the hydrothermal technique, which now is capable of producing specimens 3 inch in diameter [10].

3.2.1 Hydrothermal growth of ZnO bulk single crystals

It has been shown that best ZnO crystals are produced by the hydrothermal technology [10]. Since the ZnO substrates we used where prepared from hydrothermal ZnO, it is necessary to have a closer look into the technology.
Hydrothermal growth comprises the use of aqueous solvents and mineralizers under elevated temperature and pressure in order to dissolve and recrystallize materials, which are barely soluble under ordinary conditions. Mineralizers are particularly important since they serve to establish a suitable solubility of the solute because most of the species are rather poorly soluble in water.

The hydrothermal growth of ZnO requires the use of water in its supercritical state (T_c = 374 K and p_c = 22.1 MPa.). SC H_2O is characterized by an enhanced acidity, reduced density (0.05-0.2 gcm^{-3}) lower polarity, the diffusivity and the miscibility with gases are strongly increased in comparison to water under normal pressure and temperature [10]. The enhanced acidity favors the dissolution of ZnO. However, the solubility of ZnO in SC H_2O remains insufficient and makes the use of mineralizers necessary. The best mineralizers for ZnO are a mixture of KOH and LiOH. Pure KOH gives rise to a high growth rate which leads to low crystal quality and the growth process is hard to control. By contrast, LiOH alone is too weak to significantly increase the solubility of ZnO in SC H_2O. Li^+ is needed to reduce the number of crystal defects. It slows down the growth speed in (0001) direction and slightly increase it for the (1100) direction. This is considered to be related to a decreased positive surface charge that lowers the probability of incorporating Zn-containing negatively-charged species. A molar ratio of 3:1 of KOH:LiOH delivers the best quality [10].
Typical growth rates of high-quality ZnO crystals occur in the range up to a maximum of 0.3 mm/day for the (0001) face. The growth speed is about two times faster on the (0001) face than on the $(000\bar{1})$ face [10].
The p-T region at which large hydrothermal ZnO crystals are grown stretches between the pressure of 70-255 MPa at temperatures of 300-430°C [10].

Features of the hydrothermal method for ZnO crystals comprise:

- use of an autoclave.
- use of the solvent water.
- use of solubility increasing mineralizers (LiOH, NaOH, KOH, Li_2CO_3, H_2O_2).
- employment of a precursor (solute) e.g. sintered ZnO.
- seed crystals.
- a temperature gradient between the growth zone and the dissolution zone.
- $\Delta T \approx 0$ at the interface of the crystal to the surrounding solution.
- saturation of the solute while the seed crystal is already in contact with the undersaturated solution.

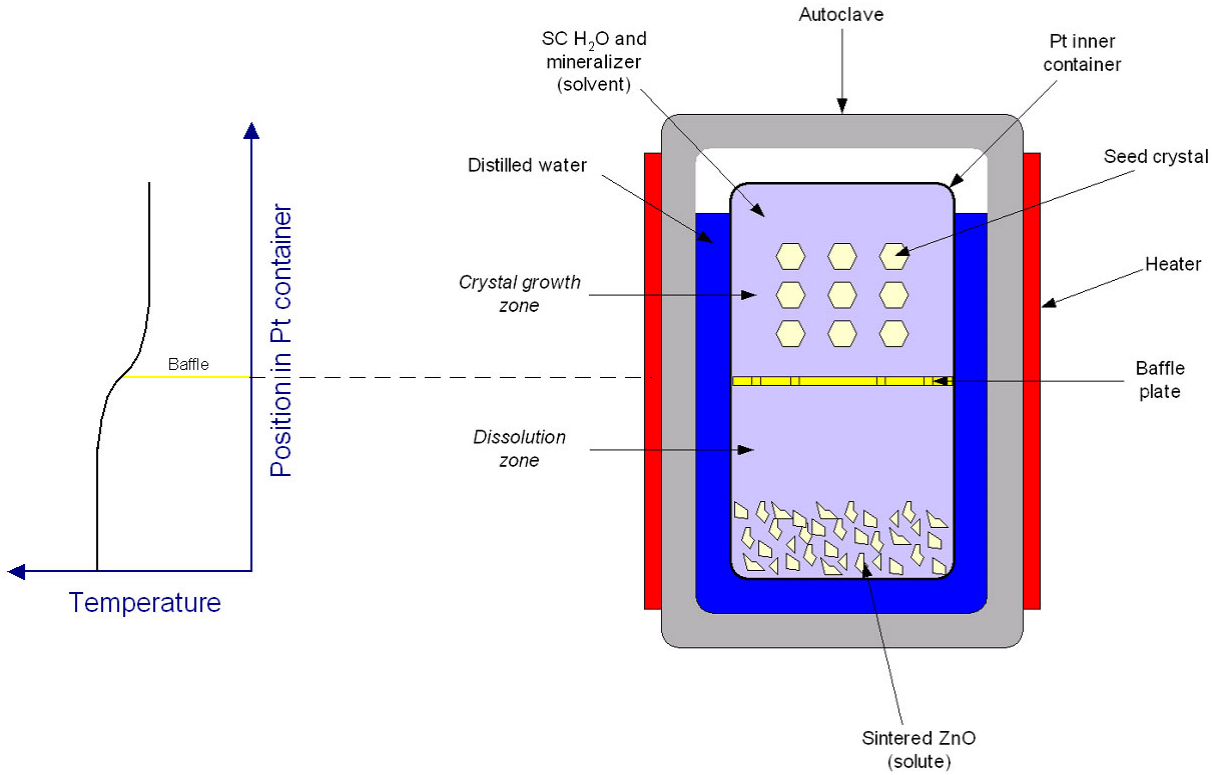

Figure 9. Schematic of the hydrothermal growth system (after: [5]).

Figure 9 shows the cross section of an autoclave used to grow ZnO single crystals. Sintered ZnO polycrystals served as precursor in an aqueous solution containing mineralizers of LiOH (1 mol/l H_2O) and KOH (3 mol/l H_2O). Because of the high concentration of the mineralizer, it would react chemically with the steel of the autoclave that leads to impurities in the ZnO crystals. Therefore, a hermetically sealed Pt inner container is employed to isolate the growth environment from the autoclave. The Pt inner container is divided by a baffle plate into two zones: the crystal growth zone and the dissolution zone. The crystals are grown from SC H_2O at high temperature (300-400°C) and high pressure (80-100 MPa). Convection between the dissolution zone (higher temperature) and the growth zone (lower temperature) is the main transport process. In order to equalize the pressure between the Pt inner container and the autoclave, a defined volume of distilled water is supplied into the gap between the autoclave and the Pt inner container.

Figure 10. Hydrothermally grown two-inch size ZnO crystals (taken from: [10]).

3.2.2 Liquid phase epitaxy

LPE is an advancement of the flux growth with a controlled supersaturation by the formation of microcrystals (same crystals which are produced in flux experiments, these crystals are catched by a baffle and ceramic shields). Additionaly, forced convection is applied to the substrate.

Basically, in LPE, a solution consisting of a solvent and solute is used to deposit a film on a single-crystalline substrate so as to preserve the crystallographic information resulting from the substrate. For a ZnO film a ZnO substrate is the ideal choice to fabricate samples with zero lattice and thermal misfits. This technique is called homoepitaxy. LPE from chloride solution is basically water-free and, consequently, hydrogen plays no role as impurity in ZnO [10].

The wafers, on which growth occurs, were hydrothermally grown (0001) ZnO (Figure 11). A diamond blade saw is used to cut wafers from the bulk single crystal. The damage induced by cutting is removed by a lapping process. A subsequent mechanical polishing serves for removal of the damage caused by lapping. High-quality surface finish is obtained by CMP, and subsequent thermal annealing at about 1000°C under oxygen-rich atmosphere. Annealing for 3h yielded the best crystallinity. Atomic steps with step spacing about 50 nm are typically found by AFM [10]. This allows for controlled 2-dimensional nucleation and growth of the films.

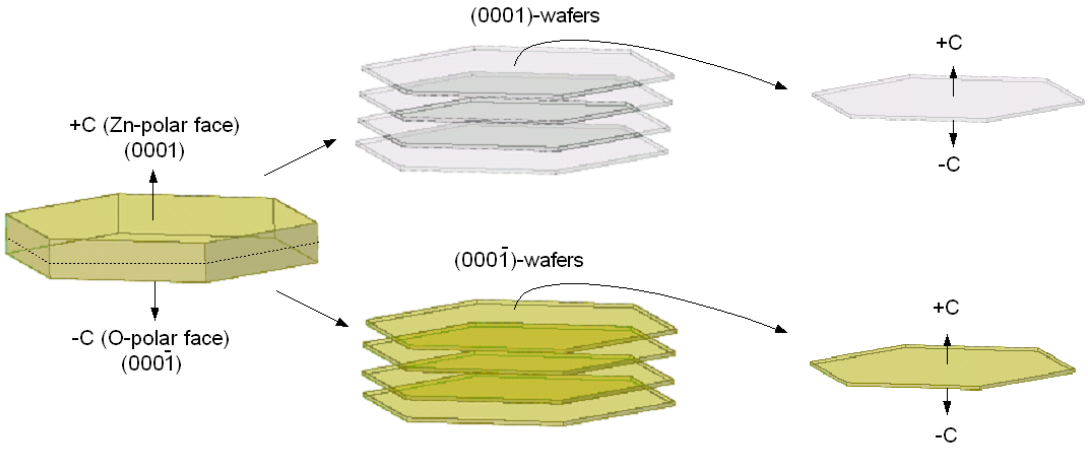

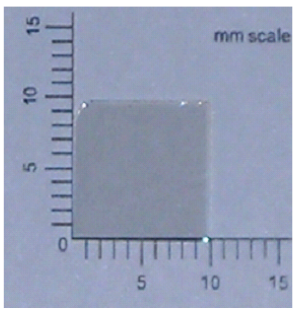

A picture of a high-grade (0001) ZnO substrate after CMP and thermal annealing

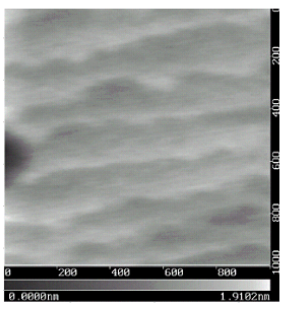

An AFM image of a high-grade (0001) ZnO substrate after CMP and thermal annealing displaying atomic steps. The scale indicates a maximum height difference of 1.9102 nm. (taken from: [6]).

Figure 11. Hydrothermally grown bulk crystal, wafers and faces.

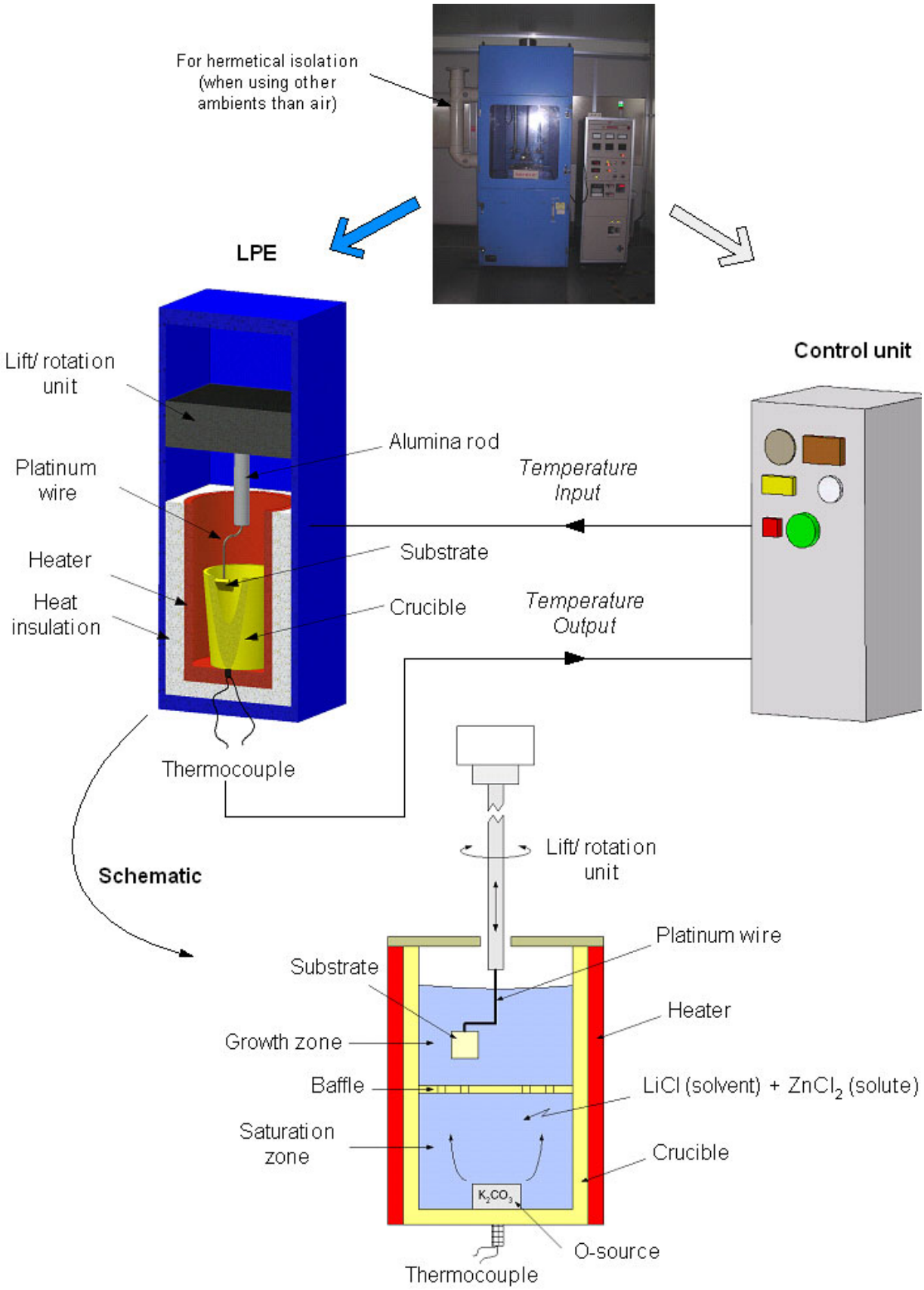

Figure 12. Schematic of the LPE setup (after: [6]).

Experiments were carried out on industrial scale LPE furnace with 3 heating zones using dipping technique (Figure 12). The liquid solution inside crucible is separated by a baffle into growth and saturation zone.
LiCl (melting point T_m = 605°C) was applied for solvent. ZnO was formed by the reaction of $ZnCl_2$ with polycristalline K_2CO_3 serving as oxygen source. Polycrystalline K_2CO_3 was obtained from powder-like K_2CO_3, which was pressed and sintered in ZrO_2 crucibles at 840°C- 870°C.
To prepare an experiment, firstly, K_2CO_3 was placed at the bottom of the crucible. After the chlorides were weighed and roughly mixed, they were filled into the crucible and immediately heated to T_G, between 630°C and 640°C. The substrate was attached to a Pt wire, which was mounted on an Al_2O_3 rod. The substrate was immersed into the liquid solution after a dwell time of ½ h and the rotation speed was slowly increased to 20 rpm. The experiments were performed under air at atmospheric pressure, and at constant temperature. The growth was finished by separating the substrate from the solution. The adhesive solvent was removed from the film by rinsing with distilled water (solvent is water soluble and so removing from the film is easy). Isopropanol was used to remove water from the sample.
The entire process does not require big efforts due to the simplicity of the equipment and process conditions, nor is high temperature or vacuum needed.

- *Chemical concept*

Alkaline metal chlorides (LiCl-NaCl-CsCl) as solvent and continuous feeding by $ZnCl_2$ and K_2CO_3 was applied. The eutectic mixture of NaCl-CsCl (T_m = 486°C) can be applied to slightly lower the melting point. The highest solubility of ZnO at 650°C was obtained in LiCl (89.5 mg/mol). The solubility of ZnO in NaCl-CsCl is about 5.3 mg/mol. Due to the comparatively high solubility in LiCl, LiCl was chosen as solvent for ZnO [10].

General reaction:

$$Solvent + ZnCl_2 + K_2CO_3 \rightarrow Solvent + ZnO + 2KCl + CO_2\uparrow$$

Used reaction:

$$\underset{42.4\,g/mol}{LiCl} + \underset{136.3\,g/mol}{ZnCl_2} + \underset{138.2\,g/mol}{K_2CO_3} \rightarrow \underset{42.4\,g/mol}{LiCl} + \underset{81.4\,g/mol}{ZnO} + \underset{74.6\,g/mol}{2KCl} + \overset{44\,g/mol}{CO_2\uparrow}$$

Input ⟶ Output

Table 4. Typical amounts of materials, for calculations see Appendix A.

	Material	[mol]
Input	LiCl	0.9756
	$ZnCl_2$	0.0122
	K_2CO_3	0.0122
Output	LiCl	0.9756
	ZnO	0.0122
	2KCl	0.0122

(CO_2 is disregarded)

The amount of formed KCl depends on the available amount of $ZnCl_2$ and K_2CO_3. The reaction results in the formation of KCl that forms a solid solution with the applied solvent (LiCl). The concentration of LiCl and K in the solid solution can be calculated:

$$\frac{2KCl_{[mol]}}{2KCl_{[mol]} + LiCl_{[mol]}} = \frac{0.012195208}{0.012195208 + 0.97561666} \approx 0.012$$

The solid solution is $K_{0.012}Li_{0.988}Cl$

A large quantity of the resulting ZnO occurs as crystals which are deposited at the bottom of the crucible. Through the formation of these crystals, the supersaturation of the solution at the beginning of an experiment is controlled.

K_2CO_3

The choice of K_2CO_3 as an oxygen source has been made due to its easy availability and high purity.
The powder is sintered to a tablet. Continuous feeding over the whole growth process is provided with the advantage to overcome the comparably low solubility of ZnO in LiCl (11 mmol at 650°C, that's 89.5 mg ZnO per 42.4 g LiCl). The powder reacts within few minutes whereas the sintered tablet serves well over 24 h. This can be explained in terms of surface size of the oxygen source, which is very large for the powder and minimized in case of the tablet.

Alkaline metal chlorides

They possess some advantageous properties like [10]

1. low melting points (LiCl 605°C, NaCl 801°C, CsCl 646°C).
2. complete dissociation to monoatomic ions when molten, which results in a low dynamic viscosity.
3. a high solubility in water, therefore cleaning of the grown film is easy.
4. availability in high purity at reasonable price.

- *General*

Crucible

A crucible of high-density Al_2O_3 never showed any corrosion, neither a weight change nor coloration. ZrO_2 as material for the crucible was slowly attacked by the $ZnCl_2$ / LiCl solution. This could cause cracking of the crucible after multiple uses. The advantage is that there is no Al in the system. In the experiments the ZrO_2 crucible was used.

Baffle and ceramic shields (Al_2O_3 as material)

Small crystals are produced as by-products during the LPE growth. The microcrystals are transported by the flow produced by natural and forced convection. The crystals would be deposited on the substrate and incorporated to form large defects.
To avoid this problem a baffle with several holes is placed in the crucible. The baffle catches most part of the crystals but some will pass in direction of the substrate. For this reason there are ceramic shields around the substrate to catch all microcrystals. Thus, C_{ZnO} will be lower but high crystallinity films can be grown. The Al content of the baffle and the ceramic shields have never been a problem with respect to the purity of the grown films.

Natural and forced convection

On top of the furnace is an aperture for passing the rotation rod, thus some heat escapes through this aperture and a little temperature difference leads to a flow within the crucible which is called natural convection. Furthermore differences in concentrations contribute to convection too. The resulting flow is not controllable which results in low-quality crystals. A rotation is applied to obtain forced convection. By the rotation of the substrate the diffusion layer is minimized and the growth speed is increased. The result is a homogeneous solution for the growth of high-quality films. Forced convection is widely used in crystal growth technology.

Rotation and attachement of the substrate

The rotation leads to a homogeneous concentration, to a reduction of the diffusion layer and to a flow effect (see forced convection). The Zn-face of the substrate is oriented against the flow. As mentioned above the substrate is attached to a Pt wire (0.5 mm diameter). The wire is mainly attached on the O-face of the substrate to establish a free surface on the Zn polar face. An angle of about 45° (between the substrate and the rod) is desired for an optimal interception of ZnO (Figure 13). A rotation of 20 rpm was applied.

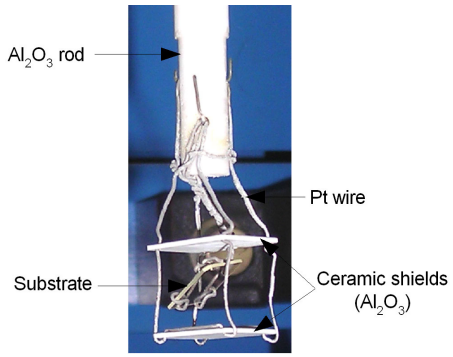

Figure 13. Attachement of the substrate.

- *Growth speed*

Films grown on $(000\bar{1})$ are generally of poorly quality and much lower thickness than those on the (0001) face. The ratio of growth speed of (0001) : $(000\bar{1})$ = (2.8-3) : 1. That is the reason why the film growth is focused on (0001). The growth rate for film growth on (0001) ranges between 0.12 µm/h ≤ $V_{(0001)}$ ≤ 0.25 µm/h [10].

3.3 Characterization

3.3.1 Selection of suitable methods

There are many different examination methods. One has to decide which analysis are reasonable. Structural and chemical quality can be investigated using optical microscopy, SEM, TEM, EDX, DIC, AFM, XRD, SIMS, PL, RL, etc. Some important examination methodes are described in the following pages.

3.3.2 Scanning electron microscopy

With an electron microscope the surface or the interior of a sample is represented by the interaction of electrons with the sample. Fast electrons have a much smaller wavelength than visible light, thus the resolution of electron microscopes is clearly higher (at present about 0.1nm).
In a typical SEM, electrons are emitted from a cathode and are accelerated towards an anode. The electron beam is focused by one or two condenser lenses into a beam with a very fine focal spot size. With coils the electron beam is focused on the sample. The primary electron beam is scanned over the surface of the sample. The energy exchange between the electron beam and the sample results in the emission of electrons and electromagnetic radiation, which can be detected to produce an image (Figure 14). The process takes place in a vaccum to avoid interactions with atoms and molecules from air.

The most important signals in SEM are:

- SE which are ejected from the sample. These electrons reproduce the topography of the sample.
- BSE. These are reflected primary electrons. The intensity of the signal depends on the atomic number. Heavy elements cause a strong backscatter, so that accordant areas appear brightly.

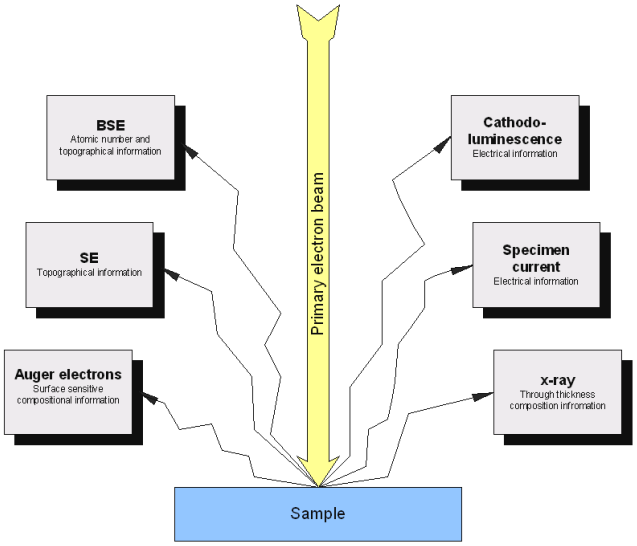

Figure 14. Different signals which can be detected (after: [22]).

EDX or WDX is often used in SEM for chemical analysis. The primary electron beam excites an electron in an inner shell of an atom of the sample. The excited electron is ejected which results in a formation of an electron hole within the atom's electronic structure. An electron from an outer, higher-energy shell then fills the hole, and the excess energy of that electron is released in the form of an x-ray. Each element has a unique electronic structure and, thus, a unique response to the excitation by the primary electron beam. By reason of this fundamental principle, the x-ray emission data can be analyzed to characterize the sample. In EDX the energy of the emitted x-ray is evaluated, whereas in WDX the wavelength is analyzed.

3.3.3 Differential interference contrast microscopy

Differential interference contrast microscopy, also known as Nomarski microscopy, is an optical microscopy illumination technique used to enhance the contrast in unstained, transparent samples. With a DIC differences in height on a surface can be seen. It employs the principle of interferometry to gain information about the optical density of the sample, to see otherwise invisible features.
DIC works by separating a polarised light source into two beams which take slightly different paths through the sample. The length of each optical path (product of refractive index and geometric path length) differs, the beams interfere when they are recombined (Figure 15). This gives the appearance of a three-dimensional physical relief corresponding to the variation of optical density of the sample.

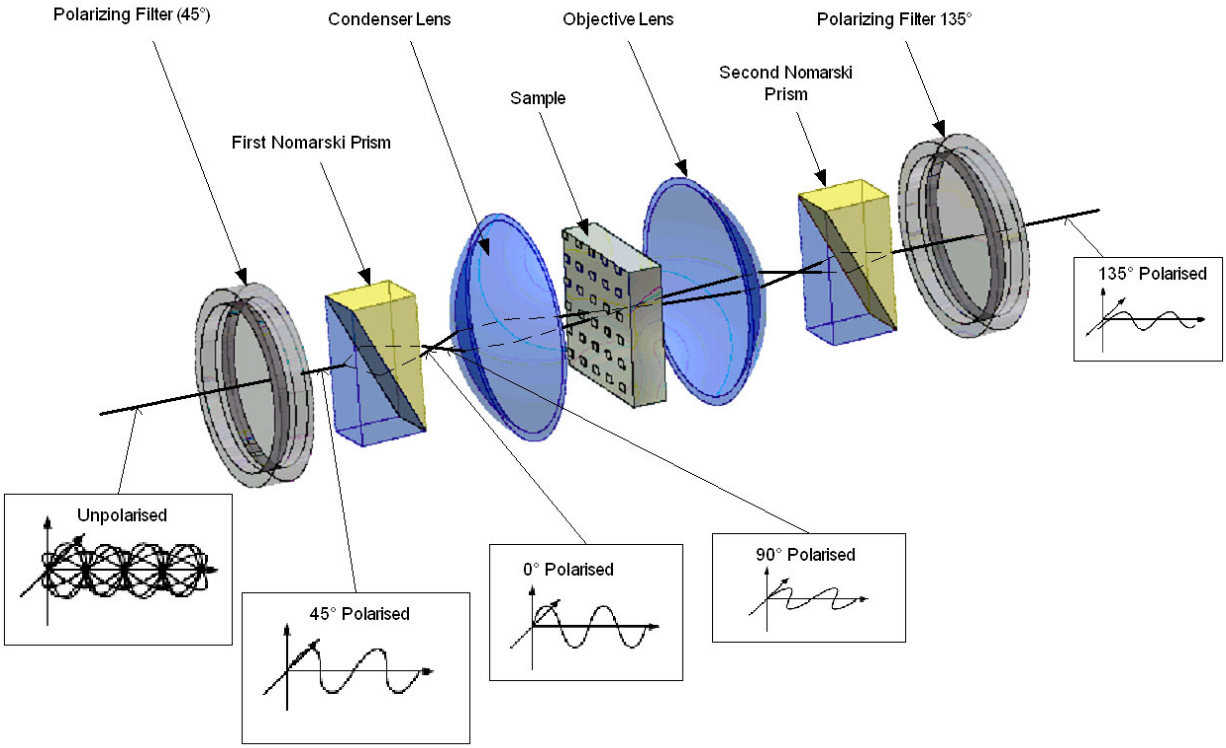

Figure 15. The light path through a DIC (after: [23]).

Unpolarised light enters the microscope and is polarised at 45°. The polarised light enters the first Nomarski prism and is separated into two rays (sampling and reference ray) polarised at 90° to each other. The two rays are focused by the condenser lens for passage through the sample. The rays will pass through two adjacent points in the sample. They will experience different optical path lengths where the areas differ in refractive index or thickness. This cause a change in phase of one ray relative to the other. Two different images are created. The rays travel through the objective lens and are focused for the second Nomarski prism. The latter recombines the two rays into one polarised at 135°. These combination of rays leads to interference.

3.3.4 X-ray diffraction

X-rays (λ between 2.5×10^{17}Hz and 6×10^{19} Hz [24]) are diffracted when they meet an object. Diffraction is concise at the moment the dimensions of the diffractive structure is comparable with the wavelength of the diffracted radiation.
There are two different derivation-methods to get the formulas for the description of concise x-ray diffraction on objects. The first method leads to the “Laue” equations and the other one leads to the equation of “Bragg”. The three Laue-formulas and the Bragg equation are identic. Subsequent, the derivation leading to the Bragg equation is demonstrated:

The blue lines (Figure 16) represent monochromatic x-ray (λ=constant) which meet, under the angle θ, on parallel lattice planes. θ is known as Bragg angle. The distance between two parallel lattice planes is called d. The lower wave train covers a longer distance than the upper one. Constructive interference takes place when the diffracted x-rays are in-phase. That means the yellow distance has to be an integer multiple of λ.

$$2\delta = n \cdot \lambda \qquad (1)$$

note: n is also known as diffraction order (Laue equations).

In Figure 16 it is obvious that,

$$\delta = d \cdot \sin(\theta) \qquad (2)$$

Introducing (2) in (1) the Bragg equation is obtained,

$$n\lambda = 2d \sin(\theta)$$

Constructive interference takes place at the moment the Bragg equation is satisfied.

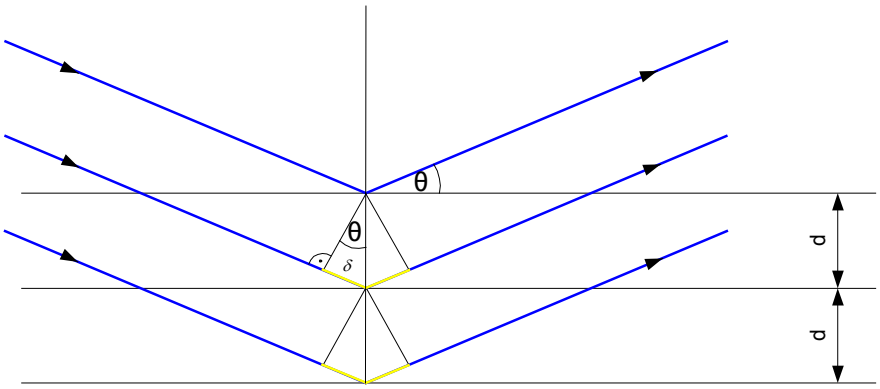

Figure 16. Diffraction of monochromatic x-ray (after: [25]).

With XRD it is possible to analyze crystals in powder form or bulk single crystals. When examining a bulk single crystal, an XRC is typically used. The resulting curve gives information about the crystallinity of the sample. Only one reflection is used which often is the (002) reflection in case of hexagonal crystals like ZnO. As smaller as the FWHM is as better is the crystallinity. That means a sharp peak relates to a high crystallinity. The angle Δω indicates the deflection to the characteristic angle θ of the particular reflection (Figure 17). A very small FWHM means practically perfect crystallinity.

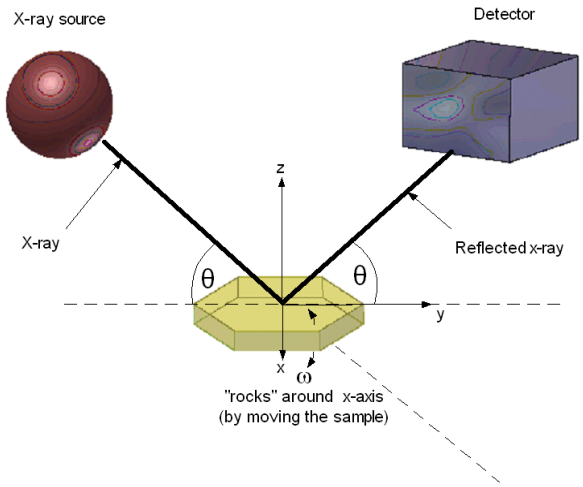

Figure 17. Principle of XRC measurement for bulk crystals (after: [26]).

When examining crystals in form of powder, the measurement gives information about the different phases, crystallinity, and composition of the powder. The different peaks e.g. peak of the (002) reflection, peak of the (102) reflection etc. depend on the 2θ-angle and on the crystallographic structure. Each phase has its own spectrum (e.g ZnO does not have the same 2θ-angle for the (002) reflection peak than GaN, because of different lattice parameters). The detector and the x-ray source move around x-axis (Figure 18). The crystals are ordered randomly. There are always crystals oriented for the desired reflection. The theoretical spectrum of ZnO is shown in Figure 19.

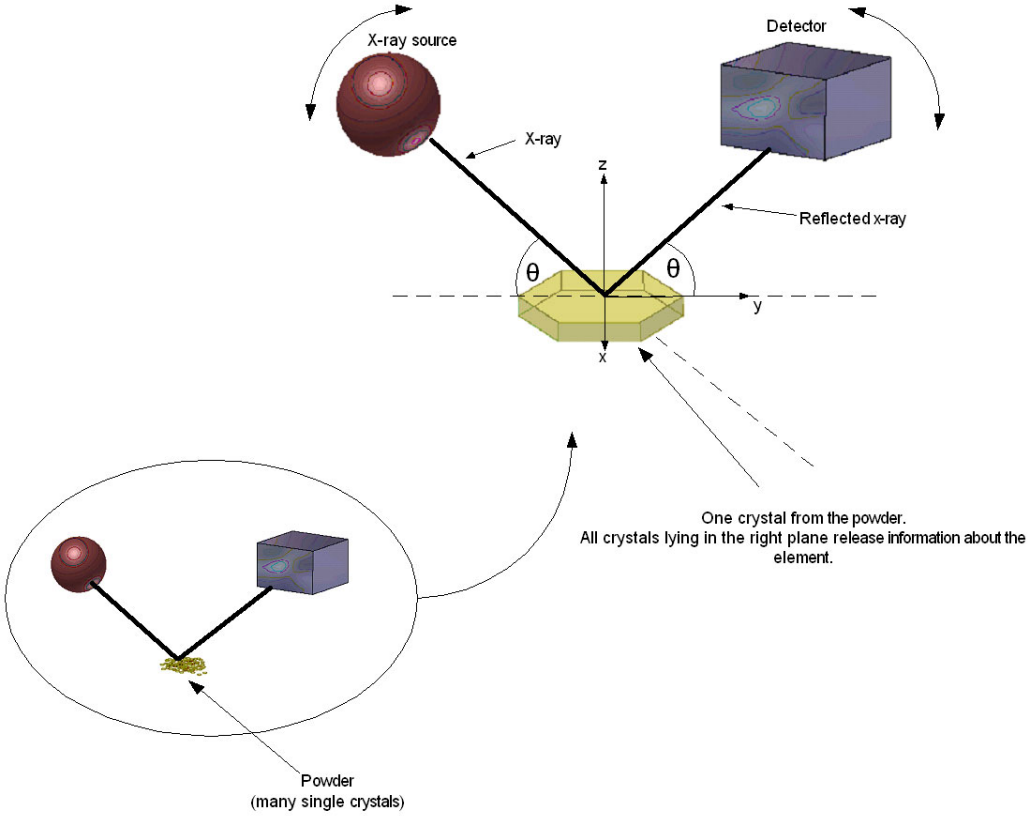

Figure 18. Principle of XRD measurement for powder (after: [26]).

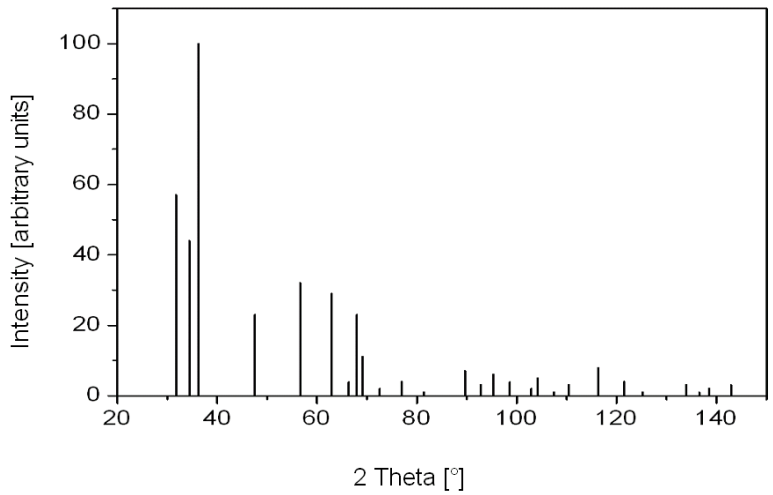

Intensity	2 teta [°]	h k l
57	31.769	1 0 0
44	34.421	0 0 2
100	36.252	1 0 1
23	47.538	1 0 2
32	56.602	1 1 0
29	62.862	1 0 3
4	66.378	2 0 0
23	67.961	1 1 2
11	69.098	2 0 1
2	72.56	0 0 4
4	76.953	2 0 2
1	81.368	1 0 4
7	89.604	2 0 3
3	92.781	2 1 0
6	95.301	2 1 1
4	98.609	1 1 4
2	102.942	2 1 2
5	104.13	1 0 5
1	107.426	2 04
3	110.388	3 0 0
8	116.274	2 1 3
4	121.567	3 0 2
1	125.183	0 0 6
3	133.925	2 0 5
1	136.513	1 0 6
2	138.505	2 1 4
3	142.91	2 2 0

Figure 19. XRD measurement of ZnO powder. The exact values are indicated in the table (after: [27]).

Often both measurements are combined, a part of the bulk crystal is taken and reduced to powder. The bulk crystal can be examined for its crystallinity and the powder gives information about phase purity and composition of the crystal.

3.3.5 Secondary ion mass spectroscopy and inductively coupled plasma mass spectroscopy

Secondary ion mass spectroscopy is a failure analysis technique used in the compositional analysis of a sample. SIMS operates on the principle that bombardment of a material with a beam of ions with high energy (1-30keV) results in the ejection or sputtering of atoms from the material. A small percentage of these ejected atoms leave as either positively or negatively charged ions, which are referred to as secondary ions.

The collection of these sputtered secondary ions and their analysis by mass-to-charge spectrometry gives information on the composition of the sample, with the elements identified through their atomic mass values. Thus, SIMS works by analyzing material removed from the sample by sputtering, and is therefore a locally destructive technique. Figure 20 shows a SIMS measurement from a LPE grown ZnO film doped with Ga.

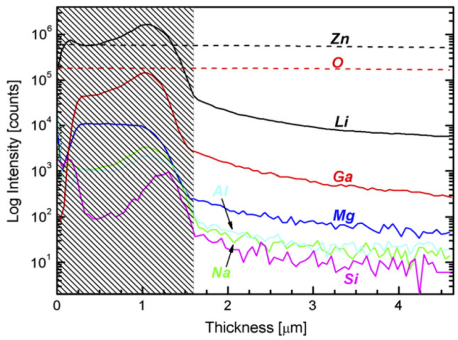

Figure 20. SIMS profile from a Ga-doped, 1.7µm thick homoepitaxial ZnO film. The hatched area comprises the cross-section of the LPE film (taken from: [10]).

Functional principle of a mass spectrometer

In Figure 21 secondary ions are collected and accelerated by a voltage U before entering a magnetic field B (streamlines of the field are perpendicular to the sketch). As moved charges these ions create a current which is forced in a circular path by the magnetic field.
The kinetic energy of the ions when entering the magnetic field is equal to the electrical power (1), on the circle path the force created by the magnetic field has to be the same as the centrifugal force (2).

$$\frac{1}{2}Mv^2 = qU \qquad (1) \qquad\qquad |q| \cdot v \cdot B = M\frac{v^2}{r} \qquad (2)$$

$$E_{kin} = \frac{1}{2}Mv^2$$

$$E_{el} = U \cdot I \cdot t = U \cdot q$$

$$F_{cent} = M\frac{v^2}{r}$$

$$\vec{F}_{Lorentz} = q \cdot \vec{v} \times \vec{B}$$

note: Because the charge moves perpendicular to the magnetic field (sinα=1) , the Lorentz force can be written as:

$$F_{Lorentz} = |q| \cdot v \times B$$

Assumption: ions are single-charged, that means $|q| = 1$.

From (2) it follows that $v = \frac{Br}{M}$ (3)

(3) in (1) is leading to $\frac{1}{2} M \left(\frac{Br}{M} \right)^2 = U$ and $M = \frac{B^2 r^2}{2U}$

Under constant conditions the radius of curvature only depends on the ionic mass. Masses are detected in different areas of the detector (because of different radiuses of curvature). Another possibility is to vary B or U so that the ions are guided to the same point of the detector. From the values of U and B, the mass can be calculated and the element is getting known.

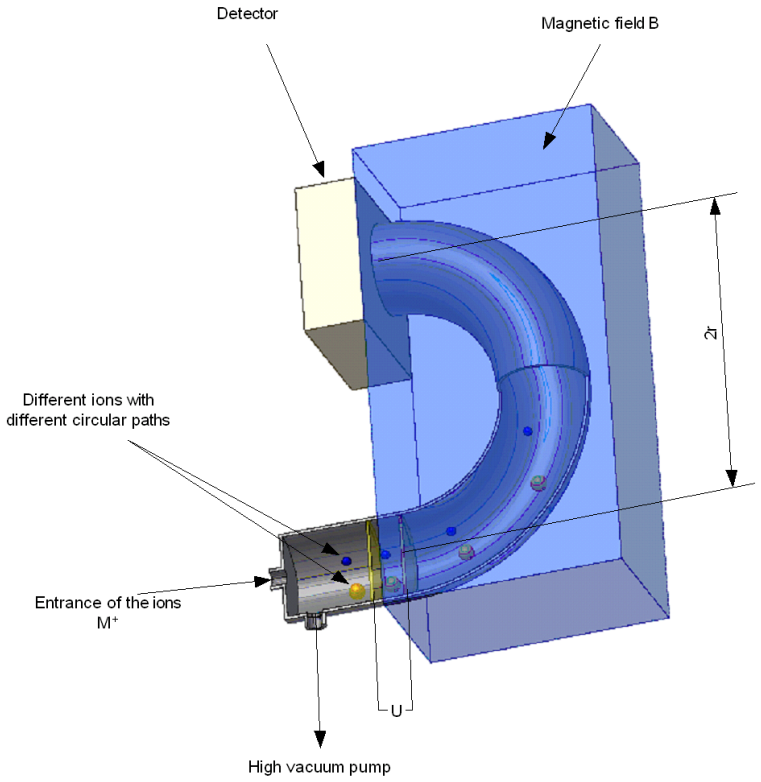

Figure 21. Functional principle of a mass spectrometer (mass analyzer). One part of the tube is cut for better view (after: [28]).

In ICP-MS, a plasma or gas consisting of ions, electrons and neutral particles is formed from Ar gas. The plasma is used to atomize and ionize the elements in a sample. The resulting ions are then passed into the high vacuum mass analyzer (Figure 21). The isotopes of the elements are identified by their mass-to-charge ratio and the intensity of a specific peak in the mass spectrum is proportional to the amount of that isotope (element) in the original sample.

3.3.6 Photoluminescence

By excitation of a semiconductor by photons, electrons are excited from the valence band into the conduction band. Electron-hole pairs are created. After a certain endurance (typically in the order of 10 ns) recombination takes place and energy is emitted e.g. as photons. These photons are detected and the measured radiation allows important insights into the examined sample properties (crystallinity, impurity). PL measurements are often done by low temperatures by cooling the sample with liquid N (77K) or He (4K) to overcome the problem of thermal ionization of the optical centers and to avoid lattice vibrations.

Device

Luminescence for the excitation is created by a laser of λ = 325.5 nm. The energy of the laser has to be higher than E_g of the excited material. The laser traverses a band pass. A mirror guides the laser to a filter where the visible light is cut (although the laser emitts at 325.5 nm, there is visible light due to incoherent lines). The chopper consists of a turning disk with holes, the laser signal is chopped, that means the laser can pass intermittently. For this reason also the sample emitts intermittently. By subtraction of the emitted radiation of the sample and the chopped signal, noise is eliminated. The laser is guided to a second mirror and to a lens which focus the laser on the sample.The emitted light of the sample and the scattered light of the laser are focused by two lenses to the monochromator. There is a filter in front of the monochromator to eliminate the scattered light from the laser. In the monochromator the radiation is spectrally decomposed and the dispersed light is guided to the detector. The optical signal is transformed into a tension signal.

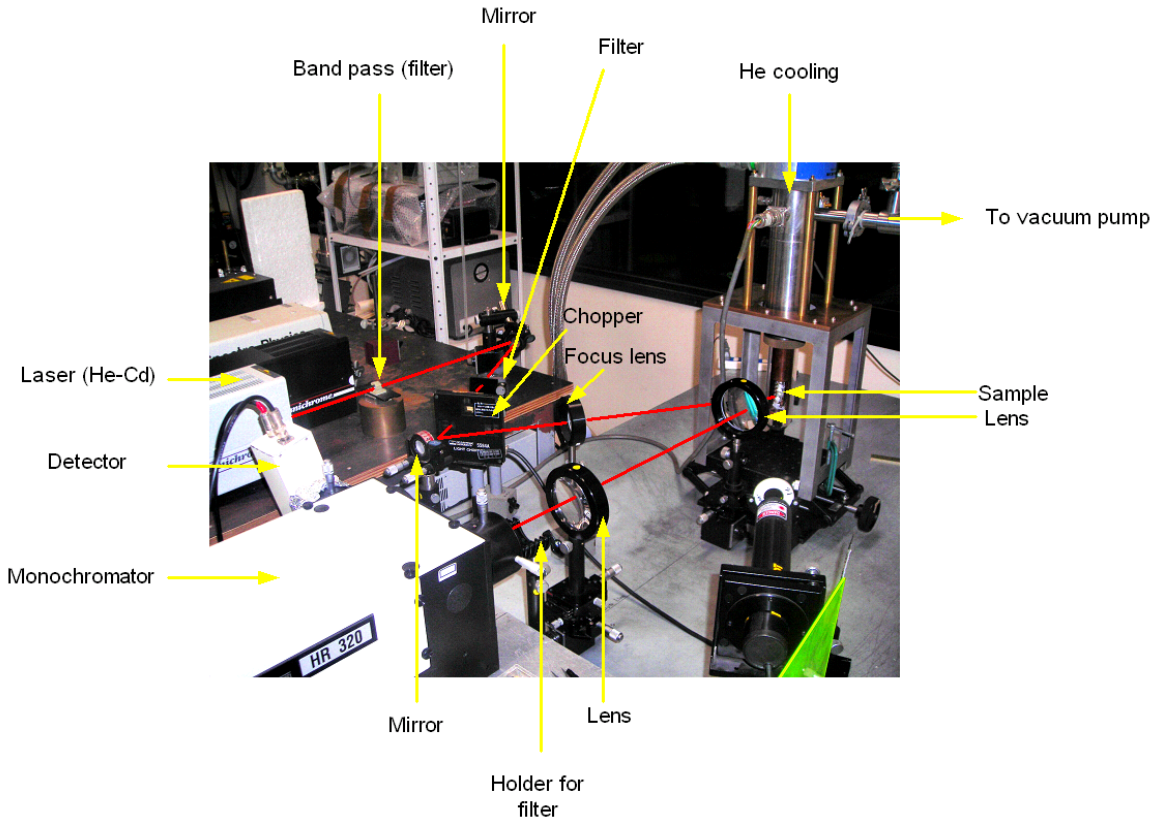

Figure 22. Device for PL measurement. The red line indicates the path of the laser.

4. Results and discussion

Note: Li is present in all experiments due to LiCl as selected solvent and acts as co-dopant.

4.1 Flux growth

4.1.1 Sb-doped ZnO

The target compound was $Sb_{0.02}Zn_{0.98}O$. For experimental conditions see Appendix B.

Visual observation

Reflections of the crystals were observed under light. The powder had a white color with a silver cast.

X-ray diffraction, Scanning electron microscopy, and Energy dispersive x-ray analysis

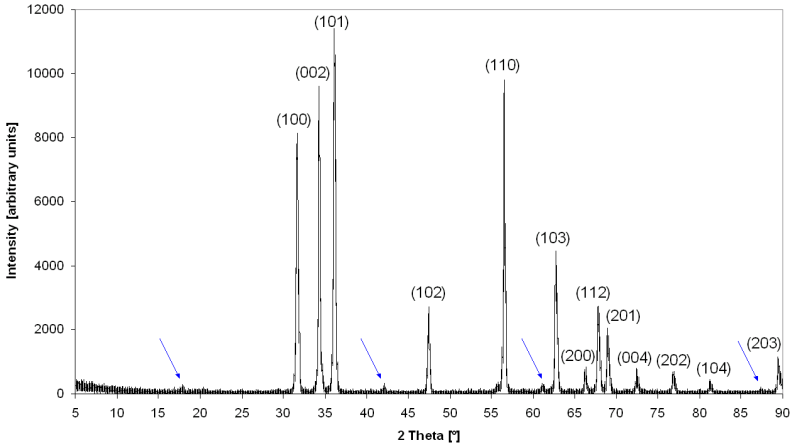

Figure 23. XRD measurement. The blue arrows indicate peaks of other phases than hexagonal ZnO.

The peaks of the hexagonal ZnO structure are indicated by the Miller Bravais indices (Figure 23). The intensities and the position of the 2θ are not exactly the same as for the theoretical ZnO spectrum (compare Figure 19). That is an indication that Sb is incorporated in ZnO, for this reason the lattice parameters vary a little resulting in the observed deviations.
The appearance of other peaks shows that there is at least one other phase. This phase could not have been indicated.

Apparently, homoepitaxial growth on first-grown ZnO crystals was visible in different areas (Figure 24c). A crystal was first formed and a film was grown on this crystal later. It was shown that growing films by this way is possible but the film is of low quality. Island growth and inclusions were observed.
The hexagonal shape of ZnO was confirmed (Figure 24d). The dark spots in the distribution maps (Figure 24b) are in accordance with the larger crystals of the SEM image (Figure 24a). These crystals are mainly composed of ZnO (sometimes few Sb was also found), they reached sizes until 0.5 mm. The presence of Sb was measured

by EDX. Sb was quite homogeneously distributed (green spots in the map of Sb). In several areas shapes with an increased concentration of Sb were found (white spots in the map of Sb). A new phase formed consisting of Sb in combination with Zn, O, and probably K (Figure 24e). That is in agreement with the obtained results by XRD. The formation of a new phase can be explained in the differences of the atomic radii [29] (see also section 4.3.3).

Following phases were found in the literature:

- ZnSb: soluble in water, T_m = 565°C, orthorhombic crystals [30].
- ZnSbO: cubic crystals [31].

The observed phase is not soluble in water for this reason it can not be ZnSb. ZnSbO could be a possibility which forms the spinel crystal structure (cubic system). For an exact statement further examinations of the phase would be necessary.

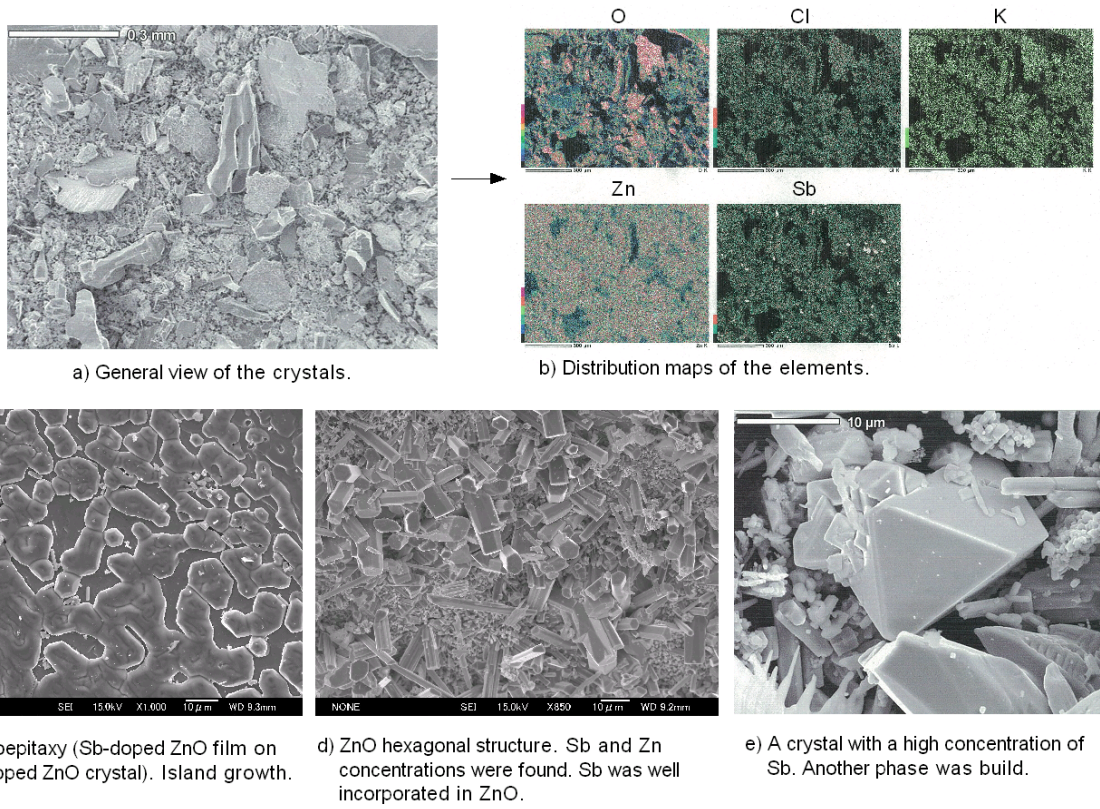

a) General view of the crystals.

b) Distribution maps of the elements.

c) Homoepitaxy (Sb-doped ZnO film on Sb-doped ZnO crystal). Island growth.

d) ZnO hexagonal structure. Sb and Zn concentrations were found. Sb was well incorporated in ZnO.

e) A crystal with a high concentration of Sb. Another phase was build.

Figure 24. SEM-EDX of Sb-doped ZnO crystals. Li is too light for detection by EDX.

4.1.2 Bi-doped ZnO

The target compound was $Bi_{0.02}Zn_{0.98}O$. For experimental conditions see Appendix B.

Visual observation

Reflections of the crystals were observed under light. The powder had a yellowish color.

X-ray diffraction, Scanning electron microscopy, and Energy dispersive x-ray analysis

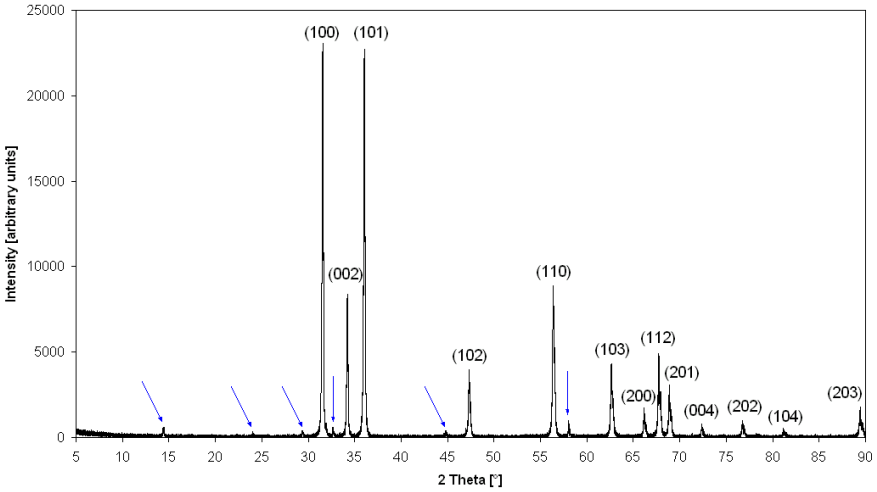

Figure 25. XRD measurement. The blue arrows indicate peaks of other phases than hexagonal ZnO.

The intensities and the position of the 2θ are close to the theoretical ZnO spectrum. Bi is not well incorporated in ZnO and formed its own phase. The lattice of ZnO was almost not influenced by Bi. This may point to the fact that the concentration of Bi in ZnO is low.
The appearance of other peaks is an indication that there is at least one other phase.

Several crystals reached sizes until 0.5mm (Figure 26a). EDX measurement showed that Bi was not homogeneously distributed (Figure 26b). It formed its own phase (Figure 26c). Many cubes with a high concentration of Bi and Cl in combination with Zn and O were found (Figure 26d, compare with e). The cubes are not soluble in water. The formation of a new phase can be explained in the differences of the atomic radii [29] (see also section 4.3.3).

Following phases were found in the literature [30]:

- BiOCl: not soluble in water, T_m = 575°C, tetragonal crystals.
- $BiCl_3$: soluble in water, T_m = 234°C, cubic crystals.

BiOCl is not soluble in water. The phase could been build when the temperature was decreased (at 640°C BiOCl is not stable). However, the new phase can not be BiOCl because Zn is missing. $BiCl_3$ is formed as cubic crystals but T_m is too low, these cubes are soluble in water, Zn and O are missing. A phase with Bi, Zn, O, and Cl could not be found in the available literature.

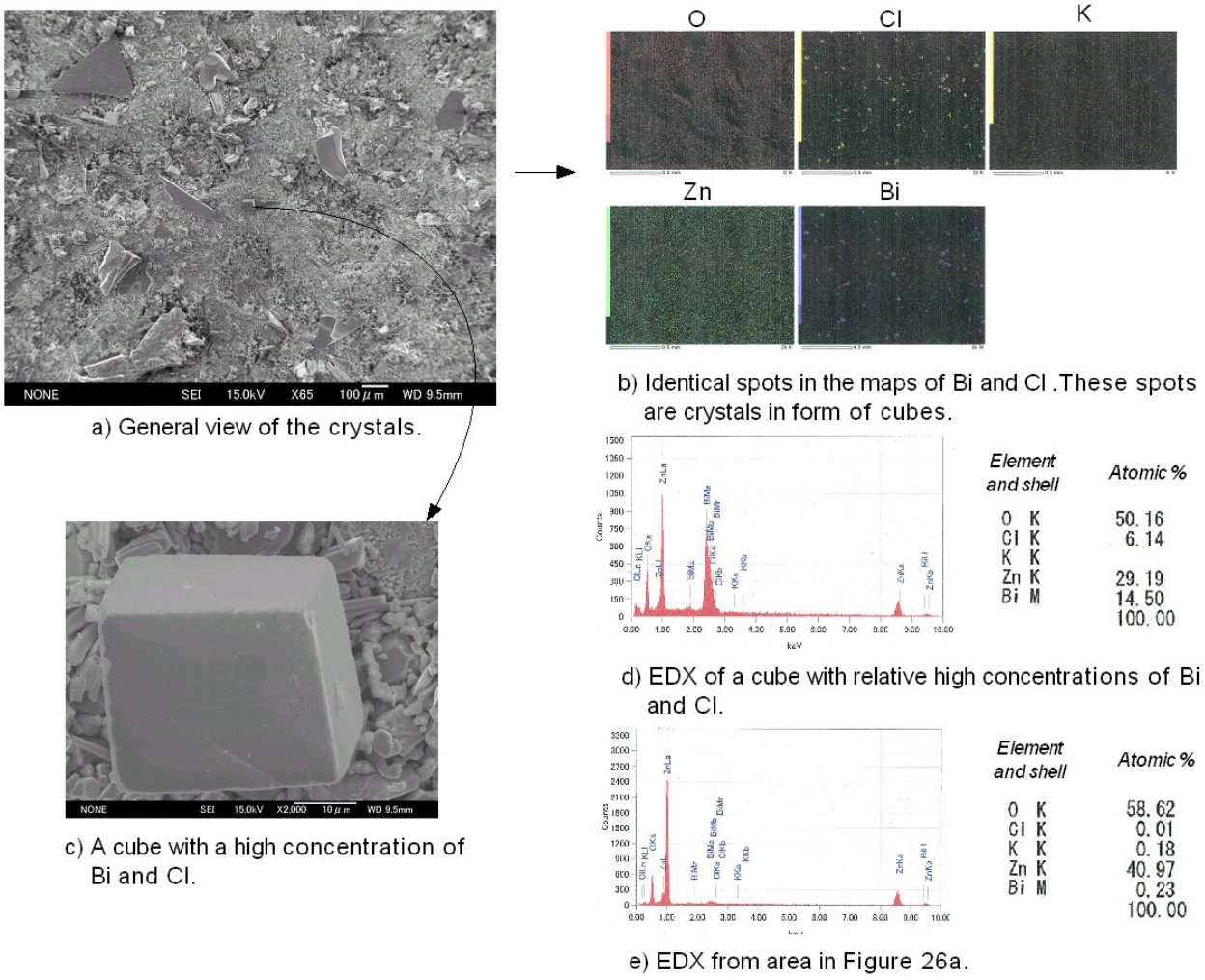

Figure 26. SEM-EDX of Bi-doped ZnO crystals.

4.1.3 In-doped ZnO

A. $In_{0.001}Zn_{0.999}O$. For experimental conditions see Appendix B.

Visual observation

Reflections of the crystals were observed under light (Figure 27). The powder had a white color.

Figure 27. Reflection of $In_{0.001}Zn_{0.999}O$ crystals under light.

X-ray diffraction, Scanning electron microscopy, and Energy dispersive x-ray analysis

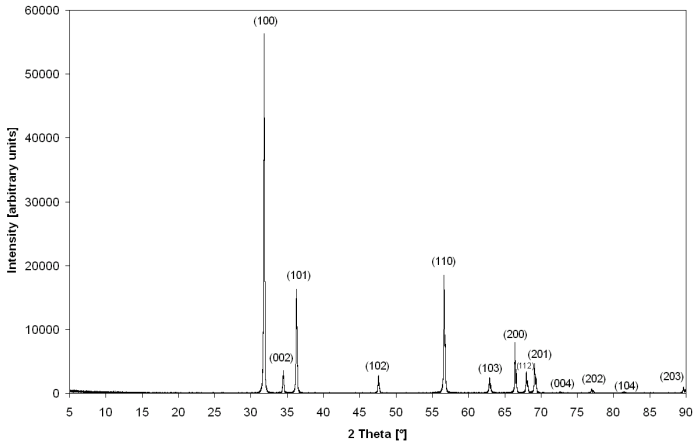

Figure 28. XRD measurement. No other peaks than hexagonal ZnO are visible.

The XRD intensities are different compared to undoped ZnO. No other peaks than hexagonal ZnO were found. In was well incorporated in the hexagonal ZnO structure.

Several crystals reached sizes up to 0.2mm (Figure 29a). The larger crystals in Figure 29a are mainly composed of ZnO but sometimes In was incorporated too. The dark spots in the distribution maps represent these larger crystals (Figure 29b). The hexagonal structure of ZnO was confirmed (Figure 29c,d). In Figure 29d, 12 instead of typically 6 prism facets are visible. It is assumed that the growth in a-direction is reduced, thus, forming a facet. In is quite homogeneously distributed all over the powder, areas of increased In concentration were not found.

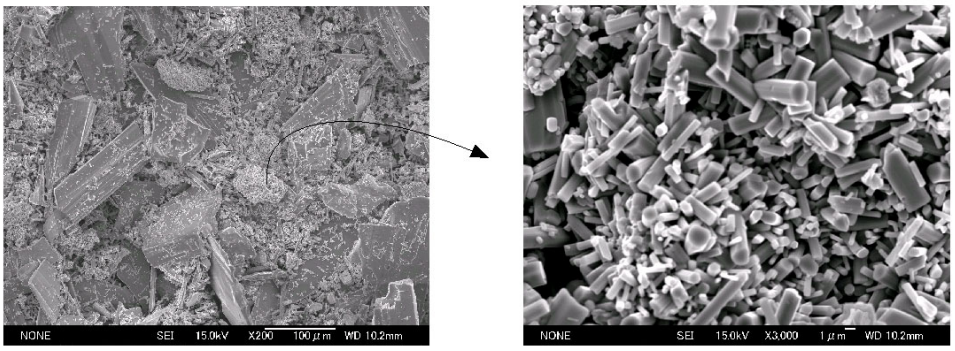

a) General view of the crystals.

c) Hexagonal ZnO.

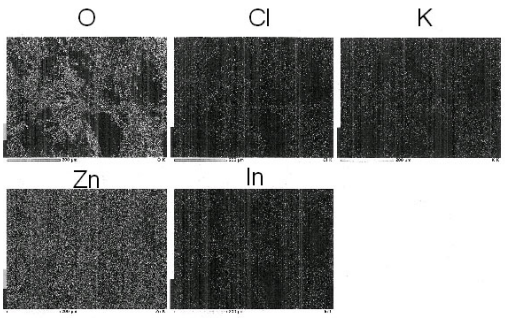

b) Distribution maps of the elements. No spots of high concentrations are observed.

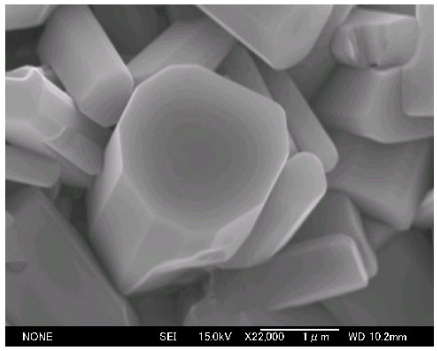

d) In-doped crystals. 12 instead of typically 6 prism facets were found.

Figure 29. SEM-EDX of 0.1mol% In-doped ZnO crystals.

B. $In_{0.02}Zn_{0.98}O$. For experimental conditions see Appendix B.

Visual observation

Reflections were not observed under light. The powder had a white color.

X-ray diffraction, Scanning electron microscopy, and Energy dispersive x-ray analysis

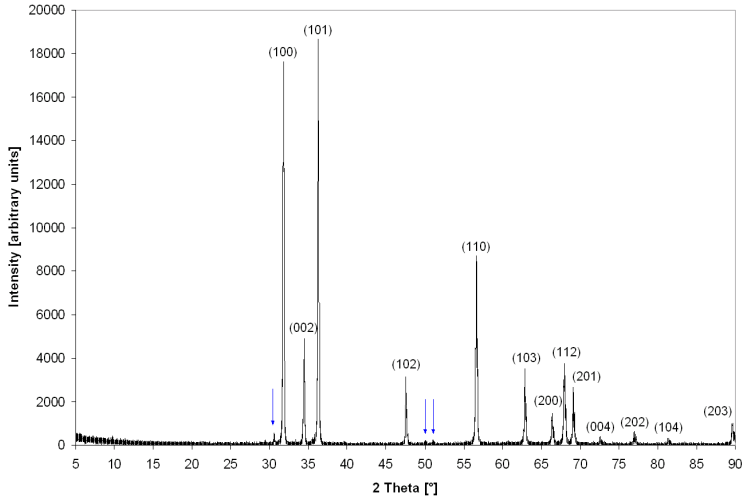

Figure 30. XRD measurement. The blue arrows indicate peaks of other phases than hexagonal ZnO.

The XRD intensities are not the same as for undoped ZnO. There is at least one other phase. In general the intensities of the reflections are much lower than for 0.1mol% In-doped ZnO.

SEM showed hexagonal crystals. The crystal size did not vary strongly (Figure 31a). Crystal sizes until 0.1 mm were observed. Mainly long crystals (needles) were formed. The dark spots in the distribution maps are areas were no powder laid (Figure 31b). Crystals with Zn, In, and O were also observed. In was incorporated but in several areas a new phase was formed consisting of In, Zn, and O (white spots in the distribution map of In). These spots have two appearances: large cubes and an arrangement of many small cubes (Figure 31c,d).
No phases of Zn in combination with In were found in the available literature.

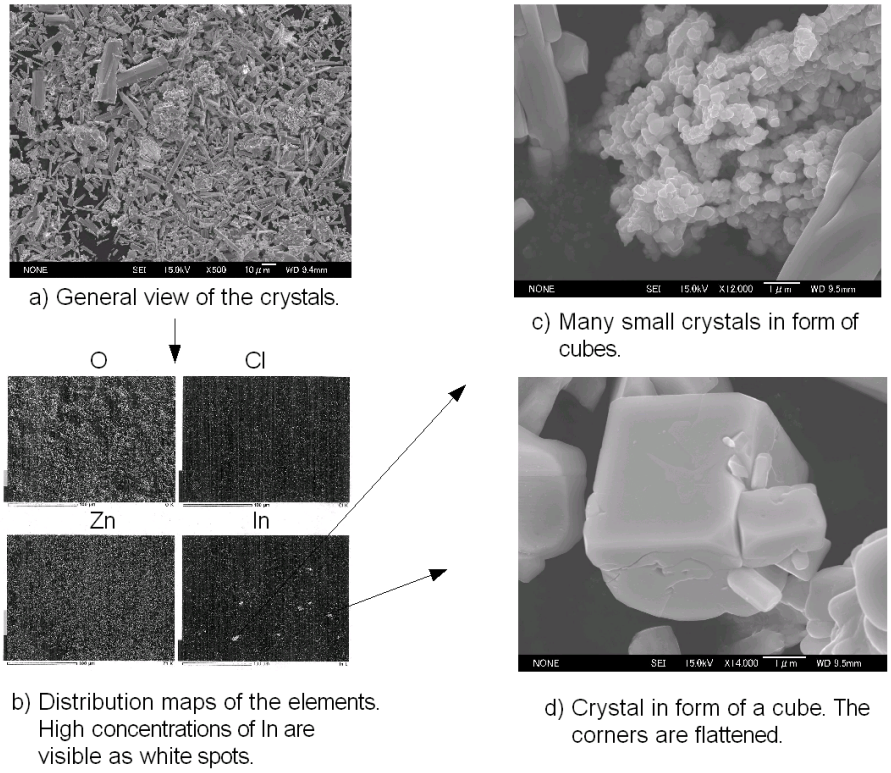

Figure 31. SEM-EDX of 2mol% In-doped ZnO crystals.

4.1.4 Mo-doped ZnO

A. $Mo_{0.001}Zn_{0.999}O$. For experimental conditions see Appendix B.

Visual observation

A reflection of the crystals was observed under light. The powder had a white color.

X-ray diffraction, Scanning electron microscopy, and Energy dispersive x-ray analysis

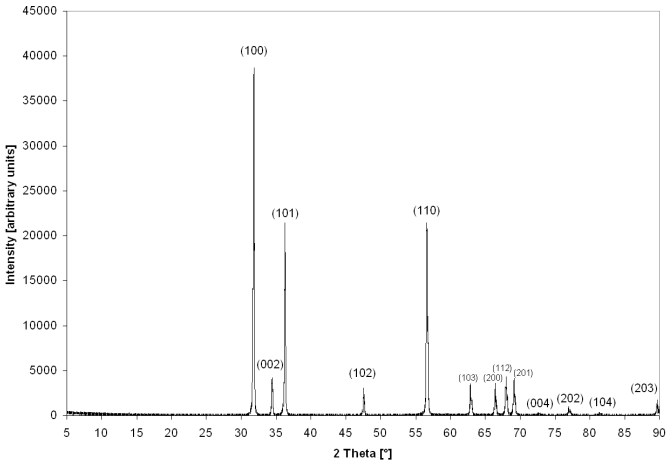

Figure 32. XRD measurement. No other peaks than hexagonal ZnO are visible.

No other than ZnO phases were found by XRD. The intensity of the XRD pattern is quite different to the undoped ZnO hexagonal structure. That means Mo is incorporated and the lattice parameters are modified.

Similar to $In_{0.02}Zn_{0.98}O$, many long crystals (needles) were observed (Figure 33a). Bigger crystals reached sizes until 0.1mm. EDX showed that the needles consist of Mo, Zn, and O. Mo was incorporated in ZnO. The crystal shape was modified by Mo. More than typically 6 prism facets are visible in Figure 33c (compare $In_{0.001}Zn_{0.999}O$). The distribution maps are quite homogeneous (Figure33 b).

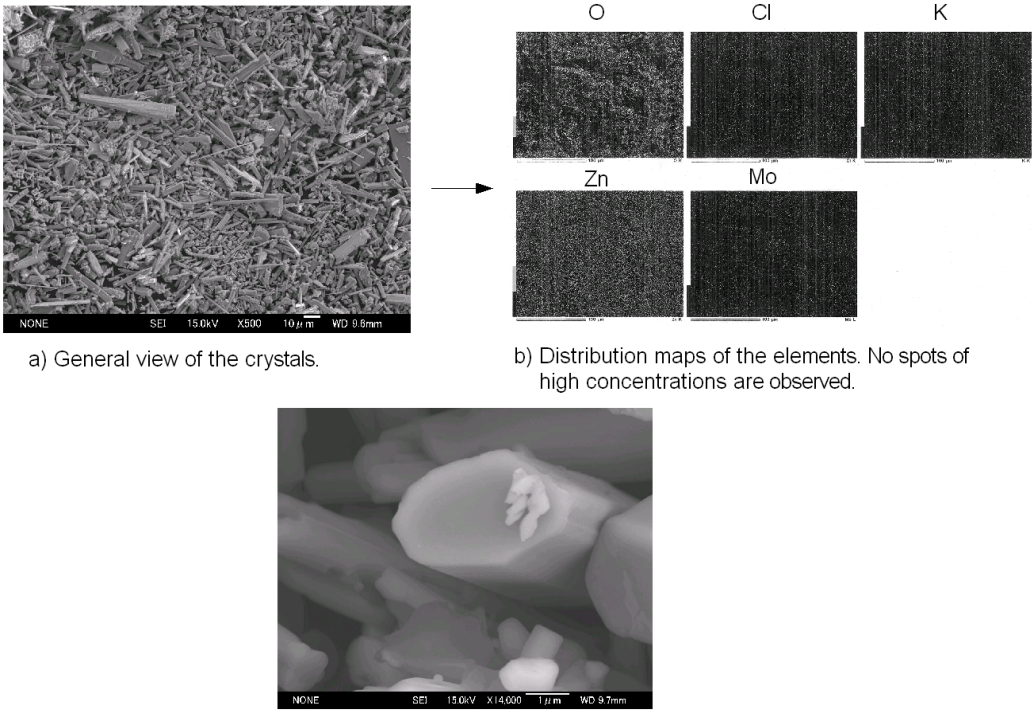

a) General view of the crystals.

b) Distribution maps of the elements. No spots of high concentrations are observed.

c) ZnO crystals with Mo content. More than 6 facets are visible (compare Figure 29 d).

Figure 33. SEM-EDX of 0.1mol% Mo-doped ZnO crystals.

B. $Mo_{0.02}Zn_{0.98}O$. For experimental conditions see Appendix B.

Visual observation

A weak reflection of the crystals was observed under light. The powder had a white color.

X-ray diffraction, Scanning electron microscopy, and Energy dispersive x-ray analysis

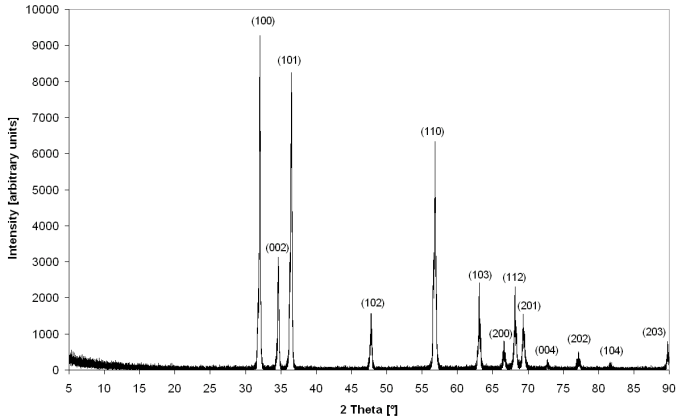

Figure 34. XRD measurement. No other peaks than hexagonal ZnO are visible.

No other than ZnO phases were found by XRD. In general the intensities of the peaks are much lower compared to 0.1 mol% Mo-doped ZnO.

The crystals reached sizes up to 0.2 mm. Mo was well incorporated in ZnO. The distribution maps are very homogeneous except the map for O (Figure 35b). Often groups of crystals were observed with Mo content (Figure 35c). A crystal with more than typically 6 prism facets is shown in Figure 35d (compare $In_{0.001}Zn_{0.999}O$ and $Mo_{0.001}Zn_{0.999}O$).

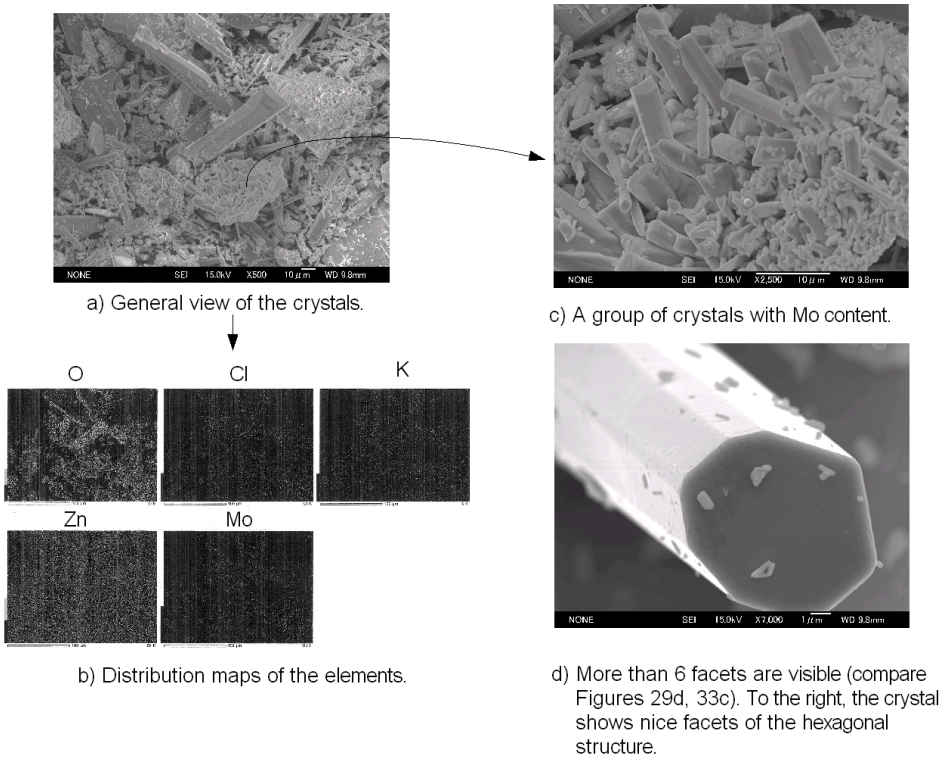

Figure 35. SEM-EDX of 2mol% Mo-doped ZnO crystals.

C. $Mo_{0.05}Zn_{0.95}O$. For experimental conditions see Appendix B.

Visual observation

A reflection of the crystals was observed under light. The powder had a white color.

X-ray diffraction, Scanning electron microscopy, and Energy dispersive x-ray analysis

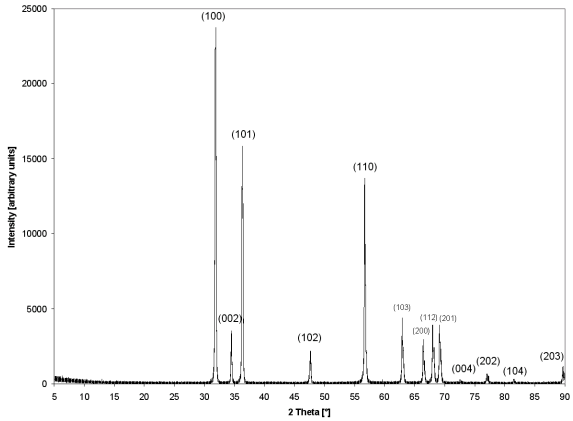

Figure 36. XRD measurement. No other peaks than hexagonal ZnO are visible.

No other than ZnO phases were found by XRD. The intensities of the peaks are higher compared to 2 mol% Mo-doped ZnO and lower compared to 0.1 mol% Mo-doped ZnO.

The crystals reached sizes up to 0.1 mm. The results are similar to 2mol% Mo-doped ZnO. There are also crystals arranged in groups with Mo content but the crystals are not as well shaped as for $Mo_{0.02}Zn_{0.98}O$ (Figure 37c).

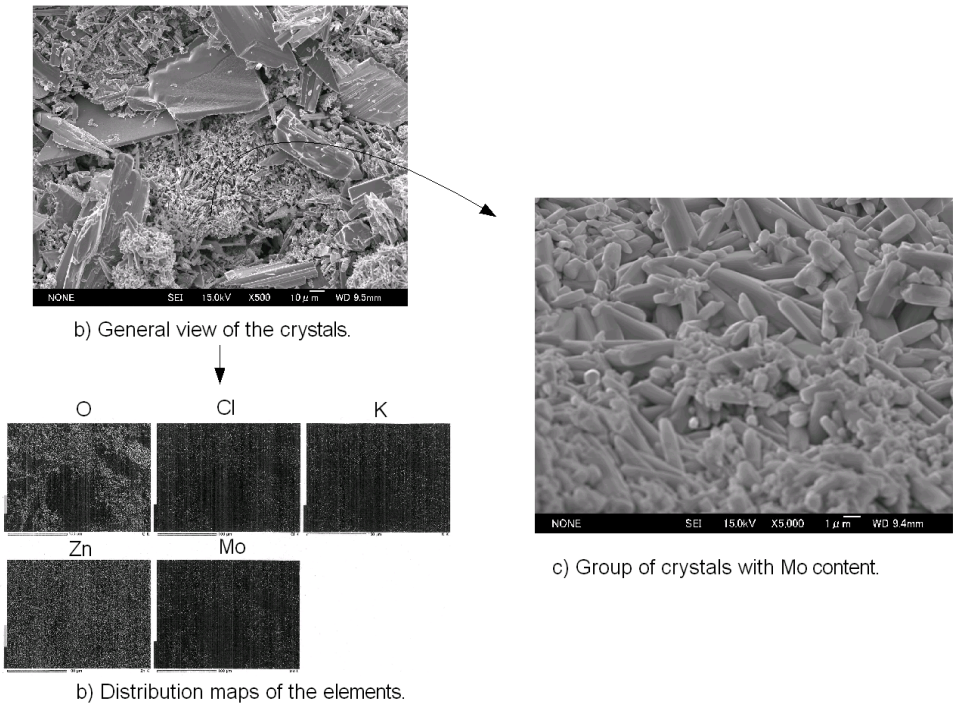

Figure 37. SEM-EDX of 5mol% Mo-doped ZnO crystals.

4.1.5 Photoluminescence

At RT and also at T_L doped ZnO emits a yellowish light. This light is a mixture of the different emission wavelengths (the laser had an energy of 3.8 eV, equivalent to λ = 325 nm, all below this energy is excited). The mixture of deep emission and blue/UV emission (NBE) results the yellowish color. The optimum case would be an emission of one wavelength with a high intensity for easy detection and high resolution. The deep emission is caused by defects like Zn vacancies, O vacancies, Li, etc. [32]. By different dopants the intensity and the color varies a little. Sb-doped ZnO showed a very high light intensity (Figure 38). The deep emission does not strikingly differ for the samples. For this reason the discussion is mainly focused on NBE.

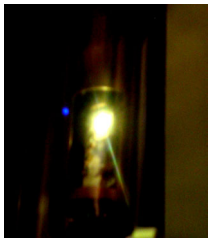

Figure 38. PL of Sb-doped ZnO showed a high light intensity. The blue spot is caused by the laser.

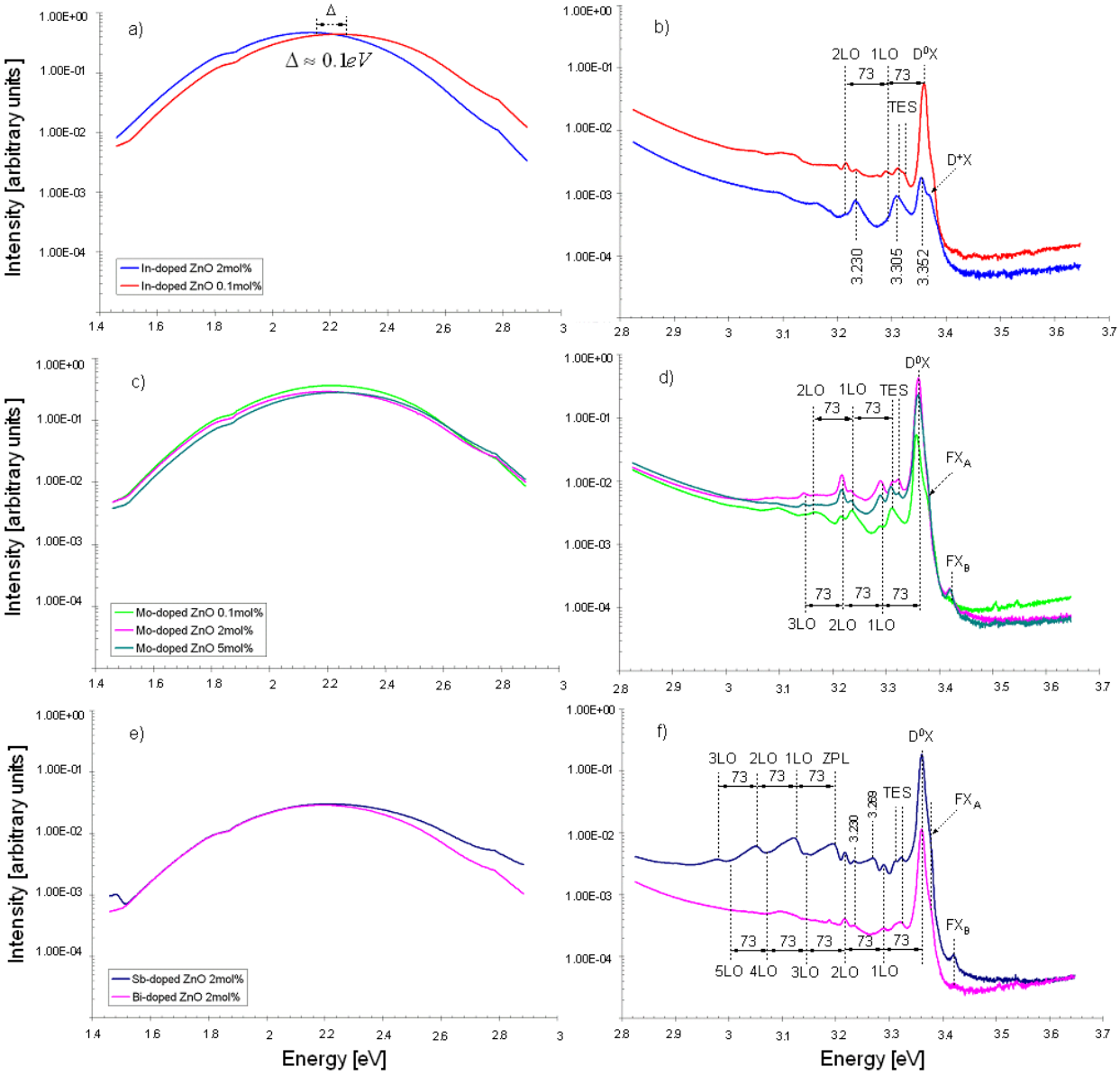

Figure 39. PL measurement, deep emission (left) and NBE (right).

In-doped ZnO (Figure 39 a,b):

The shoulder at 3.38 eV corresponds to the FX_A peak. 2mol% In results the D^+X peak at 3.366 eV. D^0X emission around 3.357 eV is clearly visible for 0.1mol% In-doped ZnO. This peak shows a high intensity but it is lower than the deep emission. The first two LOs were identified. Both TES peaks at 3.32 eV and 3.31 eV were found. The sample with 2mol% doping shows peaks at 3.352 eV, 3.305 eV, and 3.230 eV which could not be identified so far. The peak at 3.230 eV is also visible in the curve for 0.1mol% In doping (compare also Sb- and Bi-doped ZnO). The deep emission shows a shift of the main peak of about 0.1 eV.
To summarize, 2mol% In-doped ZnO results in low quality crystals. Little amounts of In can be incorporated in ZnO but higher concentrations lead to degradation of the crystal quality. In has an effective ionic radius of 0.62 Å compared to Zn with 0.60 Å, but shows sixfold coordination [12]. For this reason the incorporation of In in ZnO is limited.

Mo-doped ZnO (Figure 39 c,d):

All three curves are very similar. A strong FX_B peak at 3.42 eV is visible for 2mol% and 5mol% Mo-doped ZnO. That is a sign of high quality (high crystallinity, few trapping impurities). The curve of 0.1mol% Mo-doped ZnO does not show this peak. The FX_A shoulder at 3.38 eV can be seen for all three curves. The typical D^0X emission around 3.357eV is visible in all three cases but the intensity of 0.1mol% Mo-doped ZnO is lower. The D^0X of 2mol% Mo and 5mol% Mo curves is higher than the deep emission, whereas for 0.1mol% Mo the D^0X is lower. D^0X shows high intensities compared to the LOs. The LOs of the D^0X appear each 73 meV. The behavior of the peak intensities changes with different doping concentrations. The 1LO peak of the D^0X increase from 0.1mol% Mo to 2mol% Mo and for 5mol% Mo the peak is between the two intensities of 0.1mol% Mo and 5mol% Mo. The same behavior can be observed for 2LO and 3LO. For 0.1mol% Mo only one TES peak appeared whereas for the other two curves both peaks are visible. 0.1mol% Mo shows the highest 1LO peak of TES, this peak is lower for 2mol% Mo and for 5mol% Mo it increase again. 2LO shows the same behavior.
It can be concluded that Mo is quite easy to incorporate in ZnO (also higher amounts). Mo has an effective ionic radius of 0.41 Å (fourfold coordination) [7]. Zn can be replaced by Mo. Mo can enhance the photocatalytic effect of ZnO but it is not yet clear how Mo together with Li does (Li is always in the system).

Sb-doped ZnO (Figure 39 e,f):

A strong FX_B peak at 3.42 eV was found. FX_A peaks around 3.38 eV as a little shoulder. The typical D^0X emission around 3.357 eV is visible. D^0X shows a high intensity compared to the LOs. The D^0X peak is higher than the deep emission. The LOs peak all 73 meV (almost unvisible hillocks between the other LOs of the set ZPL). The two TES peaks are visible at 3.32 eV and 3.31 eV. The ZPL was set at 3.19 eV and LOs appear each 73 meV. These LOs could be the result of a DAP emission [12,33]. The peak at 3.269 eV can not belong to the LOs because the distance from the set ZPL to 3.269 eV is more than 73 meV. In contrast to the assumption that Sb may act as acceptor [10,33] it is suspected that Sb is the donor whereas Li is the acceptor (thus DAP emission possible). Sb-doped ZnO is interesting for superfast scintillators because of possible DAP recombination in the blue spectrum. Sb could act similar to In [6] (see also section 4.3.3). The peaks at 3.230 eV and 3.269 eV were not identified so far.
This is a quite new model thus the identification of the peaks is very difficult and would need much more examinations.

Bi-doped ZnO (Figure 39 e,f):

The presence of FX_B at 3.42 eV is visible as a low peak. The little shoulder at 3.38 eV corresponds to the FX_A peak. D^0X emission around 3.357 eV is clearly visible. D^0X shows a high intensity compared to the LOs but it is lower than the deep emission. The first two LOs were identified, higher order LOs are difficult to find. One TES peak is visible at 3.32 eV.
The PL measurement corresponds to the obtained results from SEM, EDX, and XRD. Bi is difficult to incorporate in ZnO, thus much noise is found in PL (see also section 4.3.3).

4.2 Hydrothermal crystals

The quality of the microcrystals grown by the flux method is compared to crystals grown by hydrothermal growth. T_G is much lower in hydrothermal growth (around 250°C compared to 640°C). Hydrothermal grown crystals with different Mo concentrations are shown in Figure 40. For comparison there is an image of crystals grown by flux method (Figure 40a, see also 4.1.4).

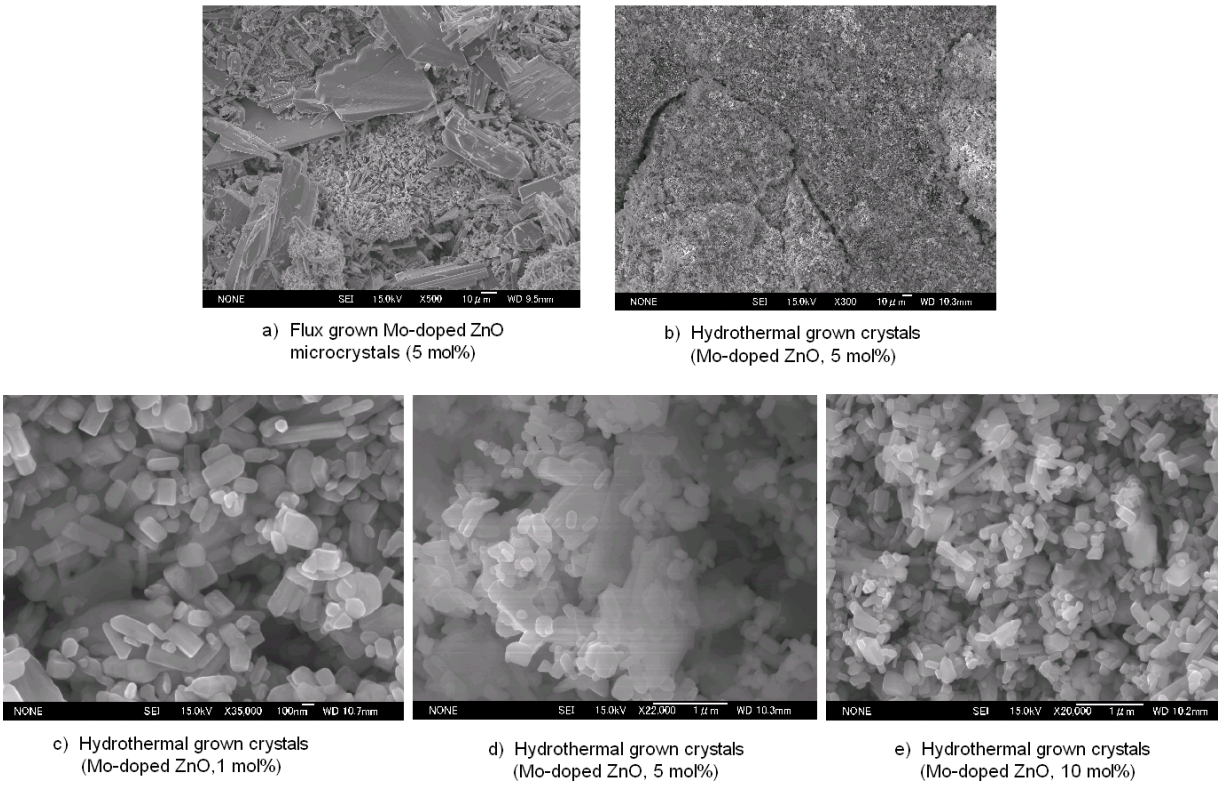

Figure 40. Hydrothermal grown crystals, a) is a picture of crystals grown by flux method for comparison.

An advantage of the hydrothermal method is that there is no Li in the growth medium. However, it seems that the crystals are of lower quality. No large size crystals were observed, the crystal size is around 10-100 nm. Crystals produced by flux growth have sizes of several micrometers and well-developed hexagonal structures. Sometimes, by influence of the dopant, more facets are visible.
The crystal size of hydrothermal grown crystals is quite constant with different dopant concentrations. Here we note that 5 mol% Mo-doped ZnO did not result in well shaped crystals which was also observed for the flux growth.
After comparison by SEM it can be said that crystals grown by the flux method are of higher quality than hydrothermal grown crystals.

Photoluminescence

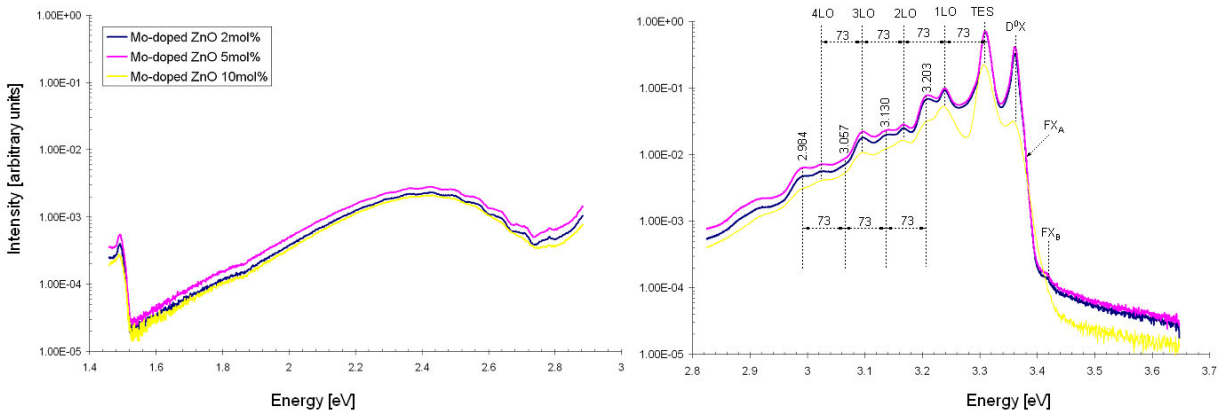

Figure 41. PL measurement, deep emission (left) and NBE (right) of hydrothermally grown Mo-doped ZnO crystals.

Compared to flux grown crystals the intensity of the deep emission is lower. The reason is possibly the absence of Li in the hydrothermal solution.
FX_B at 3.42 eV is visible for 2mol% and 5mol% Mo-doped ZnO. The curve of 10mol% Mo-doped ZnO does not show this peak. The shoulder at 3.38 eV (almost not visible) corresponds to the FX_A peak. D^0X emission around 3.36 eV is visible for all three curves but for 10mol% Mo this peak is of low intensity. The D^0X peaks show low intensities compared to TES. All three curves show only one TES peak at 3.31 eV which is higher than D^0X. The four LOs peak all 73 meV. Also, other LOs were observed which are of an unidentified origin. PL showed that the crystals are of higher quality than assumed (after SEM measurement).

4.3 Liquid phase epitaxy

4.3.1 Sb-doped ZnO film

The target compound was a $Sb_{0.02}Zn_{0.98}O$ film. For experimental conditions see Appendix C.

Visual observation

A semitransparent, milky film was visible on the Zn- and O-face. The reason of this whitish color is the roughness of the grown film. The film seemed to be quite irregular. Many spots were visible.
A film thickness of 1.57 µm on the Zn-face and an average growth speed of 0.105 µm/h was determined. On the O-face the thickness was 0.52 µm and the average growth speed was 0.035 µm/h (Appendix C, see also section 3.2.2 difference between Zn-polar face and O-polar face).

X-ray rocking curve

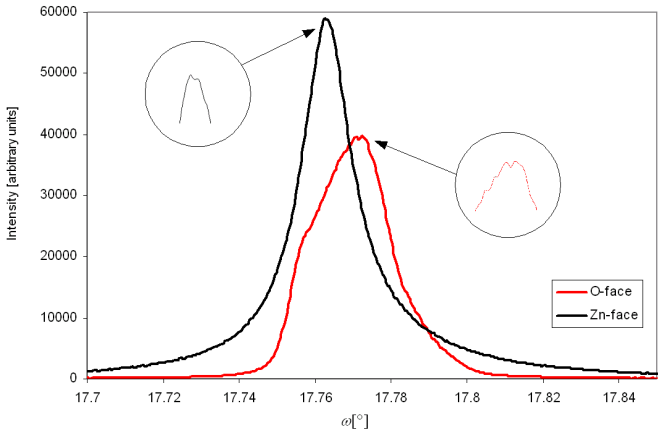

Figure 42. XRC (002) reflection of a Sb-doped ZnO film grown by LPE .

The intensity on the Zn-face is much higher than the intensity measured on the O-face. A FWHM of 60 arcsec and 92 arcsec was determined for Zn-face and O-face respectively. The substrate itself has a FWHM of about 30 arcsec [33]. The x-ray enters in the substrate, thus the measurements give information about the film and the substrate. The two XRC peaks are shifted of about 30 arcsec. The crystallinity on the Zn-face is much better than on the O-face. XRC of the O-polar face is not symmetrical. It is confirmed that impurities are preferred incorporated on the O-face. Both curves show two peaks (insets) which could be the influence of different Sb concentrations and formation of slightly different new phases (see section 4.1.1).

Differential interference contrast microscopy

The varying colors in Figure 43 show the difference in height on the surface. Island growth was observed on the O-polar face (Figure 43 a,b) and on the Zn-polar face (Figure 43 c,d). Steps were not found. The Zn-face seems to be of higher quality than the O-face. The O-face shows more hillocks. The low quality on the Zn-face is possibly affected by the loss of solution due to the formation of a crack in the crucible during the experiment run.

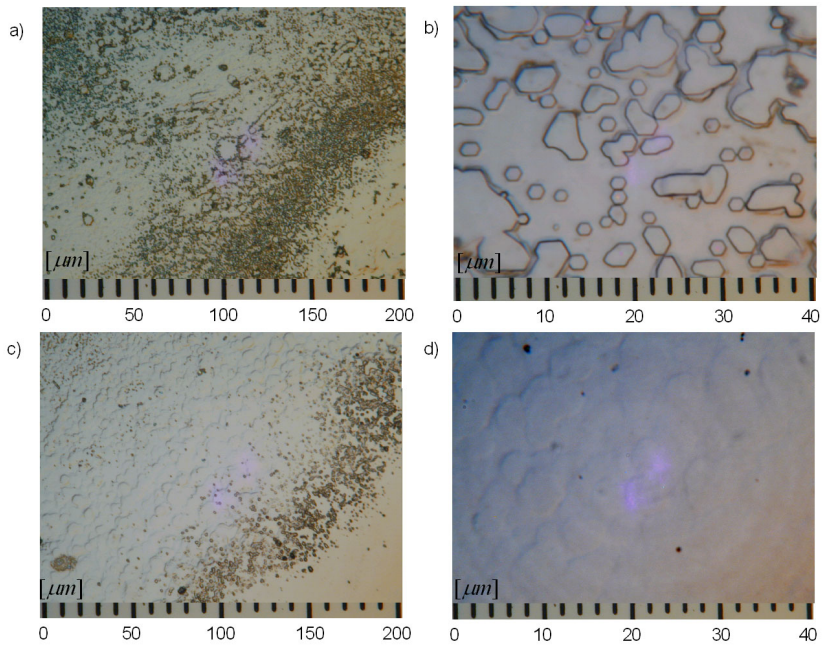

Figure 43. DIC of Sb-doped ZnO films on the O-polar face (a, b) and Zn-polar face (c, d) grown by LPE. All four images are contrast enhanced.

Scanning electron microscopy

The SEM image in Figure 44 shows the O-polar face of Sb-doped ZnO. Hillocks are visible (three dimensional growth). The interface between film and substrate is not visible. It is therefore difficult to investigate the film and its interface with the substrate. However, Figure 44 shows the surface roughness and the relatively low quality on the O-polar face.

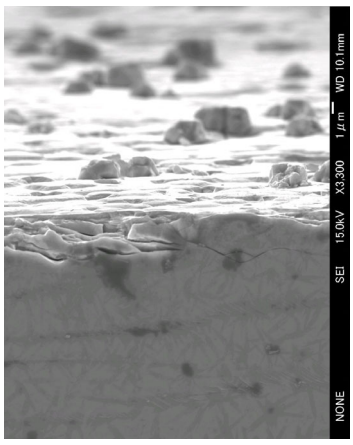

Figure 44. SEM of the Sb-doped ZnO film. O-polar face with hillocks.

Examination of microcrystals from deposit of LPE growth experiment

Although the crucible had a crack some crystals from the deposit could have been preserved and examined by SEM-EDX. The results mostly agree with the observations from the flux experiment (see section 4.1.1). In general, the crystals are smaller than flux grown crystals. The reason is likely the difference of the growth time ($t_{Growth\ LPE}$ = 15h compared to $t_{Growth\ Flux}$ = 48h).

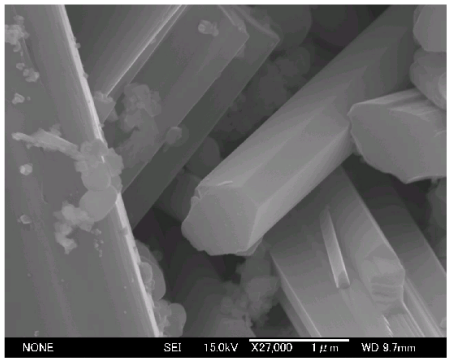

a) ZnO hexagonal structure. Sb and Zn concentrations were found by EDX. Sb was well incorporated in ZnO.

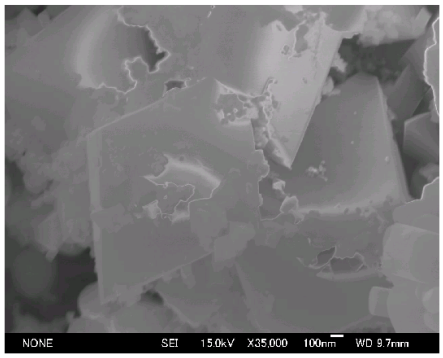

b) The new phase which was observed in the flux experiment too.

Figure 45. Left: hexagonal ZnO structure, right: the new phase with a high concentration of Sb.

4.3.2 Bi-doped ZnO film

The target compound was a $Bi_{0.02}Zn_{0.98}O$ film. For experimental conditions see Appendix C.

Visual observation

The grown film looked very regular. The reflection was much higher than for Sb-doped ZnO, and appeared as mirror-like film (Figure 46).

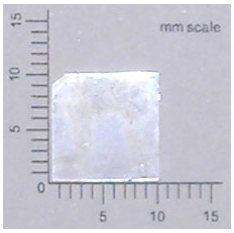

Figure 46. Bi-doped ZnO (Zn-polar face) grew as mirror-like film.

A film thickness on the Zn-face of 2.68 µm and an average growth speed of 0.179 µm/h was determined. On the O-face the thickness was of 0.89 µm and the average growth speed was 0.059 µm/h (Appendix C, see also section 3.2.2 difference between Zn-polar face and O-polar face).

X-ray rocking curve

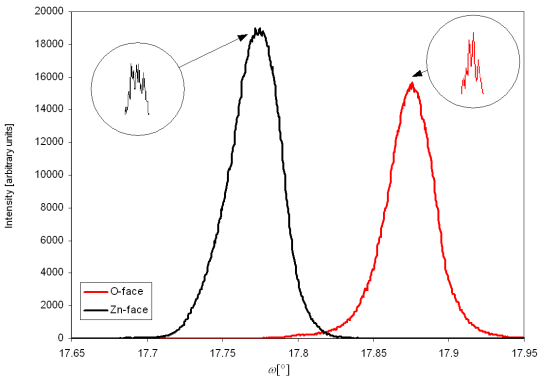

Figure 47. XRC (002) reflection of the Bi-doped ZnO film grown by LPE .

The intensity from the Zn-face is higher than the intensity measured from the O-face. A FWHM of 140 arcsec and 124 arcsec was determined for Zn-face and O-face respectively. Thus the FWHM is lower on the O-polar face. The two XRC peaks are shifted by about 368 arcsec. Both curves show several peaks. The reason for multiple peaks and shift could be the co-existence of $Bi_xZn_{1-x}O$ with different x values. In agreement to the flux experiment it is confirmed that Bi is not well incorporated in ZnO. The reason for this behavior could be the difference of the ionic radii between Zn and O compared to Bi and the possibly higher coordination number (see section 4.3.3).

Differential interference contrast microscopy

The O-polar face shows larger hexagonal islands (Figure 48a) which points to higher supersaturation for this polar face. Figure 48b shows a typical picture of different islands grown together. The grown film on the Zn-face did not show significant differences in height (Figure 48c). Growth steps were found on the Zn-polar face (Figure 48d, left part). Although with DIC the Zn-polar face seems to be of a better quality, XRC resulted in a large FWHM value which was even higher than for the O-polar face.

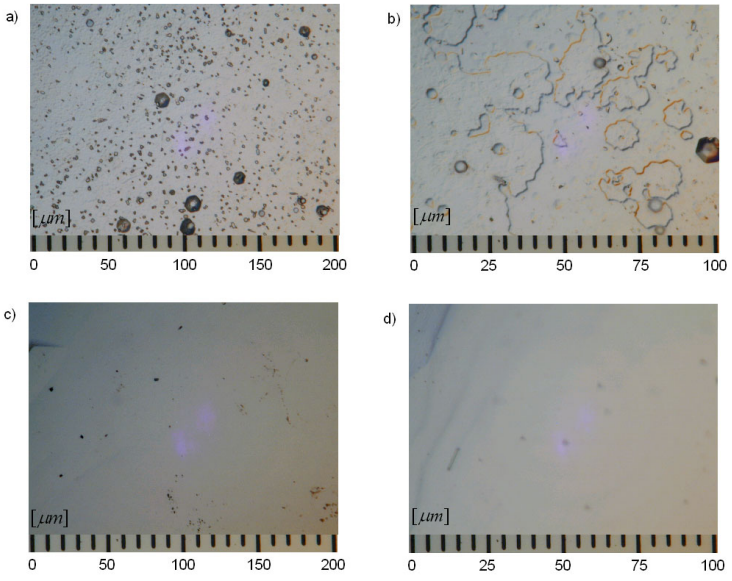

Figure 48. DIC of Bi-doped ZnO films on the O-polar face (a, b) and Zn-polar face (c, d) grown by LPE . All four images are contrast enhanced.

Examination of microcrystals from deposit of LPE growth experiment

The result agrees with the observations from the flux experiment (see section 4.1.2) with the difference that the biggest crystals reached sizes of about 0.2 mm compared to 0.5 mm for flux grown crystals (Figure 49 a,b).

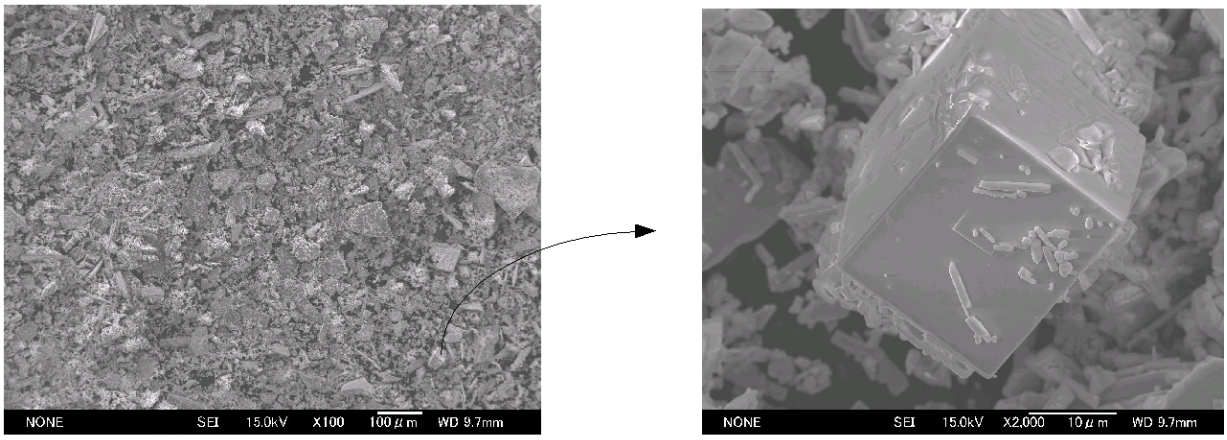

a) General view of the crystals. The crystals are smaller compared to flux grown crystals.

b) A cube of another phase with high concentration of Bi, Zn, Cl, and O is shown.

Figure 49. General view and phase segregation.

4.3.3 Photoluminescence

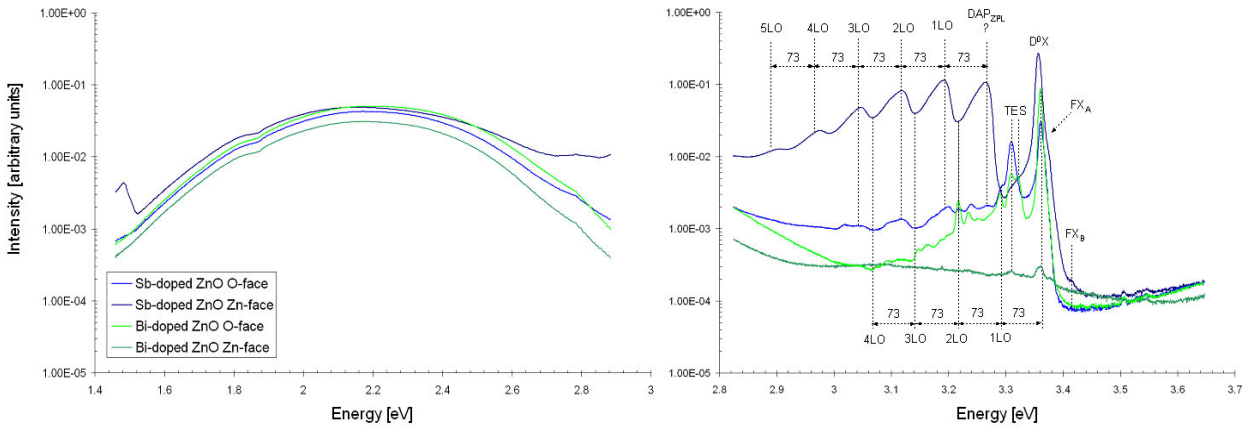

Figure 50. PL measurement, deep emission and NBE of grown films by LPE.

In Figure 50 the FX_B peak at 3.42 eV is visible for Sb-doped ZnO on the Zn-face. The shoulder at 3.38 eV corresponds to the FX_A peak. D^0X emission around 3.357 eV is visible. The Zn-face of Bi-doped ZnO shows a PL curve with much noise compared to the sharp emission peaks, what means low quality. Even the D^0X peak is very low. This confirms the results obtained by XRC. The visual observation of a mirror-like film can not be taken as reference for the crystal quality. The O-face of Bi-doped ZnO film shows the highest intensity of the D^0X peak relative to the LOs. These results are well in agreement with the XRC of Bi-doped ZnO (O-face seems to be better than the Zn-face). D^0X on the Zn-face of Sb-doped ZnO is higher than the deep emission. For the other 3 curves the intensity of the D^0X peak is always lower than the deep emission. The peak at 3.269 eV which could be the DAP_{ZPL} and its LOs as well as

LOs of D^0X emission were found on both faces of Sb-doped ZnO. The LOs of the D^0X emission can also be found on the O-face of Bi-doped ZnO. The LOs of the D^0X emission seem to be minimums (for both faces of Sb-doped ZnO) but a zoom showed peaks. These LOs peaks are well visible with Bi-doped ZnO (O-face). Both TES peaks at 3.32 eV and 3.31 eV are visible for the O-face of Bi-doped ZnO. The other curves show only one peak.
To summarize, Sb is much better incorporated in ZnO than Bi. For Sb-doped ZnO the Zn-polar face shows nice LOs of assumed DAP emission where possibly Li is the acceptor and Sb is the donor. Li has an effective ionic radius of 0.59 Å (fourfold coordinated). It can therefore easily replace Zn with 0.6 Å (fourfold coordinated). Sb has an effective ionic radius of 0.76 Å (fourfold coordinated) which is relatively close to Zn. An incorporation in ZnO is therefore possible [7]. It is confirmed that the O-face is of lower quality due to the preferred incorporation of impurities on this face.
The results from the growth of Bi-doped ZnO is opposite. The Zn-polar face which seemed to be of higher quality by visual observation and DIC is of lower quality (high FWHM value and poor PL signals) whereas the O-polar face was much better. The low quality on the Zn-face can be explained by the big radius differences between Zn (0.6 Å), O (1.38 Å) and Bi (1.03 Å). That leads to deformations of the lattice thus the crystallinity is lower. Furthermore the sixfold coordination of Bi compared to ZnO (fourfold) could be a problem [7]. It is yet not clear why the quality on the O-face is high.

5. Conclusion

Sb, Bi, In, and Mo-doped ZnO microcrystals were produced by flux technology and characterized. A Sb-doped and a Bi-doped film was grown by LPE. The solution always consisted of LiCl as solvent, K_2CO_3 tablets as O-source, and $ZnCl_2$ as Zn-source. The crystal quality was investigated by SEM, EDX, XRD, PL, and DIC.

XRD of Sb-doped ZnO microcrystals revealed the formation of an unknown phase with high Sb content. This was confirmed by SEM-EDX. Well shaped hexagonal ZnO crystals with Sb content can be produced by the applied technique. PL measurement showed emission from the FX_B peak which is a sign of high quality crystals. In contrast to the assumption that Sb may act as acceptor it is suspected that Sb could be the donor whereas Li is the acceptor. DAP emission could therefore appear.
In a LPE experiment it was confirmed that Sb can be incorporated in ZnO. The XRC resulted a high FWHM meaning low crystal quality. Despite, the PL was very intense with clearly visible emisison peaks.

The XRD of Bi-doped ZnO microcrystals showed an unknown phase. That was confirmed by SEM-EDX. Cubes with high concentrations of Bi and Cl were found. The segregation could be explained by the difference of the ionic radii of Bi compared to Zn and O. However, PL showed the FX_B peak. NBE emission was lower than the deep emission. Higher noise levels than for Sb-doped ZnO microcrystals were measured by PL.
The LPE experiment confirmed the results obtained by flux method. A mirror-like film was grown. XRC resulted high FWHM values on both faces. DIC showed a flat surface on the Zn-polar face and steps were sometimes found. PL from the Zn-polar face was highly noisy. The O-polar face was in terms of PL better. The incorporation of Bi in ZnO seems to be difficult.

XRD of $In_{0.001}Zn_{0.999}O$ showed no other phase than hexagonal ZnO, whereas for $In_{0.02}Zn_{0.98}O$ new peaks appeared. SEM-EDX of $In_{0.001}Zn_{0.999}O$ showed modified crystal shapes with more than 6 prism facets. This was explained by a reduced growth speed in a-direction. $In_{0.02}Zn_{0.98}O$ showed the creation of unknown phases (segregation) as cubes. PL of $In_{0.001}Zn_{0.999}O$ showed a high D^0X peak whereas for $In_{0.02}Zn_{0.98}O$ the peak was much lower. It is possible to incorporate In in ZnO but the amount is limited.

Mo is very interesting as dopant. XRD and SEM-EDX showed that Mo was well incorporated in ZnO. Phase segregation was not observed even not with 5mol% doping. $Mo_{0.001}Zn_{0.999}O$ and $Mo_{0.02}Zn_{0.98}O$ showed a shape modification of the crystals (more than 6 prism facets, compare $In_{0.001}Zn_{0.999}O$). PL showed very similar results. The FX_B peak was observed for $Mo_{0.02}Zn_{0.98}O$ and $Mo_{0.05}Zn_{0.95}O$. The increasing and decreasing of peaks (PL) with different Mo concentrations was observed.

Further examinations are necessary (SIMS, AFM, etc.) to fully explain the results obtained. Flux is a method to produce ZnO microcrystals by an easy way and therefore an important research instrument.

It is not yet clear what the influence of Li is (co-dopant in the system). Tests on the photocatalytic effect of Li, Mo co-doped ZnO will be conducted in India this spring.

The problem of doping ZnO p-type is not yet solved. Furthermore for an application of ZnO as blue LED it is necessary to reduce the deep emission thus to obtain a strong emission in the blue spectrum.

6. Acknowledgements

I am grateful to Prof. D. Ehrentraut for his help and support during my diploma thesis (LPE experiments, flux experiments, DIC, theory, etc), to Dr. Y. Kagamitani for help in the use of XRD, SEM-EDX measurements as well as organizational affairs, to Mr. N. Hoshino for SEM-EDX measurements, to Dr. L. Liu for XRD measurements, to Ms. S. Tohyama for organizational affairs, to Dr. K. Fujii for PL and XRC measurements as well as discussion, to Prof. T. Fukuda for his interest in my work and discussion, to Prof. H. Fukumura for discussion, to Mr. Y. Shoji for technical support with the LPE machine, to Prof. C. Yokoyama for support particularly at the initial stage of my stay, to Prof. S.F Chichibu for measurements, and to Prof. E. Carreño-Morelli for continuous support during my time in Sendai.

Particular grateful is due to Tohoku University, Haute Ecole Spécialisée de Suisse occidentale (HES-SO), and my parents for financial support and agreement to write my diploma thesis in Sendai.

7. References

[1] K. W. Krämer, P. Dorenbos, H. U. Güdel, and C. W. E. van Eijk, J. Mater. Chem., 2006, 16, 2773-2780.
[2] P.J. Simpson, R. Tjossem, A.W. Hunt, K.G. Lynn, V. Munné, Nucl. Instr. Meth. Phys. Res. A 505 (2003) 82-84.
[3] D. Ehrentraut, Y. Mikawa, and T. Fukuda, State-of-the-art of ZnO bulk crystal growth, presentation, 2007.
[4] A. Tsukazaki, A. Ohtomo, T. Onuma, M. Ohtani, T. Makino, M. Sumiya, K. Ohtani, S. F. Chichibu, S. Fuke, Y. Segawa, H. Ohno, H. Koinuma and M. Kawasaki, Nat. Mater., 4, 2005, 42-46.
[5] K. Maeda, M. Sato, I. Niikura, T. Fukuda, Semicond. Sci. Technol. 20 (2005) S49-S54.
[6] D. Ehrentraut, H. Sato, M. Miyamoto, T. Fukuda, M. Nikl, K. Maeda, I. Niikura, J. Cryst. Growth 287 (2006) 367-371.
[7] R. D. Shannon, Acta Cryst. (1976). A32, 751-753.
[8] Wurtzite structure, http://cst-www.nrl.navy.mil/lattice/struk.picts/b4.s.png.
[9] S.J. Pearton et al. Prog. Mater. Sci. 50 (2005) 293-340.
[10] D. Ehrentraut, H. Sato, Y. Kagamitani, H. Sato, A. Yoshikawa, T. Fukuda, Prog. Cryst. Growth Char. Mater. 52 (2006) 280-335.
[11] D. P. Norton, Y. W. Heo, M. P. Ivill, K. Ip, S. J. Pearton, M. F. Chisholm, and T. Steiner, Mater. Today, June 2004.
[12] D. Ehrentraut, H. Sato, Y. Kagamitani, A. Yoshikawa, T. Fukuda, J. Pejchal, K. Polak, M. Nikl, H. Odaka, K. Hatanaka and H. Fukumura, J. Mater. Chem., 2006, 16, 3369-3374.
[13] F.X. Xiu, Z. Yang, L.J. Mandalapu, D.T. Zhao, and J.L. Liu, Appl. Phys. Lett. 87, 152101 (2005).
[14] K Byrappa, A K Subramani, S Ananda, K M Lokanatha Rai, R Dinesh, and M Yoshimura, Bull. Mater. Sci., Vol. 29, No. 5, October 2006, pp. 433-438.
[15] T. Pauporté and J. Rathousky, J. Phys. Chem. C 2007, 111, 7639-7644.
[16] M. Nikl, Seminar at Tohoku University, 2005.
[17] M. Nikl, Meas. Sci. Technol. 17 (2006) R37-R54.
[18] Electromagnetic spectrum, http://de.wikipedia.org/wiki/Elektromagnetisches_Spektrum.
[19] PET basics, http://en.wikipedia.org/wiki/Positron_emission_tomography.
[20] PET basics, http://www.imaging-netzwerk-berlin.de/data/files/Downloads_intern/Beyer-Philips_Kombinierte_PET-CT_Bildgebung_1998-2008_Innovationen_med._Bildgebung_130707.pdf.
[21] PET basics, http://www.msha.com/images/Radiology/biograph1_big.jpg.
[22] SEM signals, http://mse.iastate.edu/microscopy/beaminteractions.html.
[23] DIC basics, http://en.wikipedia.org/wiki/Differential_interference_contrast_microscopy.
[24] X-ray basics, http://de.wikipedia.org/wiki/R%C3%B6ntgenstrahlung.
[25] Bragg equation, http://de.wikipedia.org/wiki/Bragg-Gleichung.
[26] XRC basics, http://www.fz-juelich.de/projects/datapool/page/284/V5a.pdf.
[27] Software of XRD machine, Rigaku Corp., Japan.
[28] Mass spectrometer, http://schulen.eduhi.at/chemie/pdf/ms0.pdf.
[29] S. Limpijumnong, S.B. Zhang, S. Wei, and C.H. Park, Phys. Rev. Lett., 92.155504.
[30] David R. Lide, Handbook of Chemistry and Physics, 88th edition, 2007-2008, CRC Press, USA.
[31] Spinel crystal structure, http://scitation.aip.org/getabs/servlet/GetabsServlet?prog=normal&id=PODIE200001800000300021900000 1&idtype.
[32] M. Willander, Q. Zhao, and O. Nur, SPIE, Newsroom, doi: 10.1117/2.1200712.0977.
[33] D. Ehrentraut, M. Miyamoto, H. Sato, J. Riegler, K. Byrappa, K. Fujii, K. Inaba, T. Fukuda, and T. Adschiri, Cryst. Growth Des., submitted.

Further readings

Books

- K. Byrappa, M. Yoshimura, Handbook of Hydrothermal Technology, 2001, William Andrew Publishing, LLC, Norwich, New York, U.S.A.
- W. Kleber, Einführung in die Kristallographie, 16. Auflage, 1985, VEB Verlag Technik Berlin.
- A. Waag, R. Triboulet, B. K. Meyer, V. Munoz-Sanjosé, Y. S. Park, European Materials Research Society 2006, Symposium K. ZnO and Related Materials.
- A Johnson Matthey Company, Research Chemicals, Metals and Materials, Alfa Aesar, 2006-07.

Papers

- F.X. Xiu, Z. Yang, L.J. Mandalapu, D.T. Zhao, and J.L. Liu, Appl. Phys. Lett. 87, 252102 (2005).
- E. Ohshima, H. Ogino, I. Niikura, K. Maeda, M. Sato, M. Ito, T. Fukuda, J. Cryst. Growth 287 (2006) 367-371.
- F.X. Xiu, Z. Yang, L.J. Mandalapu, J.A. Yarmoff, J.L. Liu, Appl. Phys. Lett. 89, 052103 (2006).
- P. Wang, N. Chen, Z. Yin, R. Dai, and Y. Bai, Appl. Phys. Lett. 89, 202102 (2006).
- L. J. Mandalapu, Z. Yang, F. X. Xiu, D. T. Zhao, and J. L. Liu, Appl. Phys. Lett. 88, 092103 (2006).
- O. Lopatiuk, L. Chernyak, A. Osinsky, and J. Q. Xie, Appl. Phys. Lett. 87, 214110 (2005).
- O. Lopatiuk-Tirpak, W. V. Schoenfeld, L. Chernyak, F. X. Xiu, J. L. Liu, S. Jang, F. Ren, S. J. Pearton, A. Osinsky, and P. Chow, Appl. Phys. Lett. 88, 202110 (2006).
- N. Jayadev Dayan, S. R. Sainkar, R. N. Karekar, R. C. Aiyer, Thin Solid Films 325 (1998) 254-258.
- S. R. Sainkar, S. Badrinarayanan, A. P. B. Sinha, S. K. Date, Appl. Phys. Lett. 39 (1), 1 July 1981.
- S. E. Derenzo, M. J. Weber, M. K. Klintenberg, Nucl. Instr. and Meth. Phys. Res. A 486 (2002) 214-219.
- E. Oshima, H. Ogino, I. Niikura, K. Maeda, M. Sato, M. Ito, T. Fukuda, J. Cryst. Growth 260 (2004) 166-170.
- B. K. Meyer, H. Alves, D. M. Hofmann, W. Kriegseis, D. Forster, F. Bertram, J. Cristen, A. Hoffmann, M. Strassburg, M. Dworzak, U. Haboeck, and A. V. Rodina, phys. stat. sol. (b) 241, No. 2 (2004).

8. Conference presentations and publications

1. D. Jossen and D. Ehrentraut, „Growth of undoped and doped ZnO films by liquid phase epitaxy“, Proceedings of KACG Meeting, Korean Association of Crystal Growth, November 1-3, 2007, Seoul, Korea. Poster presentation.

2. David Jossen, Yuji Kagamitani, Katsushi Fuji, and Dirk Ehrentraut, „Growth and characterization of undoped and doped ZnO films by liquid phase epitaxy“, IMRAM (Institute of Multidisciplinary Research for Advanced Materials) workshop, December 2007, Sendai, Japan. Poster presentation.

3. David Jossen, Tsuguo Fukuda, Katsushi Fuji, and Dirk Ehrentraut, „Flux growth and characterization of doped ZnO films by liquid phase epitaxy“, Proceedings of Flux Growth Society of Japan, December 2007, Sendai, Japan. Oral presentation.

4. David Jossen, Dirk Ehrentraut, Yuji Kagamitani, K. Byrappa, and Jürgen Riegler, “Growth and characterization of doped ZnO films and microcrystals fabricated from low-temperature solutions”, CGCT 4, The 4th Asian Conference on Crystal Growth and Crystal Technology, May 21-24, 2008, Sendai, Japan (submitted).

5. D. Ehrentraut, D.Jossen, K. Byrappa, J.Riegler, K.Fujii: “Effect of doping on ZnO microcrystals from solution“. Publication is in preparation.

GROWTH OF UNDOPED AND DOPED ZnO FILMS BY LIQUID PHASE EPITAXY

David Jossen and Dirk Ehrentraut
IMRAM Tohoku Univ., 2-1-1 Katahira, Aoba- ku, Sendai 980-8577, Japan
Tel & Fax: +81-22-217-5101
E-mail : david.jossen@gmx.ch

An increasingly important aspect is the fabrication of materials like ZnO by technologies which not only guarantee reproducibly high quality, but also facilitate one- step fabrication of the functional materials with a minimum effort in producing them by so- called green technologies. Moreover, mechanically untouched ZnO surfaces are desirable to exclude radiative losses due to a damaged surface layer.

As the doping of hydrothermal- grown bulk ZnO appears rather difficult and time consuming, we have used our recently developed growth process by liquid phase epitaxy (LPE) to obtain high quality single crystal films of several micrometer thickness. With the LPE growth technique the damaged surface layer is neutralized, at the same time doping can be realized and the sample surface is mechanically untouched.

Homoepitaxial ZnO thin films were grown from a LiCl solution at 640°C under ambient air conditions. ZnO is produced by a reaction of $ZnCl_2$ with K_2CO_3, such way providing the feeding for continous growth. Doping and formation of solid solutions with bi- tri- and tetravalent ions is enabled through employment of the relevant metal halogenides.

REFERENCES

1. D. Ehrentraut et al., J. Cryst. Growth 2006, **287**, 367.
2. D. Ehrentraut et al., J. Mater. Chem. 2006, **16**, 3369

Growth of Undoped and Doped ZnO Films by Liquid Phase Epitaxy

David Jossen and Dirk Ehrentraut

IMRAM, Tohoku University, 2-1-1 Katahira, Aoba-ku, Sendai 980-8577, JAPAN

E-mail: david.jossen@gmx.ch

Why ZnO?

- **At RT: E_g = 3.31eV (λ = 375nm), exciton binding energy 60meV.**
- **Transparency at RT:** 80%
- **Ultra-fast scintillation decay** for Ga-doped and In-doped ZnO.*
- **Emission around 400 nm → easily detectable** by photomultiplier.
- **High radiation hardness**, relatively **high density** (5.6 g/cm^3 ↔ BaF_2 = 4.8 g/cm^3)

Problem: **SELF-ABSORPTION** of undoped ZnO.

Solution: Doping donors (In, Ge, etc.) to **RED-SHIFT LUMINESCENCE.**

Technology: Liquid Phase Epitaxy for fast screening of single crystalline ZnO films.

SELF-ABSORPTION

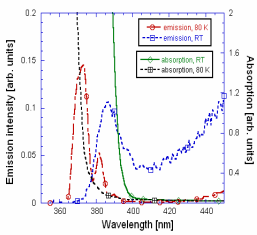

Temperature-dependent absorption edge vs. excitonic emission.

Self-absorption increasingly troublesome with rising temperature.

*S.E. Derenzo et al., NIM **A486** 214, 2002; P.J. Simpson et al., NIM **A505** 82, 2003.

Liquid Phase Epitaxy

• **New Concept - Alkaline Metal Chlorides + Continuous Feeding with ZnO**: $ZnCl_2 + K_2CO_3 \rightarrow ZnO + 2KCl + CO_2\uparrow$ *

- **Solubility** of **ZnO in LiCl = 11 mmol** at 650°C (89.5 mg ZnO per 42.4 g LiCl).
  (Solvents are water soluble; Growth under air atmosphere & normal pressure, constant temperature)
- **Simple equipment**, **Scaling-up**, **Environmentally benign conditions.**

** D. Ehrentraut et al., JCG **287**,367, 2006.*

Results

A. Film Preparation

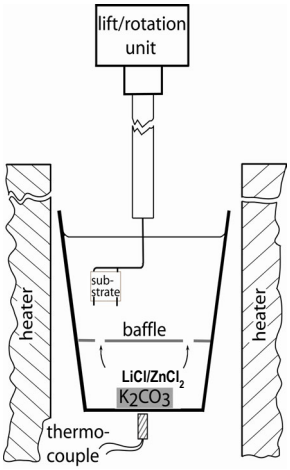

Dipping technique: Crucible with solution & substrate.

- In, Ge, Sb from halogenides.
- Growth temperature 640°C.
- Substrate rot. 5 rpm. t_{growth} = 12h.

B. (0001) and (000$\bar{1}$) ZnO Characterization

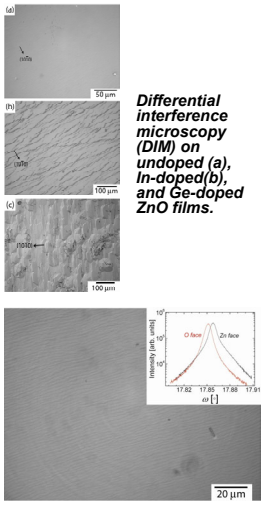

Differential interference microscopy (DIM) on undoped (a), In-doped(b), and Ge-doped ZnO films.

Optical interference micrograph from a Sb, Li codoped (0001) ZnO film shows highly uniform steps. The insets are showing XRC curves in log scale taken from the (0001) and (000$\bar{1}$) face and a contrast-enhanced magnified view of a fraction of the film.

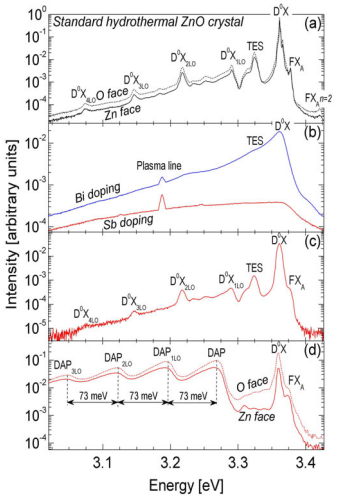

Low-temperature NBE photoluminescence from (a) the undoped hydrothermal bulk ZnO crystal, (b) Bi and Sb doped ZnO hydrothermal microcrystal, (c) Sb, Li codoped ZnO microcrystal prepared from LiCl solution, and (d) the Sb, Li codoped ZnO film prepared by LPE.

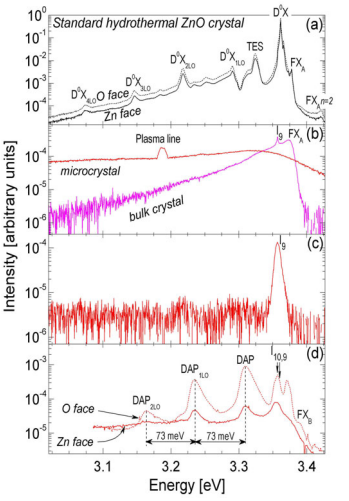

Low-temperature NBE photoluminescence from (a) the undoped hydrothermal bulk ZnO crystal, (b) In doped hydrothermal ZnO microcrystal and ZnO bulk crystal, (c) In, Li codoped ZnO microcrystal prepared from LiCl solution, and (d) the In, Li codoped ZnO film prepared by LPE.

- ***Time-resolved Photoluminescence (PL) and Decay*****

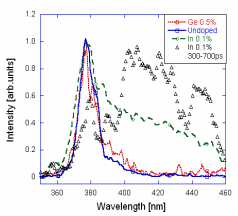

Time-resolved PL emission spectra of films doped with In and Ge in comparison to the undoped film.

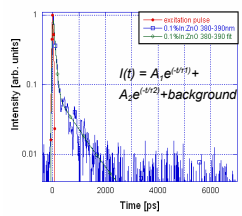

Room temperature PL decay of the 0.15 mol% In-doped film (λ_{exc} = 260 nm, 150 fs laser pulse, λ_{em} = 380-390 nm). Solid line is convolution of instrumental response with two-exponential approximation of the decay curve.

*** D. Ehrentraut et al., J. Mater. Chem. 2006, **16**,3369.*

Major Achievements

1. **High-quality undoped, In, Ge, Sb-doped ZnO films fabricated.**
2. **Phase-stabilizing effect of ZnO substrate.**
3. **Li,In co-doping: Highly intense DAP-related emission around 400-420 nm.**
4. **Ultra-short decay: 30-60 ps and 250-800 ps.**

Growth and characterization of undoped and doped ZnO films by liquid phase epitaxy

David Jossen[a], Yuji Kagamitani[a], Katsushi Fujii[b], and Dirk Ehrentraut[a]
[a]IMRAM Tohoku Univ., 2-1-1 Katahira, Aoba-ku, Sendai 980-8577, Japan
[b]CIR, Tohoku University, Aramaki aza Aoba 6-3, Aoba-ku, Sendai 980-8578, Japan
E- mail: david.jossen@gmx.ch

An increasingly important aspect is the fabrication of materials like ZnO by technologies which not only guarantee reproducibly high quality, but also facilitate one-step fabrication of the functional materials with a minimum effort in producing them by so-called green technologies. Moreover, mechanically untouched ZnO surfaces are desirable to exclude radiative losses due to a damaged surface layer.

As the doping of hydrothermally grown bulk ZnO appears rather difficult and time consuming, we have used our recently developed growth process by liquid phase epitaxy (LPE) to obtain high quality single crystal films of several micrometer thickness. With the LPE growth technique the damaged surface layer is neutralized, at the same time doping can be realized and the sample surface is mechanically untouched.

Homoepitaxial ZnO thin films were grown from a LiCl solution at 640°C under ambient air conditions. ZnO is produced by a reaction of $ZnCl_2$ with K_2CO_3, such way providing the feeding for continous growth. Doping and formation of solid solutions with ions such like Ga, Ge and Sb is enabled through employment of the relevant pure metal or metal halogenide. Highly intense donor-acceptor pair recombination is reported.

References:

1. D. Ehrentraut et al., J. Cryst. Growth 2006, **287**, 367.
2. D. Ehrentraut et al., J. Mater. Chem. 2006, **16**, 3369.
3. D. Jossen and D. Ehrentraut, „Growth of undoped and doped ZnO films by liquid phase epitaxy“, KACG Meeting November 1-3, 2007.

Growth and Characterization of Undoped and Doped ZnO Films by Liquid Phase Epitaxy

David Jossen, Yuji Kagamitani, Katsushi Fujii, and Dirk Ehrentraut

IMRAM, Tohoku University, 2-1-1 Katahira, Aoba-ku, Sendai 980-8577, JAPAN

E-mail: david.jossen@gmx.ch

Why ZnO?

- **At RT: E_g = 3.31eV (λ = 375nm), exciton binding energy 60meV.**
- **Transparency at RT:** 80%
- **Ultra-fast scintillation decay** for Ga-doped and In-doped ZnO.*
- **Emission around 400 nm → easily detectable** by photomultiplier.
- **High radiation hardness**, relatively **high density** (5.6 g/cm^3 ↔ BaF_2 = 4.8 g/cm^3)

Problem: **SELF-ABSORPTION** of undoped ZnO.

Solution: Doping donors (In, Ge, etc.) to **RED-SHIFT LUMINESCENCE.**

Technology: Flux + Liquid Phase Epitaxy for fast screening of single crystalline ZnO microcrystals and films.

SELF-ABSORPTION

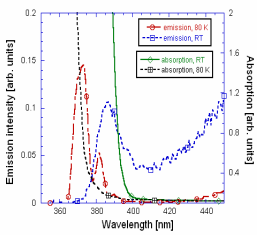

Temperature-dependent absorption edge vs. excitonic emission.

Self-absorption increasingly troublesome with rising temperature.

S.E. Derenzo et al., NIM **A486 214, 2002; P.J. Simpson et al., NIM **A505** 82, 2003.*

Liquid Phase Epitaxy

• **New Concept - Alkaline Metal Chlorides + Continuous Feeding with ZnO**: $ZnCl_2 + K_2CO_3 \rightarrow ZnO + 2KCl + CO_2\uparrow$ *

- ➟ **Solubility** of **ZnO in LiCl = 11 mmol** at 650°C (89.5 mg ZnO per 42.4 g LiCl).
  (Solvents are water soluble; Growth under air atmosphere & normal pressure, constant temperature)
- ➟ **Simple equipment**, **Scaling-up**, **Environmentally benign conditions.**

** D. Ehrentraut et al., JCG **287**,367, 2006.*

Results

LPE

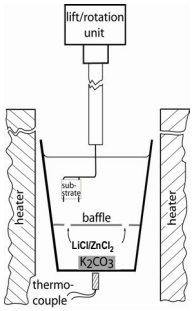

Dipping technique: Crucible with solution & substrate.

- ***In, Sb, Bi from halogenides.***
- ***Growth temperature 640°C.***
- ***Substrate rot. 5 rpm. t_{growth} = 12h.***

LPE

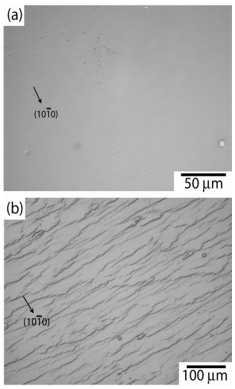

Differential interference microscopy (DIM) on undoped (a), and In-doped(b) ZnO films.

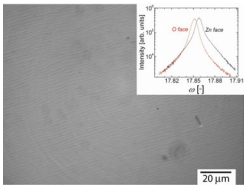

Differential interference microscopy (DIM) from a Sb, Li codoped (0001) ZnO film shows highly uniform steps. The insets are showing XRC curves in log scale taken from the (0001) and (0001) face and a contrast-enhanced magnified view of a fraction of the film.

Flux (Sb-doped ZnO)

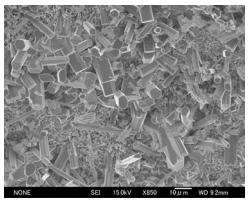

SEM from Sb-doped ZnO crystals. The ZnO structure is visible.

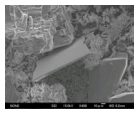

SEM from Sb-doped ZnO crystals. In several shapes, like this plate, Sb and Zn were found.

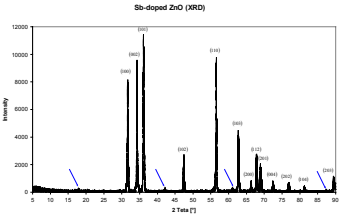

XRD measurement of Sb-doped ZnO crystals. The blue arrows indicate peaks of other phases than ZnO.

Flux (Bi-doped ZnO)

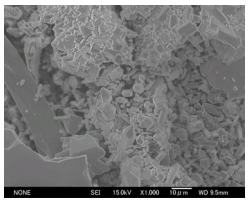

SEM from Bi-doped ZnO crystals.

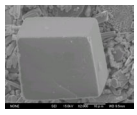

Segregation

SEM from Bi-doped ZnO crystals. Shapes in form of cubes showed a high concentration of Bi and Cl (segregation). It seems to be difficult to incorporate Bi into the ZnO lattice.

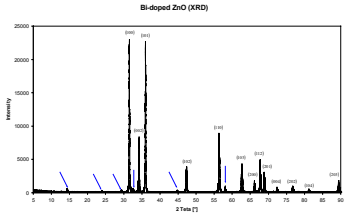

XRD measurement of Bi-doped ZnO crystals. The blue arrows indicate peaks of other phases than ZnO.

- ***Time-resolved Photoluminescence (PL) and Decay*****

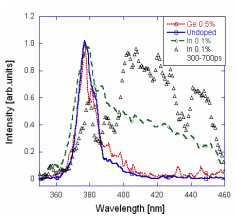

Time-resolved PL emission spectra of films doped with In and Ge in comparison to the undoped film.

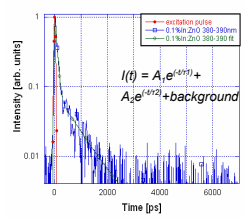

Room temperature PL decay of the 0.15 mol% In-doped film (λ_{exc} = 260 nm, 150 fs laser pulse, λ_{em} = 380-390 nm). Solid line is convolution of instrumental response with two-exponential approximation of the decay curve.

*** D. Ehrentraut et al., J. Mater. Chem. 2006, **16**,3369.*

Major Achievements

1. **High-quality undoped, In, Sb, Bi-doped ZnO microcrystals & films fabricated.**
2. **Li,In co-doping: Highly intense DAP-related emission around 400-420 nm.**
3. **Ultra-short decay: 30-60 ps and 250-800 ps.**

Flux growth and characterization of doped ZnO films by liquid phase epitaxy

David Jossen[a], Tsuguo Fukuda[a], Katsushi Fujii[b], and Dirk Ehrentraut[a]
[a]IMRAM Tohoku Univ., 2-1-1 Katahira, Aoba-ku, Sendai 980-8577, Japan
[b]CIR, Tohoku University, Aramaki aza Aoba 6-3, Aoba-ku, Sendai 980-8578, Japan
E- mail: david.jossen@gmx.ch

An increasingly important aspect is the fabrication of materials like ZnO by technologies which not only guarantee reproducibly high quality, but also facilitate one-step fabrication of the functional materials with a minimum effort in producing them by so-called green technologies. Moreover, mechanically untouched ZnO surfaces are desirable to exclude radiative losses due to a damaged surface layer.

As the doping of hydrothermally grown bulk ZnO appears rather difficult and time consuming, we have used our recently developed growth process by liquid phase epitaxy (LPE) to obtain high quality single crystal films of several micrometer thickness. With the LPE growth technique the damaged surface layer is neutralized, at the same time doping can be realized and the sample surface is mechanically untouched.

In spite of the limited potential flux systems for ZnO, i.e. H_2O requires the use of solubility-enhancing mineralizers and PbO-PbF_2 leads to high concentration of Pb in ZnO, the group-I element chlorides turned out to be useful.

Homoepitaxial ZnO thin films were grown from a LiCl solution at 640°C under ambient air conditions. ZnO is produced by a reaction of $ZnCl_2$ with K_2CO_3, such way providing the feeding for continous growth. Doping and formation of solid solutions with ions such like Ga, Ge and Sb is enabled through employment of the relevant pure metal or metal halogenide. Highly intense donor-acceptor pair recombination is reported.

References:

1. D. Ehrentraut et al., J. Cryst. Growth 2006, **287**, 367.
2. D. Ehrentraut et al., J. Mater. Chem. 2006, **16**, 3369.
3. D. Jossen and D. Ehrentraut, „Growth of undoped and doped ZnO films by liquid phase epitaxy“, KACG Meeting November 1-3, 2007.

Growth and characterization of doped ZnO films and microcrystals fabricated from low-temperature solutions

David Jossen[1], Dirk Ehrentraut[1*], Yuji Kagamitani[1], Katsushi Fujii[2], K. Byrappa[3], and Jürgen Riegler[1,4]

[1] IMRAM Tohoku Univ., 2-1-1 Katahira, Aoba- ku, Sendai 980-8577, Japan

[2] CIR Tohoku Univ., Aramaki aza Aoba 6-3, Aoba-ku, Sendai 980-8578, Japan

[3] Dept. Geology, University of Mysore, Manasagangothri, Mysore 570 006, India

[4] New address: Fraunhofer Institute, 70569 Stuttgart, Germany

E-mail : david.jossen@gmx.ch

* *Presenting author*

Zinc oxide is a wide bandgap semiconductor (E_g = 3.3 eV) with a large exciton binding energy of 60 meV. It therefore has a wide application field in modern technology such as transparent conductor in the vis-IR wavelength range, UV-blue light-emitting devices, ferromagnetic devices, piezoelectric transducers, surface acoustic devices, photocatalyst, superfast scintillator, spin functional devices, gas sensors, varistors, etc. [1].

Homoepitaxial ZnO thin films and microcrystals were grown from a LiCl solution at 640°C under ambient air conditions. ZnO is produced by a reaction of $ZnCl_2$ with K_2CO_3, such way providing the feeding for continous growth [2]. Low-temperature (90-150°C) hydrothermal growth under alkali-free conditions yielded well-shaped microcrystal [3]. Doping and formation of solid solutions with ions such like Bi, Sb, Mo, In, etc. was enabled through employment of the relevant pure metal, metal halogenide or metal oxide.

The crystal quality has been investigated by secondary electron microscopy, x-ray diffraction, photoluminescence, and electron diffraction spectroscopy. For example, the co-doping of Li and Sb resulted in highly intense donor-acceptor pair recombination and luminescence from free excitons was clearly observed [4].

References

[1] S.J. Pearton, D.P. Norton, K. Ip, Y.W. Heo, T. Steiner, *Prog. Mater. Sci.* **50** (2005) 293. [2] D. Ehrentraut, H. Sato, Y. Kagamitani, H. Sato, A. Yoshikawa, T. Fukuda, *Prog. Cryst. Growth Char. Mater.* **52** (2006) 280. [3] D. Ehrentraut, H. Sato, Y. Kagamitani, A. Yoshikawa, T. Fukuda, J. Pejchal, K. Polak, M. Nikl, H. Odaka, K. Hatanaka, and H. Fukumura, *J. Mater. Chem.* **16** (2006) 3369. [4] D. Jossen, D. Ehrentraut, „Growth of undoped and doped ZnO films by liquid phase epitaxy“, KACG Meeting November 1-3, 2007, poster presentation.

9. Appendix

Appendix A

Production of K_2CO_3 tablets

Crucibles for sintering

Producer:	Metoxit AG
Material:	ZrO_2 (90%)/Y_2O_3 (10%), FSZ white color or yellow color. The yellow crucible has a lower purity
$V_{crucible}$:	49 ml (yellow crucible) and 42 ml (white crucible).
Density:	5.8 g/cm^3
Max. working temperature:	2000°C

Figure 51. The crucibles of 49ml (left) and 42ml (right) volume.

Before using, the crucible was cleaned in a supersonic bath of distilled water and 2-propanol during 10 minutes. After that the crucible was rinsed with 2-propanol and dried in a furnace for 10 minutes (70°C). The advantage of 2-propanol is that it evaporates well and absorbes H_2O.

Supersonic bath

Type: AS ONE, Ultra Sonic washer

Figure 52. Supersonic bath.

K_2CO_3 powder

Potassium carbonate is stocked in a dryed cabinet (humidity 40%, temperature 20°C).

Figure 53. K_2CO_3 powder.

Distributor:	Alfa Aesar Puratronic
Purity:	99.997%
Stock #:	10838
Lot #:	23092

Potassium carbonate was weighed and filled in a crucible. 2-propanol and a punch were used to compact the powder. The crucible was covered (cover ZrO_2) and put in the furnace.

Used scale

Type: Mettler AE 163 (min. resolution 0.00001g, max. weight 30g)

Figure 54. Mettler AE 163 scale.

Sintering

Type: Muffle Furnace FO200 (Yamato), max.Temperature 1200°C, air-atmosphere, programmable.

Figure 55. Muffle furnace.

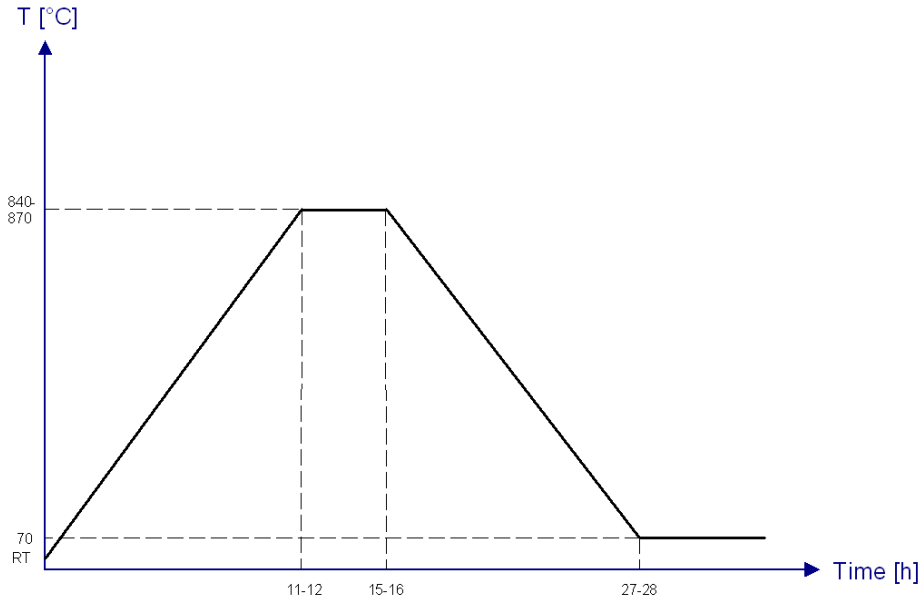

Figure 56. Temperature profile of sintering process .

870° C is just under T_m of K_2CO_3 (see Table 6).
After thermal treatment, the tablets were stocked in a cabinet with humidity absorbent material.

Table 5. Weighed masses of powder and tablets .

Tablet No.	M_{K2CO3} [g] (powder)	M_{K2CO3} [g] (tablet)	M_{lost} [%]	Used crucible[ml]	T [°C]
1	2.00100	1.78700	10.69	42	840
2	3.00030	2.73030	9.10	42	870
3(1)	2.50050	-	-	42	870
4	2.49950	2.32800	6.86	42	870
5	2.49900	2.34110	6.32	42	870
6(2)	2.49249	2.40300	3.59	42	870
7	2.50673	2.36712	5.57	49	870
8(3)	2.50300	2.29920	8.14	49	870
9(4)	2.49910	-	-	42	870
10(5)	2.50143	1.94320	22.32	42	855
11	2.49760	2.24890	9.96	42	860
12(6)	2.49220	2.32521	6.70	49	860

(1) This tablet could not be used (not stable enough, too less 2-propanol was used for compaction).
(2) The tablet was molten in the crucible. The crucible with the tablet was weighed and after the experiment the crucible was back-weighed.
(3) The crucible cracked during thermal treatment (figure 7) but the tablet could be used.
(4) The tablet was molten. This tablet was not used. The crucible with the tablet was put in water to dissolve K_2CO_3.
(5) A lot of the powder was not sintered.
(6) Identical crucible to the cracked one was used.

Figure 57. Cracked crucible.

The crucible in Figure 57 shows a white coloration due to increased Li content. This crucible was also used for flux experiments. A formation of a Li-Zr-O-Cl phase has taken place. This can lead to cracking.

Figure 58. Left: tablet no. 2 / Right: tablet no. 5

The mass of a sintered tablet is always lower than the mass of powder. That can be explained by evaporation of water from the powder and partly decomposition of K_2CO_3 powder. The tablet no. 1 lost over 10% (no 2-propanol was used for binding the powder, for this reason the tablet was not sintered completely). The tablet no. 10 was not sintered completely (T too low, over 20% of the mass was lost).

Calculation

All data were taken from the Alfa Aesar 2006/07 catalogue (flux experiments and LPE).

Table 6. Material properties .

Material	ρ [g/cm^3]	T_m [°C]	Molweight [g/mol]
K_2CO_3	2.428	891	138.2058
LiCl	2.068	605	42.3937
$ZnCl_2$	2.910	290	136.2854
ZnO	5.606	1975	81.3794

V_{LiCl} = 20cm^3 is used for flux experiments and LPE. From this value the mass of K_2CO_3 required for the experiments can be calculated. A concentration of 0.0125 mol ZnO per mol LiCl is desired.

Table 7. Calculated amounts of the chlorides, K_2CO_3, and formed ZnO.

Material	[mol]	M [g]	V [cm^3]
LiCl	0.9756	41.36000	**20.00**
$ZnCl_2$	0.0122	1.66203	0.57
ZnO	0.0122	0.99244	0.18
K_2CO_3	0.0122	1.68545	0.69

Following equations were used:

(1) $$M_{LiCl} = V_{LiCl} \times \rho_{LiCl}$$

(2) $$LiCl[mol] = \frac{M_{LiCl}[g]}{Molweight_{LiCl}}$$

(3) $$ZnO[mol] = 0.0125 \times LiCl[mol]$$

(4) $$M_{ZnO} = ZnO[mol] \times Molweight_{ZnO}$$

(5) $$V_{ZnO} = \frac{M_{ZnO}}{\rho_{ZnO}}$$

(6) $$ZnO[mol] = ZnCl_2[mol] = K_2CO_3[mol]$$

(7) $$M_{ZnCl_2} = ZnCl_2[mol] \times Molweight_{ZnCl_2}$$

(8) $$V_{ZnCl_2} = \frac{M_{ZnCl_2}}{\rho_{ZnCl_2}}$$

(9) $$M_{K_2CO_3} = K_2CO_3[mol] \times Molweight_{K_2CO_3}$$

(10) $$V_{K_2CO_3} = \frac{M_{K_2CO_3}}{\rho_{K_2CO_3}}$$

Tablets with a larger mass were produced. K_2CO_3 which would not be used in the experiment remains on the ground of the crucible and has no influence on the experiment.

Appendix B

Flux Experiments

Crucibles

Same crucibles as for production of K_2CO_3 tablets and the following one were used.

Company:	C.C. Japan
Material:	Al_2O_3 (95%)/SiO_2(3%), SSA-H
$V_{crucible}$:	42 ml
Density:	3.7 g/cm^3
Max. working temperature:	1600°C

Figure 59. Al_2O_3 crucible.

Materials and processing

The volume of LiCl was 20 cm^3 (for calculations of the masses see “Appendix A”)

Table 8. Used materials.

Material	Properties	Purity [%]	Distributor	Lot #	Calculated mass [g]
LiCl	white color,	99.999	MV Laboratories, INC	E305LIA1	41.36000
$ZnCl_2$	Brown cast (almost transparent)	99.999	High Purity Chemicals	69520	1.66203
K_2CO_3	white color	99.997	Alfa Aesar Puratronic	23092	1.68545
Sb	silver color	99.990	High Purity Chemicals	746960	-
Bi_2O_3	yellow color	99.990	High Purity Chemicals	32382G	-
$InCl_3$	white color, evaporates very fast	99.999	Alfa Aesar	E11P17	-
MoO_3	grey color, little globes	Heavy metals (as Pb) 0.001%, SO_4 0.005%, SiO_2 0.005%, NH_4 0.005%, Cl 0.002%	Wako Pure Chemical Industries, LTD	WDQ 3091	-

LiCl, $ZnCl_2$ and K_2CO_3 are used in all experiments and the adequate dopant was added (e.g. Sb, Bi_2O_3 etc.). LiCl was weighed in two steps. It's not possible to weigh more than 30g with the used scale. LiCl consists of many clumps which were reduced to powder (Figure 60). Otherwise mixing of the chlorides would be difficult. K_2CO_3 was placed at the bottom of the crucible. $ZnCl_2$ and LiCl were mixed and filled in the crucible. The dopant was added, the crucible was covered with an Al_2O_3 lid and put in the furnace.
After the experiment the crucible was placed in a glassbeaker filled with water. The water was changed several times. The advantage is that ZnO, oxide of the dopant and the dopant are not water soluble but all the other components of the flux are. At the end only the ZnO will remain at the bottom of the glassbeaker and the empty crucible can be taken out. The supersonic bath was used for accelerating the process.
The glassbeaker with the ZnO and water was stored for about 24h. After this time the material was deposited at the bottom. The water was drained and 2-propanol was used to separate all water from the powder.
The powder was dried for about 24h at ambient temperature, weighed and collected for examination.

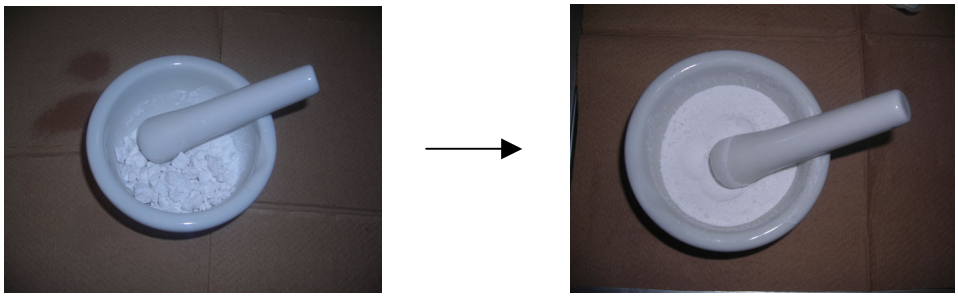

Figure 60. LiCl clumps were reduced to powder .

Scales

Two scales were used:

1. Mettler AE 163 (min. 0.00001g, max. 30g).
2. AND GX 600 (min. 0.02g, max. 610g).

Figure 61. AND GX 600.

Supersonic bath

Type: AS ONE, Ultra Sonic washer.

Furnace and temperature profile

Type: Muffle Furnace FO200 (Yamato), max.Temperature 1200°C, air-atmosphere, programmable.

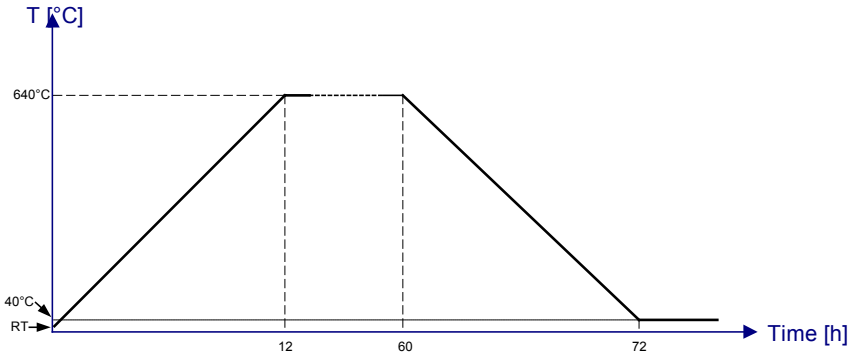

Figure 62. Temperature profile for flux experiments.

Examination

SEM-EDX

Type: JEOL, SM-71010, Japan
Voltage: 15 kV

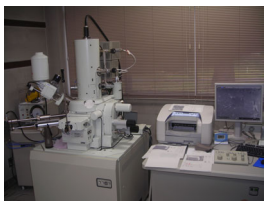

Figure 63. JEOL, SM-71010.

PL

Laser: Series 56 Omnichrome, He-Cd, λ = 325 nm
Monochromator: Groupe Horiba HR 320
Filters: 34U (all wavelength under 340 nm are cut) and L42 (all wavelength under 420 nm are cut)
Temperature: PL was measured at low temperature (12K)

XRD

Type: Rigaku x-ray Diffractometer, Rint 2000 (for powder examination), Japan
Scanning type: Continous scanning
X-ray: 40kV/40mA
Step width: 0.002°
Scan range (2θ): 5°-90°
Scanning speed: 2 °/min

Figure 64. Rigaku x-ray Diffractometer, Rint 2000.

Crucible

Material: ZrO_2 (90%)/Y_2O_3 (10%)
$V_{crucible}$: 42 ml

K_2CO_3

Used K_2CO_3: Tablet no. 1 (1.78700g)

Doping: (Sb)

2mol% SbO is desired; source is pure Sb. Sb needs the oxygen of K_2CO_3 to form SbO.

$$Sb + O_2 \rightarrow SbO + \frac{1}{2}O_2$$
$$ZnCl_2 + Sb + K_2CO_3 \rightarrow Sb_{0.02}Zn_{0.98}O + \ldots$$

Table 9. Calculated and weighed masses and molar concentrations.

Material	Molweight [g/mol]	Calculated		Weighed	
		M [g]	mol]	M [g]	[mol]
K_2CO_3	138.2058	1.68545	0.0122	1.78700	0.0129
$ZnCl_2$	136.2854	1.62879	0.0120	1.66020	0.0122
LiCl	42.3937	41.36000	0.9756	41.27590	0.9736
$Sb_{0.02}$ $Zn_{0.98}O$	82.5068	1.00619	0.0122	0.73116	0.0089
SbO	137.7494	0.03360	0.0002		
Sb	121.7500	0.02970	0.0002	0.02976	0.0002

The values of 0.0122 for K_2CO_3 and 0.9756 for LiCl are known from the calculations in “Appendix A” (LiCl = 20 cm^3). Instead to form 0.0122 mol of ZnO it is needed to form 0.0122 mol of the solid solution $Sb_{0.02}$ $Zn_{0.98}O$.

Calculation:

(1) $Sb_{0.02}Zn_{0.98}O_{[mol]} = 0.0122$

(2) $M_{=[mol]} \times Molweight$

(3) $SbO_{[mol]} = 0.02 \times Sb_{0.02}Zn_{0.98}O_{[mol]}$; $ZnCl_{2[mol]} = ZnO_{[mol]} = 0.98 \times Sb_{0.02}Zn_{0.98}O_{[mol]}$

(4) $SbO_{[mol]} = Sb_{[mol]}$

Weighed:

(5) $[mol] = \frac{M}{Molweight}$

The masses of LiCl and $ZnCl_2$ in the crucible are not exactly the weighed values. It is important to mix these two materials what leads to losses. All other components do not change the weighed values.

LiCl and $ZnCl_2$ in the crucible:

42.35300g (without losses it would be 41.27590+1.66020=42.93510g, see Table 9).

Table 10. Real amounts of LiCl and $ZnCl_2$ in the crucible.

Material	M weighed [g]	Mass %	$M_{substracted}$ [g]	M in crucible [g]
LiCl	41.27590	96.14	0.56059	40.71531
$ZnCl_2$	1.66020	3.86	0.02251	1.63769
LiCl+$ZnCl_2$	42.93510	100	0.58310	42.35300

(6) $LiCl_{M\ substracted} = 0.9614 \times 0.5831$

(7) $ZnCl_{2\,M\ substracted} = 0.0386 \times 0.5831$

(8) $M_{incrucible} = M_{weighed} - M_{substracted}$

Table 11. Used and formed amounts.

Material	In crucible M [g]	In crucible [mol]	**Formed materials** [mol%] (calculated with the values "In crucible")	$C_{ZnO\ in\ LiCl}$ [mol%]
K_2CO_3	1.78700	0.0129		
$ZnCl_2$	1.63769	0.0120		
LiCl	40.71531	0.9604		100
SbO formed	0.03367	0.0002	1.9936	
ZnO formed	0.97791	0.0120	98.0064	1.2512
Sb	0.02976	0.0002		

(9) $SbO_{formed\ [mol]} = Sb_{[mol]}$

(10) $ZnO_{formed\ [mol]} = ZnCl_{2[mol]}$

(11) $[mol] = \frac{M}{Molweight}$

Notes

All was molten and a crust on the surface was visible.

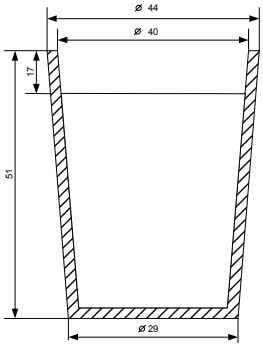

Figure 65. Dimension of the crucible after thermal treatment (filled with solution).

Figure 66. The doped ZnO is deposited at the bottom of the glassbeaker.

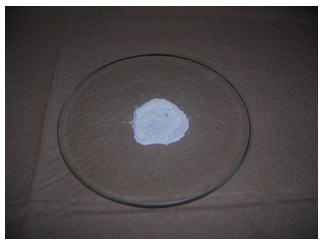

Figure 67. Dried powder.

The obtained amount of powder: 0.73116g

$\frac{0.73116}{1.00619} \approx 0.7267 \approx 73\%$ of the calculated value, the remaining 27% contain the formation of a solid solution and losses by mixing the chlorides.

Crucible

Material: ZrO_2 (90%)/Y_2O_3 (10%)
$V_{crucible}$: 49 ml

K_2CO_3

Used K_2CO_3: Tablet no. 4 (2.32800g)

Doping: (Bi)

2mol% BiO is desired; source is Bi_2O_3. Bi_2O_3 does not need the oxygen from K_2CO_3 to form BiO. The dopant already contains O.

$$Bi_2O_3 \rightarrow 2BiO + \frac{1}{2}O_2$$

$$ZnCl_2 + Bi_2O_3 + K_2CO_3 \rightarrow Bi_{0.02}Zn_{0.98}O + ...$$

Table 12. Calculated and weighed masses and molar concentrations.

Material	Molweight [g/mol]	Calculated		Weighed	
		M [g]	mol]	M [g]	[mol]
K_2CO_3	138.2058	1.68545	0.0122	2.32800	0.0168
$ZnCl_2$	136.2854	1.62879	0.0120	1.66650	0.0122
LiCl	42.3937	41.36000	0.9756	41.34810	0.9753
$Bi_{0.02}$ $Zn_{0.98}O$	84.5141	1.03067	0.0122	0.76722	0.0091
BiO	224.9798	0.05487	0.0002		
Bi_2O_3	465.9589	0.05682	0.0001	0.05689	0.0001

The values of 0.0122 for K_2CO_3 and 0.9756 for LiCl are known from the calculations in “Appendix A” (LiCl = 20 cm^3). Instead to form 0.0122 mol of ZnO it is wished to form 0.0122 mol of the solid solution $Bi_{0.02}$ $Zn_{0.98}O$.

Calculation:

(1) $Bi_{0.02}Zn_{0.98}O_{[mol]} = 0.0122$

(2) $M = [mol] \times Molweight$

(3) $BiO_{[mol]} = 0.02 \times Bi_{0.02}Zn_{0.98}O_{[mol]}$; $ZnCl_{2[mol]} = ZnO_{[mol]} = 0.98 \times Bi_{0.02}Zn_{0.98}O_{[mol]}$

(4) $Bi_2O_{3[mol]} = \frac{1}{2}BiO_{[mol]}$

Weighed:

(5) $[mol] = \frac{M}{Molweight}$

LiCl and $ZnCl_2$ in the crucible:

42.54100g (without losses it would be 41.34810+1.66650=43.01460g, see Table 12).

Table 13. Real amounts of LiCl and $ZnCl_2$ in the crucible.

Material	M weighed[g]	Mass %	$M_{substracted}$ [g]	M in crucible [g]
LiCl	41.3481	96.13	0.45527	40.89283
$ZnCl_2$	1.6665	3.87	0.01833	1.64817
LiCl+$ZnCl_2$	43.0146	100	0.47360	42.54100

(6) $LiCl_{M\ substracted} = 0.9613 \times 0.4736$

(7) $ZnCl_{2M\ substracted} = 0.0387 \times 0.4736$

(8) $M_{incrucible} = M_{weighed} - M_{substracted}$

Table 14. Used and formed amounts.

Material	In crucible M [g]	[mol]	**Formed materials** [mol%] (calculated with the values "In crucible")	$C_{ZnO\ in\ LiCl}$ [mol%]
K_2CO_3	2.32800	0.0168		
$ZnCl_2$	1.64817	0.0121		
LiCl	40.89283	0.9646		100
BiO formed	0.05494	0.0002	1.98	
ZnO formed	0.98449	0.0121	98.02	1.2542
Bi_2O_3	0.05689	0.0001		

(9) $BiO_{formed\ [mol]} = 2Bi_2O_{3[mol]}$

(10) $ZnO_{formed\ [mol]} = ZnCl_{2[mol]}$

(11) $[mol] = \frac{M}{Molweight}$

Notes

All was molten and a crust was visible but not as distinct like in Flux1 D.J.

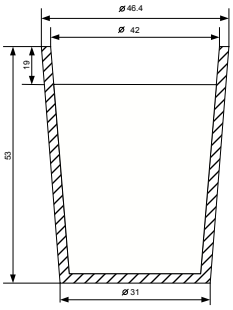

Figure 68. Dimension of the crucible after thermal treatment (filled with solution).

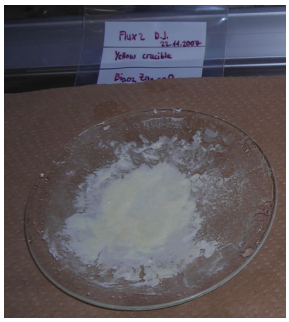

Figure 69. Powder before drying.

The obtained amount of $Bi_{0.02}Zn_{0.98}O$: 0.76722g

$\frac{0.76722}{1.03067} \approx 0.74439 \approx 74\%$ of the calculated value.

Crucible

Material: ZrO_2 (90%)/Y_2O_3 (10%)
$V_{crucible}$: 49 ml

K_2CO_3

Used K_2CO_3: Tablet no. 2 (2.73030g)

Doping: (In)

2mol% InO is desired; source is $InCl_3$. $InCl_3$ needs the oxygen of K_2CO_3 to form InO.

$$InCl_3 + O_2 \rightarrow InO + 3Cl + \frac{1}{2}O_2$$
$$ZnCl_2 + InCl_3 + K_2CO_3 \rightarrow In_{0.02}Zn_{0.98}O + \ldots$$

Table 15. Calculated and weighed masses and molar concentrations.

Material	Molweight [g/mol]	Calculated		Weighed	
		M [g]	mol]	M [g]	[mol]
K_2CO_3	138.2058	1.68545	0.0122	2.73030	0.0198
$ZnCl_2$	136.2854	1.62879	0.0120	1.66260	0.0122
LiCl	42.3937	41.36000	0.9756	41.32360	0.9748
$In_{0.02}$ $Zn_{0.98}O$	82.36816	1.00450	0.0122	0.58135	0.0071
InO	130.8174	0.03191	0.0002		
$InCl_3$	221.1761	0.05395	0.0002	0.05420	0.0002

The values of 0.0122 for K_2CO_3 and 0.9756 for LiCl are known from the calculations in “Appendix A” (LiCl = 20 cm^3). Instead to form 0.0122 mol of ZnO it is needed to form 0.0122 mol of the solid solution $In_{0.02}$ $Zn_{0.98}O$.

Calculation:

(1) $In_{0.02}Zn_{0.98}O_{[mol]} = 0.0122$

(2) $M_{=[mol]} \times Molweight$

(3) $InO_{[mol]} = 0.02 \times In_{0.02}Zn_{0.98}O_{[mol]}$; $ZnCl_{2[mol]} = ZnO_{[mol]} = 0.98 \times In_{0.02}Zn_{0.98}O_{[mol]}$

(4) $InO_{[mol]} = InCl_{3[mol]}$

Weighed:

(5) $[mol] = \frac{M}{Molweight}$

LiCl and $ZnCl_2$ in the crucible:

42.54400g (without losses it would be 41.32360+1.66260=42.98620, see Table 15).

Table 16. Real amounts of LiCl and $ZnCl_2$ in the crucible.

Material	M weighed [g]	Mass %	$M_{substracted}$ [g]	M in crucible [g]
LiCl	41.3236	96.13	0.42509	40.89851
$ZnCl_2$	1.6626	3.87	0.01711	1.64549
LiCl+$ZnCl_2$	42.9862	100	0.44220	42.54400

(6) $LiCl_{M_{substracted}} = 0.9613 \times 0.4422$

(7) $ZnCl_{2\,M_{substracted}} = 0.0387 \times 0.4422$

(8) $M_{incrucible} = M_{weighed} - M_{substracted}$

Table 17. Used and formed amounts.

Material	In crucible M [g]	In crucible [mol]	**Formed materials** [mol%] (calculated with the values "In crucible")	$C_{ZnO\ in\ LiCl}$ [mol%]
K_2CO_3	2.73030	0.0198		
$ZnCl_2$	1.64549	0.0121		
LiCl	40.89851	0.9647		100
InO_{formed}	0.03206	0.0002	1.9893	
ZnO_{formed}	0.98256	0.0121	98.0107	1.2515
$InCl_3$	0.05420	0.0002		

(9) $InO_{formed\,[mol]} = InCl_{3[mol]}$

(10) $ZnO_{formed\,[mol]} = ZnCl_{2[mol]}$

(11) $[mol] = \frac{M}{Molweight}$

Notes

- The cover sticked together with the crucible (during thermal treatment).
- The crucible and the cover were placed in the glassbeaker with water. After several minutes, the cover separated from the crucible.
- A crust was visible.
- The powder looked like a paste after drying (Figure 70). That is an indication that LiCl was not dissolved entirely. For this reason the powder was mixed with water again and stocked for several hours to dissolve all LiCl.

Figure 70. LiCl is not dissolved entirely.

The obtained amount of powder: 0.58135g

$\frac{0.58135}{1.00450} \approx 0.5787 \approx 58\%$ of the calculated value.

Crucible

Material: ZrO_2 (90%)/Y_2O_3 (10%)
$V_{crucible}$: 42 ml

K_2CO_3

Used K_2CO_3: Tablet no. 5 (2.34110g)

Doping: (In)

0.1 mol% InO is desired; source is $InCl_3$. $InCl_3$ needs the oxygen of K_2CO_3 to form InO.

$$InCl_3 + O_2 \rightarrow InO + 3Cl + \frac{1}{2}O_2$$
$$ZnCl_2 + InCl_3 + K_2CO_3 \rightarrow In_{0.001}Zn_{0.999}O + \ldots$$

Table 18. Calculated, weighed masses and mol of used and formed materials.

Material	Molweight [g/mol]	Calculated		Weighed	
		M [g]	mol]	M [g]	[mol]
K_2CO_3	138.2058	1.68545	0.0122	2.34110	0.0169
$ZnCl_2$	136.2854	1.66037	0.0122	1.66240	0.0122
LiCl	42.3937	41.36000	0.9756	41.31940	0.9747
$In_{0.001}$ $Zn_{0.999}O$	81.4288	0.99304	0.0122	0.76673	0.0094
InO	130.8174	0.00160	0.00001		
$InCl_3$	221.1761	0.00270	0.00001	0.00350	0.00002

The values of 0.0122 for K_2CO_3 and 0.9756 for LiCl are known from the calculations in “Appendix A” (LiCl = 20 cm^3). Instead to form 0.0122 mol of ZnO it is wished to form 0.0122 mol of the solid solution $In_{0.001}$ $Zn_{0.999}O$.

Calculation:

(1) $In_{0.001}Zn_{0.999}O_{[mol]} = 0.0122$

(2) $M_{=[mol]} \times Molweight$

(3) $InO_{[mol]} = 0.001 \times In_{0.001}Zn_{0.999}O_{[mol]}$; $ZnCl_{2[mol]} = ZnO_{[mol]} = 0.999 \times In_{0.001}Zn_{0.999}O_{[mol]}$

(4) $InO_{[mol]} = InCl_{3[mol]}$

Weighed:

(5) $[mol] = \frac{M}{Molweight}$

LiCl and $ZnCl_2$ in the crucible:

42.44200g (without losses it would be 41.31940+1.66240=42.98180g, see Table 18).

Table 19. Real amounts of LiCl and $ZnCl_2$ in the crucible.

Material	M weighed [g]	Mass %	$M_{substracted}$ [g]	M in crucible [g]
LiCl	41.3194	96.13	0.51891	40.80049
$ZnCl_2$	1.6624	3.87	0.02089	1.64151
LiCl+$ZnCl_2$	42.9818	100	0.53980	42.44200

(6) $LiCl_{M_{substracted}} = 0.9613 \times 0.5398$

(7) $ZnCl_{2\,M_{substracted}} = 0.0387 \times 0.5398$

(8) $M_{incrucible} = M_{weighed} - M_{substracted}$

Table 20. Used and formed amounts.

Material	In crucible M [g]	In crucible [mol]	**Formed materials** [mol%] (calculated with the values "In crucible")	$C_{ZnO\ in\ LiCl}$ [mol%]
K_2CO_3	2.34100	0.0169		
$ZnCl_2$	1.64151	0.0120		
LiCl	40.80049	0.9624		100
InO_{formed}	0.00207	0.00002	0.1312	
ZnO_{formed}	0.98019	0.0120	99.8688	1.2515
$InCl_3$	0.00350	0.00002		

(9) $InO_{formed\,[mol]} = InCl_{3[mol]}$

(10) $ZnO_{formed\,[mol]} = ZnCl_{2[mol]}$

(11) $[mol] = \frac{M}{Molweight}$

Notes

- It is very difficult to weigh such a little amount of $InCl_3$. Another problem is that $InCl_3$ is hydrophobic.
- The cover sticked together with the crucible.
- A crust was visible when the cover separated from the crucible.

The obtained amount of powder: 0.76673g

$\frac{0.76673}{0.99304} \approx 0.7721 \approx 77\%$ of the calculated value.

Crucible

Material: ZrO_2 (90%)/Y_2O_3 (10%)
$V_{crucible}$: 42 ml

K_2CO_3

Used K_2CO_3: Tablet no. 6 (2.40300g)

Doping: (Mo)

0.1 mol% MoO is desired; source is MoO_3. MoO_3 does not need the oxygen from K_2CO_3 to form MoO. The dopant already contains O.

$$MoO_3 \rightarrow MoO + O_2$$
$$ZnCl_2 + MoO_3 + K_2CO_3 \rightarrow Mo_{0.001}Zn_{0.999}O + ...$$

Table 21. Calculated and weighed masses and molar concentrations.

Material	Molweight [g/mol]	Calculated		Weighed	
		M [g]	mol]	M [g]	[mol]
K_2CO_3	138.2058	1.68545	0.0122	2.40300	0.0174
$ZnCl_2$	136.2854	1.66037	0.0122	1.66200	0.0122
LiCl	42.3937	41.36000	0.9756	41.39150	0.9764
$Mo_{0.001}$ $Zn_{0.999}O$	81.4100	0.99281	0.0122	0.67060	0.0082
MoO	111.9394	0.00137	0.00001		
MoO_3	143.9382	0.00176	0.00001	0.00192	0.00001

The values of 0.0122 for K_2CO_3 and 0.9756 for LiCl are known from the calculations in "Appendix A" (LiCl = 20 cm^3). Instead to form 0.0122 mol of ZnO it is needed to form 0.0122 mol of the solid solution $Mo_{0.001}$ $Zn_{0.999}O$.

Calculation:

(1) $Mo_{0.001}Zn_{0.999}O_{[mol]} = 0.0122$

(2) $M_{[mol]} = [mol] \times Molweight$

(3) $MoO_{[mol]} = 0.001 \times Mo_{0.001}Zn_{0.999}O_{[mol]}$; $ZnCl_{2[mol]} = ZnO_{[mol]} = 0.999 \times Mo_{0.001}Zn_{0.999}O_{[mol]}$

(4) $MoO_{[mol]} = MoO_{3[mol]}$

Weighed:

(5) $[mol] = \frac{M}{Molweight}$

LiCl and $ZnCl_2$ in the crucible:

42.86300g (without losses it would be 41.39150+1.66200=43.05350, see Table 21).

Table 22. Real amounts of LiCl and $ZnCl_2$ in the crucible.

Material	M weighed [g]	Mass %	$M_{substracted}$ [g]	M in crucible [g]
LiCl	41.39150	96.14	0.18315	41.20835
$ZnCl_2$	1.66200	3.86	0.00735	1.65465
LiCl+$ZnCl_2$	43.05350	100	0.19050	42.86300

(6) $LiCl_{M\ substracte\ d} = 0.9614 \times 0.1905$

(7) $ZnCl_{2\,M\ substracte\ d} = 0.0386 \times 0.1905$

(8) $M_{incrucible} = M_{weighed} - M_{substracte\ d}$

Table 23. Used and formed amounts.

Material	In crucible M [g]	In crucible [mol]	**Formed materials** [mol%] (calculated with the values "In crucible")	$C_{ZnO\ in\ LiCl}$ [mol%]
K_2CO_3	2.40300	0.0174		
$ZnCl_2$	1.65465	0.0121		
LiCl	41.20835	0.9720		100
MoO $_{formed}$	0.00149	0.00001	0.1097	
ZnO $_{formed}$	0.98803	0.0121	99.8903	1.2490
MoO_3	0.00192	0.00001		

(9) $MoO_{formed\ [mol]} = MoO_{3[mol]}$

(10) $ZnO_{formed\ [mol]} = ZnCl_{2[mol]}$

(11) $[mol] = \frac{M}{Molweight}$

Notes

- A crust was visible. Crystallization was visible under the crust.

Figure 71. Crust and crystallization.

The obtained amount of powder: 0.67060g

$\frac{0.67060}{0.99281} \approx 0.6755 \approx 68\%$ of the calculated value.

Crucible

Material: Al_2O_3 (95%)/SiO_2(3%)
$V_{crucible}$: 42 ml

K_2CO_3

Used K_2CO_3: Tablet no. 7 (2.36712g)

Doping: (Mo)

2 mol% MoO is desired; source is MoO_3. MoO_3 does not need the oxygen from K_2CO_3 to form MoO. The dopant already contains O.

$$MoO_3 \rightarrow MoO + O_2$$
$$ZnCl_2 + MoO_3 + K_2CO_3 \rightarrow Mo_{0.02}Zn_{0.98}O + ...$$

Table 24. Calculated and weighed masses and molar concentrations.

Material	Molweight [g/mol]	Calculated		Weighed	
		M [g]	mol]	M [g]	[mol]
K_2CO_3	138.2058	1.68545	0.0122	2.36712	0.0171
$ZnCl_2$	136.2854	1.62879	0.0120	1.66040	0.0122
LiCl	42.3937	41.36000	0.9756	41.36920	0.9758
$Mo_{0.02}$ $Zn_{0.98}O$	81.9906	0.99989	0.0122	0.66750	0.0081
MoO	111.9394	0.02730	0.0002		
MoO_3	143.9382	0.03511	0.0002	0.03650	0.0003

The values of 0.0122 for K_2CO_3 and 0.9756 for LiCl are known from the calculations in “Appendix A” (LiCl = 20 cm^3). Instead to form 0.0122 mol of ZnO it is needed to form 0.0122 mol of the solid solution $Mo_{0.02}$ $Zn_{0.98}O$.

Calculation:

(1) $Mo_{0.02}Zn_{0.98}O_{[mol]} = 0.0122$

(2) $M = [mol] \times Molweight$

(3) $MoO_{[mol]} = 0.02 \times Mo_{0.02}Zn_{0.98}O_{[mol]}$; $ZnCl_{2[mol]} = ZnO_{[mol]} = 0.98 \times Mo_{0.02}Zn_{0.98}O_{[mol]}$

(4) $MoO_{[mol]} = MoO_{3[mol]}$

Weighed:

(5) $[mol] = \frac{M}{Molweight}$

LiCl and $ZnCl_2$ in the crucible:

42.58100g (without losses it would be 41.36920+1.66040=43.02960, see Table 24).

Table 25. Real amounts of LiCl and $ZnCl_2$ in the crucible.

Material	M weighed [g]	Mass %	$M_{substracted}$ [g]	M in crucible [g]
LiCl	41.3692	96.14	0.43128	40.93792
$ZnCl_2$	1.6604	3.86	0.01732	1.64308
LiCl+$ZnCl_2$	43.0296	100	0.44860	42.58100

(6) $LiCl_{M_{substracted}} = 0.9614 \times 0.4486$

(7) $ZnCl_{2M_{substracted}} = 0.0386 \times 0.4486$

(8) $M_{incrucible} = M_{weighed} - M_{substracted}$

Table 26. Used and formed amounts.

Material	In crucible M [g]	In crucible [mol]	**Formed materials** [mol%] (calculated with the values "In crucible")	$C_{ZnO\ in\ LiCl}$ [mol%]
K_2CO_3	2.36712	0.0171		
$ZnCl_2$	1.64308	0.0121		
LiCl	40.93792	0.9657		100
MoO_{formed}	0.02839	0.0003	2.06	
ZnO_{formed}	0.98113	0.0121	97.94	1.2485
MoO_3	0.03650	0.0003		

(9) $MoO_{formed[mol]} = MoO_{3[mol]}$

(10) $ZnO_{formed[mol]} = ZnCl_{2[mol]}$

(11) $[mol] = \frac{M}{Molweight}$

Notes

- The cover sticked together with the crucible.

The obtained amount of powder: 0.66750g

$\frac{0.66750}{0.99989} \approx 0.6676 \approx 67\%$ of the calculated value.

Crucible

Material: Al_2O_3 (95%)/SiO_2(3%)
$V_{crucible}$: 42 ml

K_2CO_3

Used K_2CO_3: Tablet no. 8 (2.29920g)

Doping: (Mo)

5 mol% MoO is desired; source is MoO_3. MoO_3 does not need the oxygen from K_2CO_3 to form MoO. The dopant already contains O.

$$MoO_3 \rightarrow MoO + O_2$$
$$ZnCl_2 + MoO_3 + K_2CO_3 \rightarrow Mo_{0.05}Zn_{0.95}O + ...$$

Table 27. Calculated and weighed masses and molar concentrations.

Material	Molweight [g/mol]	Calculated		Weighed	
		M [g]	mol]	M [g]	[mol]
K_2CO_3	138.2058	1.68545	0.0122	2.29920	0.0166
$ZnCl_2$	136.2854	1.57893	0.0116	1.66272	0.0122
LiCl	42.3937	41.36000	0.9756	41.37470	0.9760
$Mo_{0.05}$ $Zn_{0.95}O$	82.9074	1.01107	0.0122	0.65145	0.0079
MoO	111.9394	0.06826	0.0006		
MoO_3	143.9382	0.08777	0.0006	0.08725	0.0006

The values of 0.0122 for K_2CO_3 and 0.9756 for LiCl are known from the calculations in “Appendix A” (LiCl = 20 cm^3). Instead to form 0.0122 mol of ZnO it is needed to form 0.0122 mol of the solid solution $Mo_{0.05}$ $Zn_{0.95}O$.

Calculation:

(1) $Mo_{0.05}Zn_{0.95}O_{[mol]} = 0.0122$

(2) $M_{=[mol]} \times Molweight$

(3) $MoO_{[mol]} = 0.05 \times Mo_{0.05}Zn_{0.95}O_{[mol]}$; $ZnCl_{2[mol]} = ZnO_{[mol]} = 0.95 \times Mo_{0.05}Zn_{0.95}O_{[mol]}$

(4) $MoO_{[mol]} = MoO_{3[mol]}$

Weighed:

(5) $[mol] = \frac{M}{Molweight}$

LiCl and $ZnCl_2$ in the crucible:

42.59700g (without losses it would be 41.37470+1.66272=43.03742, see Table 27).

Table 28. Real amounts of LiCl and $ZnCl_2$ in the crucible.

Material	M weighed [g]	Mass %	$M_{substracted}$ [g]	M in crucible [g]
LiCl	41.3747	96.14	0.42342	40.95128
$ZnCl_2$	1.6627	3.86	0.01700	1.64572
LiCl+$ZnCl_2$	43.0374	100	0.44042	42.59700

(6) $LiCl_{M\ substracte\ d} = 0.9614 \times 0.44042$

(7) $ZnCl_{2\,M\ substracte\ d} = 0.0386 \times 0.44042$

(8) $M_{incrucible} = M_{weighed} - M_{substracte\ d}$

Table 29. Used and formed amounts.

Material	In crucible M [g]	In crucible [mol]	**Formed materials** [mol%] (calculated with the values "In crucible")	$C_{ZnO\ in\ LiCl}$ [mol%]
K_2CO_3	2.29920	0.0166		
$ZnCl_2$	1.64572	0.0121		
LiCl	40.95128	0.9660		100
MoO_{formed}	0.06785	0.0006	4.7798	
ZnO_{formed}	0.98270	0.0121	95.2202	1.2501
MoO_3	0.08725	0.0006		

(9) $MoO_{formed\,[mol]} = MoO_{3[mol]}$

(10) $ZnO_{formed\,[mol]} = ZnCl_{2[mol]}$

(11) $[mol] = \frac{M}{Molweight}$

Notes

- The cover sticked together with the crucible.

The obtained amount of powder: 0.65145g

$\frac{0.65145}{1.01107} \approx 0.6443 \approx 64\%$ of the calculated value.

Appendix C

LPE Experiments

Used crucibles

Material: ZrO_2 (90%)/Y_2O_3 (10%)
$V_{crucible}$: 49 ml

Materials and processing

The volume of LiCl should be 20 cm^3 (for calculations of the required masses see “Appendix A”)

Table 30. Used materials.

Material	Properties	Purity [%]	Distributor	Lot #	Required mass [g]
LiCl	white color	99.999	MV Laboratories, INC	E305LIA1	41.36000
$ZnCl_2$	almost transparent, hydrophobic	99.999	High Purity Chemicals	69520	1.66203
K_2CO_3	white color	99.997	Alfa Aesar Puratronic	23092	1.68545
Bi_2O_3	yellow color	99.990	High Purity Chemicals	32382G	-
Sb	silver color	99.990	High Purity Chemicals	746960	-

Firstly, K_2CO_3 was placed at the bottom of the crucible. After the chlorides were weighed and roughly mixed, they were filled in the crucible. The baffle was placed at about middle height of the crucible. The crucible was filled to ¾ by the chlorides. The wished dopant was added and covered by the remaining chlorides. The crucible was heated to T_G (635°C-660°C). The substrate was attached to a Pt wire, which was mounted on an Al_2O_3 rod. The substrate was immersed into the liquid solution after a dwell time of ½ h and the rotation speed was slowly increased to 20 rpm. The dwell time is important to homogenize the solution. When heating, the substrate should not be too close to the solution because some chlorides evaporate and would deposit on the substrate. The experiments were performed under air at atmospheric pressure, and constant temperature. The growth was finished by seperating the substrate from the solution. The adhesive solvent was removed from the film by rinsing with water (solvent is water soluble and so removing from the film is easy). Isopropanol was used to remove water from the sample.

Scales

Two scales were used:

1. Mettler AE 163 (min. 0.00001g, max. 30g).
2. AND GX 600 (min. 0.02g, max. 610g).

Supersonic bath

Type: AS ONE, Ultra Sonic bath.

Temperature profile and LPE machine

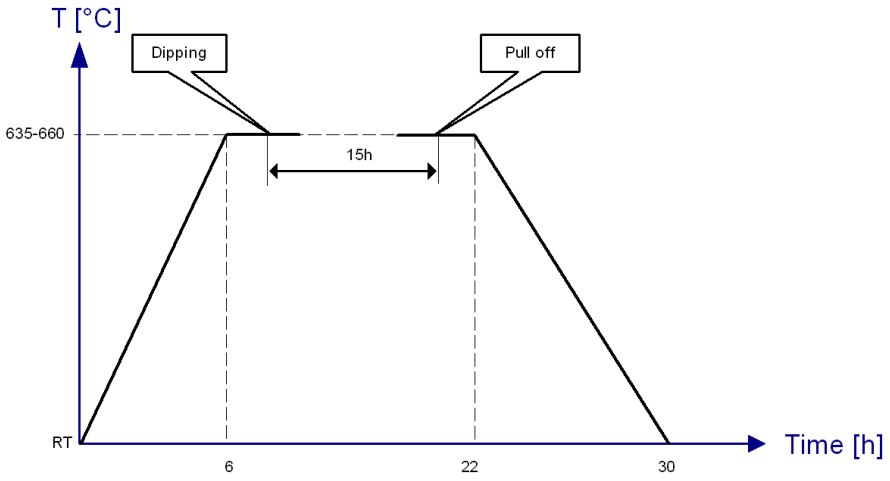

Figure 72. Temperature profile.

LPE machine: Techno search, Japan, 3 heaters (lower, middle, and upper), control unit.

Figure 73. LPE machine from Techno search.

Examination

SEM-EDX and PL

See “Appendix B”, Flux general.

DIC

Type: Nikon, Eclipse, ME600.

Figure 74. DIC, Nikon.

XRC

Type:	PHILIPS X'PERT MRD (Material Research Diffractometer)
Scanning type:	Continuous scanning (ω-scan)
X-ray:	45kV/40mA
Scan step size:	0.0005°

Figure 75. Philips X'Pert MRD.

Crucible

Material: ZrO_2 (90%)/Y_2O_3 (10%)
$V_{crucible}$: 49 ml

K_2CO_3

Used K_2CO_3: Tablet no. 10 (1.94320g)

Substrate

0.29493 g
TEW (0.5°-off axis to m)
Lot #: JZN-3215-027
Annealing: TEW (1100°C, 2h). TEW is the company name.
Dimensions: 10 x 10 x 0.5 [mm^3]

Rotation: 20 rpm

Atmosphere: Air

Materials:

2mol% SbO is desired; source is pure Sb. Sb needs the oxygen from K_2CO_3 to form SbO.

$$Sb + O_2 \rightarrow SbO + \frac{1}{2}O_2$$

$$ZnCl_2 + Sb + K_2CO_3 \rightarrow Sb_{0.02}Zn_{0.98}O + \ldots$$

Table 31. Calculated and weighed masses and molar concentrations.

Material	Molweight [g/mol]	Calculated		Weighed	
		M [g]	[mol]	M [g]	[mol]
K_2CO_3	138.2058	1.68545	0.0122	1.94320	0.0141
$ZnCl_2$	136.2854	1.62879	0.0120	1.65450	0.0121
LiCl	42.3937	41.36000	0.9756	41.35070	0.9754
$Sb_{0.02}$ $Zn_{0.98}O$	82.5068	1.00619	0.0122	*0.00117	0.0965
SbO	137.7494	0.03360	0.0002		
Sb	121.7500	0.02970	0.0002	0.02970	0.0002

** see page 79 (ΔM). It's the mass of the grown film on Zn-face and O-face.*

The values of 0.012195208 for K_2CO_3 and 0.9756 for LiCl are known from the calculations in "Appendix A" (LiCl = 20 cm^3). Instead to form 0.0122 mol of ZnO it is needed to form 0.0122 mol of the solid solution $Sb_{0.02}$ $Zn_{0.98}O$.

Calculation:

(1) $Sb_{0.02}Zn_{0.98}O_{[mol]} = 0.0122$

(2) $M =_{[mol]} \times Molweight$

(3) $SbO_{[mol]} = 0.02 \times Sb_{0.02}Zn_{0.98}O_{[mol]}$; $ZnCl_{2[mol]} = ZnO_{[mol]} = 0.98 \times Sb_{0.02}Zn_{0.98}O_{[mol]}$

(4) $SbO_{[mol]} = Sb_{[mol]}$

Weighed:

(5) $[mol] = \frac{M}{Molweight}$

LiCl and $ZnCl_2$ in the crucible:

42.80600g (without losses it would be 41.35070+1.65450=43.00520g, see Table 31).

Table 32. Real amounts of LiCl and $ZnCl_2$ in the crucible.

Material	M weighed [g]	Mass %	$M_{substracted}$ [g]	M in crucible [g]
LiCl	41.3507	96.15	0.19153	41.15917
$ZnCl_2$	1.6545	3.85	0.00767	1.64683
LiCl+$ZnCl_2$	43.0052	100	0.19920	42.80600

(6) $LiCl_{M_{substracted}} = 0.9615 \times 0.1992$

(7) $ZnCl_{2\,M_{substracted}} = 0.0385 \times 0.1992$

(8) $M_{incrucible} = M_{weighed} - M_{substracted}$

Table 33. Used and formed (calculated) amounts.

Material	In crucible M [g]	In crucible [mol]	Formed materials [mol%] (calculated with the values "In crucible")	$C_{ZnO\ in\ LiCl}$ [mol%]
K_2CO_3	1.94320	0.0141		
$ZnCl_2$	1.64683	0.0121		
LiCl	41.15917	0.9709		100
SbO_{formed}	0.03360	0.0002	1.9788	
ZnO_{formed}	0.98336	0.0121	98.0212	1.2446
Sb	0.02970	0.0002		

(9) $SbO_{formed\,[mol]} = Sb_{[mol]}$

(10) $ZnO_{formed\,[mol]} = ZnCl_{2[mol]}$

(11) $[mol] = \frac{M}{Molweight}$

Calculation of the film thickness

The film thickness is calculated as a result of the mass difference before and after film growth.
The mass after film growth: 0.29610g.
ΔM = 0.29610-0.29493 = 0.00117g.

(12) $V = \frac{M}{\rho_{ZnO}} = \frac{0.00117}{5.606} = 2.08704959 \times 10^{-4}\,cm^3$ (volume of the grown film)

(13) $d = \frac{V}{A_{Substrate}} = \frac{2.08704959 \times 10^{-4}}{1} = 2.08704959 \times 10^{-4}\,cm$ (film thickness on O-, and Zn-face)

The ratio of growth speed:

$$\frac{Zn-face}{O-face} = \frac{3}{1}$$

The film thickness on the Zn-face can be calculated:

$$d_{Zn-face} = (2.08704959 \times 10^{-4}) \times \frac{3}{4} = 1.565287192 \times 10^{-4} cm \approx 1.57 \mu m$$

The film thickness on the O-face:

$$d_{O-face} = 2.08704959 \times 10^{-4} - 1.565287192 \times 10^{-4} \approx 0.52 \mu m$$

Growth speed

$$\frac{1.57 \mu m}{15h} \approx 0.105 \frac{\mu m}{h}$$ (Zn-face)

$$\frac{0.52 \mu m}{15h} \approx 0.035 \frac{\mu m}{h}$$ (O-face)

Notes

After the experiment the crucible was empty. It is possible that a part of the solution evaporated. 3 heaters were used (upper, middle, and lower). When observing the crucible more in detail it was clear that most of the solution was lost due to a crack at the bottom of the crucible. The basement of the crucible could be separated (Figure 76). In spite of, some microcrystals at the bottom were preserved and examined. The crucible must have been cracked at the end of the experiment (otherwise no film would have been grown).

Figure 76. Cracked crucible.

1.00619g (100%) of the solid solution should be formed (see Table 31). From this value only 0.00117g (0.1163%) is used for the film growth. 0.10720g (10.6541%) microcrystals were formed and the rest was lost (cracked crucible).

Crucible

Material: ZrO_2 (90%)/Y_2O_3 (10%)
(identical crucible to the cracked one in LPE 1D.J)
$V_{crucible}$: 49 ml

K_2CO_3

Used K_2CO_3: Tablet no. 11 (2.24890g)

Substrate

0.29760 g
TEW (0.5°-off axis to m)
Lot #: JZN-3215-027
Annealing: TEW (1100°C, 2h).
Dimensions: 10 x 10 x 0.5 [mm^3]

Rotation: 20 rpm

Atmosphere: Air

Materials:

The amount of LiCl was set to 50g.

Table 34. Needed masses of LiCl, $ZnCl_2$, and K_2CO_3 (calculations see "Appendix A" formulas (1) - (10)).

Material	[mol]	M [g]	V [cm^3]
LiCl	1.1794	**50.00000**	24.18
$ZnCl_2$	0.0147	2.00922	0.69
ZnO	0.0147	1.19976	0.21
K_2CO_3	0.0147	2.03753	0.84

2mol% BiO is wished. The source is Bi_2O_3. Bi_2O_3 does not need the oxygen of K_2CO_3 to form BiO. The dopant already contains O.

$$Bi_2O_3 \rightarrow 2BiO + \frac{1}{2}O_2$$

$$ZnCl_2 + Bi_2O_3 + K_2CO_3 \rightarrow Bi_{0.02}Zn_{0.98}O + \ldots$$

Table 35. Calculated and weighed masses and molar concentrations.

Material	Molweight [g/mol]	Calculated		Weighed	
		M [g]	[mol]	M [g]	[mol]
K_2CO_3	138.2058	2.03753	0.0147	2.24890	0.0163
$ZnCl_2$	136.2854	1.96904	0.0144	2.01085	0.0148
LiCl	42.3937	**50.00000**	1.1794	49.95772	1.1784
$Bi_{0.02}$ $Zn_{0.98}O$	84.5141	1.24597	0.0147	*0.00200	0.00002
BiO	224.9798	0.06634	0.0003		
Bi_2O_3	465.9589	0.06870	0.0001	0.06895	0.00015

** see page 82 (ΔM). It's the mass of the grown film on Zn-face and O-face.*

The values of 0.0147 for K_2CO_3 and 1.1794 for LiCl are known from Table 34. Instead to form 0.0147 mol of ZnO it is wished to form 0.0147 mol of the solid solution $Bi_{0.02}$ $Zn_{0.98}O$.

Calculation:

(1) $Bi_{0.02}Zn_{0.98}O_{[mol]} = 0.0147$

(2) $M_{=[mol]} \times Molweight$

(3) $BiO_{[mol]} = 0.02 \times Bi_{0.02}Zn_{0.98}O_{[mol]}$; $ZnCl_{2[mol]} = ZnO_{[mol]} = 0.98 \times Bi_{0.02}Zn_{0.98}O_{[mol]}$

(4) $Bi_2O_{3[mol]} = \frac{1}{2} BiO_{[mol]}$

Weighed:

(5) $[mol] = \frac{M}{Molweight}$

LiCl and $ZnCl_2$ in the crucible:

51.71900g (without losses it would be 49.95772+2.01085=51.96857g, see Table 35).

Table 36. Real amounts of LiCl and $ZnCl_2$ in the crucible.

Material	M weighed [g]	Mass %	$M_{substracted}$ [g]	M in crucible [g]
LiCl	49.95772	96.13	0.23991	49.71781
$ZnCl_2$	2.01085	3.87	0.00966	2.00120
LiCl+$ZnCl_2$	51.96857	100	0.24957	51.71900

(6) $LiCl_{M_{substracted}} = 0.9613 \times 0.24957$

(7) $ZnCl_{2M_{substracted}} = 0.0387 \times 0.24957$

(8) $M_{incrucible} = M_{weighed} - M_{substracted}$

Table 37. Used and formed amounts.

Material	In crucible M [g]	In crucible [mol]	**Formed materials** [mol%] (calculated with the values "In crucible")	$C_{ZnO\ in\ LiCl}$ [mol%]
K_2CO_3	2.24890	0.0163		
$ZnCl_2$	2.00119	0.0147		
LiCl	49.71781	1.1728		100
BiO $_{formed}$	0.06658	0.0003	1.9757	
ZnO $_{formed}$	1.19496	0.0147	98.0243	1.2521
Bi_2O_3	0.06895	0.0001		

(9) $BiO_{formed\ [mol]} = 2Bi_2O_{3[mol]}$

(10) $ZnO_{formed\ [mol]} = ZnCl_{2[mol]}$

(11) $[mol] = \frac{M}{Molweight}$

Calculation of the film thickness

The film thickness is calculated as a result of the mass difference before and after film growth.
The mass after film growth: 0.29960g.
ΔM = 0.29960-0.29760 = 0.00200g.

(12) $V = \frac{M}{\rho_{ZnO}} = \frac{0.002}{5.606} = 3.567606136 \times 10^{-4} cm^3$ (volume of the grown film)

(13) $d = \frac{V}{A_{Substrate}} = \frac{3.567606136 \times 10^{-4}}{1} = 3.567606136 \times 10^{-4} cm$ (film thickness on O-, and Zn-face)

The ratio of growth speed:

$$\frac{Zn - face}{O - face} = \frac{3}{1}$$

The film thickness on the Zn-face can be calculated:

$$d_{Zn-face} = (3.567606136 \times 10^{-4}) \times \frac{3}{4} = 2.675704602 \times 10^{-4} cm \approx 2.68 \mu m$$

The film thickness on the O-face:

$$d_{O-face} = 3.567606136 \times 10^{-4} - 2.675704602 \times 10^{-4} \approx 0.89 \mu m$$

Growth speed

$\frac{2.68 \mu m}{15h} \approx 0.179 \frac{\mu m}{h}$ (Zn-face)

$\frac{0.89 \mu m}{15h} \approx 0.059 \frac{\mu m}{h}$ (O-face)

Notes

Figure 77. Crucible filled with the solution after the experiment. The Pt-wires of the baffle are visible.

1.24597g (100%) of the solid solution should be formed (see Table 35). From this value 0.00200g (0.1605%) was used for the film growth. 0.89880g (72.1365%) microcrystals were formed and the rest did not form the wished solid solution.